INTERFACIAL HEAT TRANSFER DURING SOLIDIFICATION OF COMMERCIALLY PURE ALUMINIUM

by

Md. Abdul Gafur

B.Sc. Engg. (Metallurgical), M. Sc. Engg. (Metallurgical)

A thesis submitted to The Department of Materials and Metallurgical Engineering *in partial fulfillment of requirements for the degree of **DOCTOR** of **PHILOSOPHY*** in Metallurgical Engineering
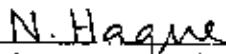
Bangladesh University of Engineering and Technology
Dhaka-1000, Bangladesh
July 1999

#935777#

Certification of thesis work

A thesis on "INTERFACIAL HEAT TRANSFER DURING SOLIDIFICATION OF COMMERCIALLY PURE ALUMINIUM" by Md. Abdul Gafur has been accepted as satisfactory in partial fulfilment of the requirements for the degree of **Doctor of Philosophy in Metallurgical Engineering** and certify that the student demonstrated a satisfactory knowledge of the field covered by this thesis in an oral examination held on 12 July, 1999.

Dr. Md. Nasrul Haque
Professor
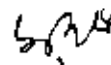Dept. of MME. BUET. Dhaka

N. Haque
Chairman (Supervisor)
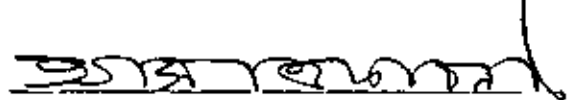
Head
Dept. of MME, BUET, Dhaka

E. Haque
Member

Dr. Ehsanul Haque
Professor
Dept. of MME, BUET, Dhaka

E. Haque
Member

Dr. Md. Mohafizul Haque
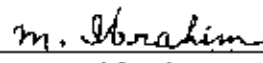Professor
Dept. of MME, BUET, Dhaka

Member

Dr. A S W Kurny
Professor
Dept. of MME. BUET, Dhaka

Member

Dr. Md. Wahhaj Uddin
Professor
Dept of ME, BUET, Dhaka

Member

Prof. M. Ibrahim
House No. 31, Road No. 4
Dhanmondi R/A. Dhaka

m. Ibrahim
Member

Prof. Md. Serajul Islam
256/2A Sultangonj Rd
Rayer Bazar, Dhaka

Member

Dr. K. Narayan Prabhu
Manchester Materials Sceince Centre
University of Manchester and UMIST
United Kingdom

Member (External)

DECLARATION

No portion of the work contained in this thesis has been submitted in support of an application for another degree or qualification of this or any other university or institution.

Md. Abdul Gafur

July, 1999

CONTENTS

ABSTRACT
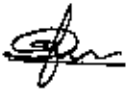
Theoretical and experimental investigations have been carried out on different casting systems. In the theoretical investigations, the casting variables used are casting thickness, superheat of molten metal, initial mould temperature, mould thickness, and interfacial heat transfer coefficient. It is found that solidification time decreases with the increase of mould thickness upto a critical value, called semi-infinite mould thickness. Further up, above the critical value, the solidification time is not affected by the mould thickness. With the variations of casting material, mould material, superheat of molten metal, interfacial heat transfer coefficient (HTC) and initial mould temperature, the solidification time has been estimated using the semi-infinite mould model and found that, with any combination of casting and mould variables, it increases linearly with interfacial thermal resistance. It is also found that the solidification time increases with the increase of casting thickness, superheat of molten metal, and initial mould temperature quadratically. To validate the model, aluminium castings are cast in semi-infinite sand mould. Using Beck's non-linear estimation procedure the interfacial heat flux (HF) and interfacial HTC are obtained. Taking average HTC, the castings are simulated. The experimental results are in good agreement with the simulated results.

The experimental works have been done using metal moulds to evaluate the unknown heat transfer at the casting-mould interface. Three shapes of castings, namely bar-shape, plate-shape, and cylindrical-shape, are used to find the effects of superheat, chill thickness, casting thickness, and initial mould temperature. Commercially pure aluminium has been used as casting material. The effects of superheat (45-140 C) and chill thickness (24mm, 47mm and 70mm) have been studied using bar shaped (1-Bar and 3-Bar) sand mould casting with cast iron chill at the end. Plate shaped casting is used to find the effects of superheat (90 -290 C) and casting thickness (68mm, 52mm and 36mm). The effects of superheat and initial mould temperature are investigated using cylindrical casting. Gray cast iron has been used as mould materials for both plate shaped and cylindrical shaped castings. Kiethly 740 Scan Thermometer and IEE488 interfacing card are used to

obtain temperature of the casting and mould at various locations at an interval of 1 sec. The interfacial heat flux has been estimated by Beck's non-linear estimation procedure.

The temperature of the inner surface of the mould or chill initially increases at a faster rate for higher superheat and higher initial mould temperature. Chill thickness or casting thickness initially does not affect the rate of increase of temperature of the inner surface of mould. The effect of chill thickness on the inner surface temperature is only observed when the heat from the interface reaches the outer surface of the chill or mould and due to increase of outer surface temperature, the temperature gradient at the inner surface of the mould reduces.

For all casting systems, that is, for all shapes of castings, with the variations of superheat, casting thickness, chill thickness, and initial mould temperature, HF is found to increase from a low value to a peak value (HFmax). The HFmax is obtained at the end of filling due to maximum metallostatic pressure. HFmax increases with the increase of superheat and initial mould temperature. The chill thickness and casting thickness are found to have no effect on HFmax.

The effect of superheat on HF diminishes with time from the end of filling. The effect of chill thickness and casting thickness on HF is observed after the occurrence of HFmax. Higher HF is found for higher chill thickness and also for higher casting thickness.

The HTC is found to be higher for higher superheat. No significant effect of chill thickness on HTC is observed.

ACKNOWLEDGEMENTS

NOMENCLATURE

A - A point at the centre of casting

a - Constant

B- A point near the interface in casting

b - Constant

C - A point near the interface in mould /chill

C_1, C_2 - Constants

C_l - Specific heat of liquid

C_m- Specific heat of metal

C_s - Specific heat of solid

CM- Casting material

CT- Casting thickness

ChT- Chill thickness

D - A point near the external surface in mould/chill

DX- Space spacing

DT- Time spacing

G- Temperature gradient

g1, g2- Temperature jump distances

H- Enthalpy

HF- Interfacial heat flux

HF_s . Interfacial heat flux due to metal-mould contact

HF_c -Interfacial heat flux due to gas conduction

HF_r -Interfacial heat flux due to radiation

HFmax- Maximum heat flux

HN- Hardness of the softer material

HTC- Interfacial heat transfer coefficient

HTCs- Heat transfer coefficient due to metal-mould contact

HTC_c- Heat transfer coefficient due to gas conduction

HTC_r- Heat transfer coefficient due to radiation

HTC_e- Heat transfer coefficient at the external surface

$HTCmax$- Maximum heat transfer coefficient

I- Upper limit of F, Equation [2.16]

ITR-Interfacial thermal resistance

K - Thermal conductivity

K_m - Thermal conductivity of mould

K_{hm} - Harmonic mean of the thermal conductivity

K_g - Thermal conductivity of gas

k- Chvorinov's constant

L- Latent heat

l- Ordinal number of iteration

MM- Mould material

MT- Initial mould temperature

MMT- Mould thickness

M_c - Modulus of casting

m- Small integer

n_s - Number of sensor

n_f - Number of future temperature

n_p - Number of parameters

P- Pressure

PT - Pouring temperature

r- Number of future temperature + 1

R- Growth rate

S- Cooling modulus

SDAS- Secondary dendrite arm spacing

SH- superheat $(PT-T_f)$

T- Temperature

T1 -Measured temperature at point A

T2 - Measured temperature at point B

T3 - Measured temperature at point C

T4 - Measured temperature at point D

T_c- Casting surface temperature

T_m- Mould surface temperature

T_a, AT, Ta - Ambient temperature

T_f- Freezing point of metal

T_o - Initial mould temperature

T_i. Interface temperature

ΔT - Temperature drop at the interface

t_f- Solidification time

t -Time

V- Volume

V_c- Volume of casting

V_m - Volume of mould

VR - Volume ratio of mould and casting

$(V/SA)_L$ - Local cooling rate

w_1- The first order regularization constant

w_j - Weighing constant for the temperature measurements from jth sensor

X1- Distance from interface to point C

X2- Distance from interface to point D

x - Distance

x_2 - Mould thickness

x_3 - Coating thickness

x_g - Void spacing

Y- Measured temperature

α- Thermal diffusivity

α_s- Thermal diffusivity of solid

α_m- Thermal diffusivity of mould

β - Parameter

φ- Sensitivity coefficient

ε - Small value

ε_1 . Emissivity of casting

ε_2 . Emissivity of mould

ρ- Density

ρ_m- Density of mould

η- Time index for temperature

0- Time index for temperature

σ-Stefan-Boltzman constant

CHAPTER 1

INTRODUCTION

Foundry occupies an important position in the manufacturing industries. As a method of fabrication, casting is the initial and primary process followed by subsequent machining of the product. The technique of metal casting can offer the advantages of flexibility and low cost. Casting is a very traditional technology which has been in existence for hundreds of years. In recent years, numerical modelling of casting is receiving increasing interest because of its potential in overcoming the expensive and time-consuming trial-and-error experimentation. Computer simulation for the solidification of casting can offer a basis of predicting the solidification pattern and parameters with greater accuracy, efficiency and economy, both in time and money than empirical methods, provided both numerical model and thermal properties are suitably applied. The attractive feature of CAD of casting is that the casting design is reviewable ahead of experimentation. CAD of casting can offer a number of advantages: increased casting yield, improved casting quality, enhanced productivity, easier implementation and evaluation of engineering application, and enhanced ability to deal with batch production of castings of different design.

Casting modelling can be used to design casting furnishing the location, and size of sprues, gates, runners, and feeders, along with the orientation of the casting and to select the process variables such as pouring temperature, and mould materials to eliminate the porosity, segregation, and cold shuts, and to predict residual stresses. Suitable location, properties of materials, cooling modulus of feeder are very essential to eliminate the piping in casting.

Casting modelling can also be used to estimate the parameters like local and total solidification times, local cooling rate, temperature gradient, growth rate, etc. These parameters are related to porosity, segregation, grain size, grain structure, secondary dendrite arm spacing (SDAS), etc. The mechanical properties of a casting largely depend on the soundness of castings, SDAS and its microstructure. The

1

solidification time is very useful to obtain sound casting. The location and size of feeder, fluidity of metal, etc. affect the soundness of casting. The location and size of feeder are to be such that it can supply liquid metal to compensate the shrinkage of casting. The condition of supplying liquid metal is achieved by using higher solidification time for feeder than that of casting. Feeder size is generally estimated on the basis of solidification time predicted by Chvorinov's rule (1). Chvorinov's rule assumes zero superheat and perfect contact. Metal are poured having sufficient superheat for suitable feeding and perfect contact between the casting and mould are rarely obtained. In casting design, directional solidification is also accomplished. To achieve the directional solidification, the feeder is to be placed such that it can supply the liquid metal to the last position of solidification. This requires the estimation of solidification time. The growth rate (R) and temperature gradient (G) control the microstructure of the castings. These are related to the local solidification time. Moreover, the SDAS of casting alloy is also related to solidification time. A model incorporating casting variables (superheat of molten metal, casting thickness, mould temperature, etc.) to estimate solidification pattern and solidification time would be extremely useful.

Castings made in metal moulds have better strength compared to those cast in sand moulds due to the faster rate of cooling in metal moulds. They also have better surface finish compared to sand castings. A significant portion of non-ferrous alloys are cast in metal mould. The soundness of casting depends on the thermal conditions during its solidification (2). The soundness of metal mould casting and the structure-properties relationships, have been studied experimentally and computationally (2-9). Casting-mould interfacial resistance controls the heat transfer significantly. It happens when the metal and the mould have reasonably good rates of heat conductance. The interface becomes overriding when an insulating die coat is applied and/or the casting shrinks away from mould surface leaving a gap between two surfaces. These circumstances are common in the die casting of light alloys.

The interfacial heat transfer plays the most important role in achieving good simulation results. A number of investigators (10-12) studied the metal-mould interface to arrive at a viable physical representation. To find the heat flow, the most critical and unpredictable parameter is the resistance of the casting-mould interface. It is difficult to measure the interfacial resistance or heat flow directly. It can be estimated by measuring the temperature distributions in the mould and castings. With a slight variation, the interfacial condition changes and results in significant change in heat transfer. Therefore, for useful solidification modelling, a through investigation of the interfacial heat transfer is required by varying the casting variables like type of metals/alloys, superheat of molten metal, casting thickness, roughness of the mould, casting orientation, metallostatic pressure, presence of coating material, coating thickness, etc.

In simulation works, the interface is treated by using either interfacial heat flux or interfacial heat transfer coefficient. The availability of a reliable and experimentally validated model of heat flux or heat transfer coefficient under various casting conditions mentioned above would be extremely useful for a solidification modeller.

Most of the investigators (10-14) used 1-D heat flow using water cooled chill. But casting without cooling may be more useful. Issac et al. (15) studied the effect of casting size on HTC. Their results are self contradictory. Durham and Berry (13) assumed constant HTC to simulate the solidification front of lead casting on water cooled brass mould. Higher heat transfer coefficient has been used for higher superheat. The estimated solidification front presented did not well matched with the experimental which shows that assumption of a constant HTC is not valid. The effect of superheat on the interfacial heat transfer is not well known. Sully (16) related the peak HTC at the end of filling. Kumar and Prabhu (7) found the occurrence of peak heat flux after the end of filling. Further study to identify the timing of peak HTC/HF is, therefore, needed. Sully reported that initial rise of HTC from a low value would only be observed for metals poured at lower superheat. This

3

can be investigated by using wide range of superheat. The effect of chill thickness on HF studied by Kumar and Prabhu (7) is not convincing.

In theoretical works, a model has been developed to find out the effect of casting variables on solidification pattern and to relate them with solidification time for semi-infinite mould model. To verify the model plate shaped aluminium castings are cast in semi-infinite sand mould.

In experimental works, three shapes of castings, bar shape, plate shape and cylindrical shape are chosen and the effects of superheat of molten metal, casting thickness, mould temperature and chill thickness on the interfacial heat transfer have been investigated. For bar shaped casting, superheat and chill thickness are varied. In the plate shaped casting, the casting thickness and superheat are the variables whereas superheat and mould temperature are varied for cylindrical shaped casting.

CHAPTER 2

LITERATURE REVIEW

2.1 INTRODUCTION

The soundness of a casting depends on the thermal conditions during solidification (2). Castings made in metal mould have better strength compared to those in sand due to the faster rate of cooling in the metal moulds and also they have better surface finish compared to sand castings. Non-ferrous alloys are generally cast in metal moulds. The thermal conditions are determined by the rate of heat extraction from the casting by the mould.

2.2 RESITANCES IN THE HEAT FLOW PATH OF CASTING

Solidification is the process of transformation of liquid to solid. The hot liquid metal takes time to lose its heat and solidify. Flemings (17) found that the rate at which a casting can liberate heat is controlled by a number of resistances. The resistances to the heat flow from the interior of the casting are those of the liquid metal, the solidified metal, the metal-mould interface, the mould, and the surroundings of the mould.

2.2.1 Resistance by liquid and surroundings of the mould

In casting the resistance offered by the liquid metal is negligible due to its high state of agitation. For semi-infinite thick mould, the resistance offered by the surroundings has no effect on solidification. But for metal mould, the surrounding environment has a significant effect on the solidification. Iron casting made in Croning shell moulds solidifies faster when the shell is thicker, but the solidification is delayed in thinner mould due to the effect of surroundings.

2.2.2 Resistance by solidified metal

The resistance offered by solidified metal is not significant in metal casting, especially for metal with high thermal conductivity in mould of low thermal

5

conductivity. But when the conductivity of mould is relatively high, this resistance becomes important, for example. Pb-Sn casting in steel dies, steel casting in copper mould, etc. (18).

2.2.3 Resistance by metal-mould interface

Resistance at the mould-metal interface controls the heat flow significantly in many important casting processes. This occurs when both the metal and the mould have reasonably good rates of heat conductance, leaving the boundary between the two as the dominant one. The interface resistance becomes prominent when an insulating mould coat is applied, or when a gap is formed between mould and casting due to the shrinkage of casting and expansion of the mould.

2.2.4 Resistance by mould material

This resistance controls the heat absorption rate from the casting. When a metal at its melting temperature T_f is poured in an infinite mould, initially at a temperature, T_0 and whose inner surface is instantly raised to a temperature T_f at the time t=0, then the cooling modulus is given by the Flemings's solution of one dimensional heat flow equation is:

$$S = \frac{V}{SA} = \left(\frac{T_f - T_0}{\rho_s L}\right) \frac{2\sqrt{K_m \rho_m} C_m}{\sqrt{\pi}} \sqrt{t_f} \qquad [2.1]$$

The product $K_m \rho_m C_m$ is a useful parameter for assessing the rate at which various moulding materials can absorb heat. The freezing time, t_f, of a casting is one of the important thermal parameters which depends on the rate of heat extraction.

2.3 SOLIDIFICIATION TIME

Solidification of a casting begins near the mould wall and proceeds towards the centre. The time at which the last solidifying point in the casting crosses the freezing or solidus temperature is taken as the freezing time or solidification time, t_f. Solidification time plays an important role in controlling the soundness and microstructure of castings. One of the most important criteria of suitable gating

system to yield sound casting is the filling time. This is related to solidification time. On the other hand, the SDAS (secondary dendrite arm spacing) and grain size of castings are controlled by the heat extraction rate, that is, by solidification time. Almost always, a shorter solidification time produces finer grain size and stronger castings (19). Quantitative relationships have been developed between casting soundness and freezing time (20).

The presence of an air gap between the solidifying casting and its metallic mould reduces the heat extraction rate owing to the insulating nature of the gases present in this gap. This, in turn, affects the freezing time of the casting. Similarly, a number of factors affect the heat extraction from the casting, which, in turn, affect its solidification time.

2.3.1 Factors affecting solidification time

Experimental results show that the solidification time depends on the thermal properties of casting and mould, interfacial condition, and pressure acting on the casing (21-31). The factors are:

2.3.1.1 Mould material

With the variation of mould material, the solidification time is markedly varied. Equation [2.1] implies that mould material having higher thermal conductivity, higher specific heat and density results in a lower solidification time, that is, mould material having higher heat diffusivity ($K_m \rho_m C_m$) yields lower solidification time. It was found that t_f is lesser in copper moulds compared to cast iron and anodised moulds (21).

2.3.1.2 Volume ratio and modulus coefficient

Solidification time, t_f, is influenced by volume ratio (VR) (volume of mould / volume of casting) if it is less than 5.0 (21,32). But, according to Mohan (33), it is not the only parameter for predicting t_f. In the case of cast iron castings in permanent mould, it was observed that t_f is proportional to the modulus coefficient given by $(V_c/SA)^{1.5}(VR)^{-0.5}$ (33,34). Here, V_c is the volume of casting, and SA the

surface area of casting. The chilling action of mould/chill will be fully utilised if the mould is very thick. For a chill of low thickness, the chilling action denoted by the heat diffusivity will be utilised initially but it will be limited as the chill/mould will be saturated with heat because of its limited thickness (18). So, the concept of volumetric heat capacity (ρCV) is introduced. The higher is the volumetric heat capacity of a chill, the lower is the solidification time of the casting.

2.3.1.3 Mould preheat

With an increase of the preheat of a mould, the solidification time of casting increases (35,36). Solidification time, t_f, increases marginally with the increase in mould preheat in the case of cast iron solidifying in cast iron mould (33).

2.3.1.4 Mould surface roughness

Prates and Biloni (37) and Morales et al. (38) found that with an increases in the roughness of the mould surface, there is an increase in freezing time. The faster rate of heat extraction by a smoother mould surface was demonstrated by a shift in the centre line of the casting, poured in a mould with opposite walls of different roughness. Assar (39) also found that the solidification time increases with roughness for zinc casting in steel mould.

2.3.1.5 Mould coatings

The effect of mould coatings on t_f was studied by a number of investigators (32, 33, 40) who found that insulating mould coatings increase the resistance to the heat flow and, consequently, increase the solidification time. The effects of different types of coatings on t_f was also investigated by Nehru (32) and he found that silica mould coats increase t_f and there is an optimum coat thickness at which the freezing time is maximum.

2.3.1.6 Casting material

For the unidirectional heat flow from a metal poured exactly at its melting point, T_f,

8

in a mould initially at a temperature MT, the transient heat flow equation is

$$\frac{\partial T}{\partial t} = \alpha_s \frac{\partial^2 T}{\partial x^2} \qquad [2.2]$$

The solution of the equation [2.2] is $S = 2 \gamma (\alpha t)^{0.5}$. It reveals that the higher is the thermal diffussivity ($\alpha = K/\rho C$), the lower is the solidification time. Metals having lower latent heat solidify ahead of those having higher latent heat (41).

2.3.1.7 Types of alloy

Pure metal solidifies ahead of its alloy. Nehru (32) found that copper solidifies before gunmetal. Long freezing alloys have higher solidification time than the short freezing alloys. Patterson et al. (42) found that the solidification time of copper-tin alloys increases with an increase in the solidification range of the alloy. Shrinvasan et al. (21) found that, in aluminium alloys, the value of t_f was higher for Al-4.5% Cu and Al-10%Mg for similar casting conditions compared to pure aluminium.

2.3.1.8 Pouring temperatures

The solidification time of casting increases with an increase in the pouring temperature (43). This can be attributed to the increase in the average mould temperature during heat extraction for higher pouring temperature, resulting in a lower heat extraction rate. With the increase of pouring temperature, the heat content of casting increases, consequently, the solidification time also increases (41).

2.3.1.9 Casting geometry

The solidification time is influenced by the casting geometry. For given casting thickness, casting material, mould preheat temperature, and mould wall thickness, Mohan (33) found that in the case of cast iron solidifying in a metal mould,

t_f(cylinder) < t_f (square) < t_f(plate)

9

Srinivasan et al. (44) found that in a given metallic mould, for a particular volume/surface area ratio, for Zn and Zn-5%Al alloy,

t_f(cylinder) < t_f (rectangle) < t_f (square) < t_f(plate)

2.3.1.10 Pressure

The solidification time decreases with the increase of applied pressure on the molten metal. It can be attributed to the increase in heat extraction caused by better contact between the casting and the mould (45,46). Davies (47) reported that freezing time decreases with the increase in pressure up to 0.2 bar but the increase in pressure above 0.2 bar does not cause further reduction in freezing time.

2.3.2 Relationship between solidification time and casting variables

Many investigators (1, 21, 32, 33) developed a number of relationships between solidification time and a number of casting variables. Some of them are discussed here:

According to Chvorinov (1),

$$t_F = k\left(\frac{V_c}{SA}\right)^2 \qquad\qquad [2.3]$$

where, t_f = solidification time, k = Chvorinov's constant, V_c = Volume of casting, and SA= cooling surface area.

This equation is valid for castings solidifying in insulating sand mould and zero degree superheat. Convincing demonstrations of its accuracy have been made many times. Chovrinov himself showed in his paper published in 1940 that it applied to steel casting form 12 to 65,000 kg in green sand moulds. It is one of the most useful guides untill to calculate the solidification time.

According to Flemings's (17) three dimensional equation, $\dfrac{\partial T}{\partial t} = \alpha_m \dfrac{\partial^2 T}{\partial r^2} + \dfrac{n \partial T}{\partial r}$, here. n=0 for plate shape, n=1 for cylindrical shape and n=2 for a spherical shape castings. The solution of the equation is

$$\frac{V}{SA} = \left(\frac{2}{\sqrt{\pi}} \sqrt{K_m \rho_m C_m} \sqrt{t_f} + \frac{nK_m t_f}{2r} \right) \left(\frac{T_m - MT}{\rho_c L} \right)$$ [2.4]

Nehru (32), Chinnathambi (34) and Ayyampernumal (48) found that a general relation between the casting modulus, volume ratio and freezing time is :

$$t_f = kM_c = k\left(\frac{V_c}{SA} \right)^{15} (VR)^{-0.5}$$ [2.5]

where, M_c = modulus of casting = $(V_c/SA)^{15}(VR)^{-0.5}$ and k is a constant.

Nehru (32) also developed a nomogram to obtain the freezing time for plate shaped copper and gunmetal castings whose volume. mould wall thickness, mould coat thickness are all known. Bishop et al.(49) working on steel casting in gray cast iron mould found that, with the increase of mould wall thickness, t_f decreases. This happens because, as the mould thickness decreases. the thermal heat capacity of the mould decreases and thus more time is required to solidify the casting.

An empirical relationship was obtained by Srinivasan et al. (21) between two dimensionless parameters as,

$$t_f = \frac{\left(\dfrac{V_c}{SA} \right)^3}{V_m} (k.SA.VR)$$ [2.6]

Here V_m = volume of mould, V_c = volume of casting, SA= surface area of casting, t_f = freezing time of casting, VR= volume ratio of casting and mould, and k is Chvorinov's constant.

Mohan and Senoy (31) found the following relationship

$$t_t = \alpha\left(\frac{V}{SA}\right)_L^2 + \beta\left[\frac{x_2 + x_3}{x_2^2}\right] * \left[1 + \frac{PT}{PT - MT} + \frac{PT - Ta}{MT}\right]\left(\frac{V}{SA}\right)_L \qquad [2.7]$$

Here, x_2 = mould thickness, x_3 = coating thickness, PT = pouring temperature, MT = initial mould temperature, Ta = ambient temperature. α and β are solidification constants, $(V/SA)_L$ = local cooling modulus.

2.4 MOULD-METAL INTERFACE

2.4.1 Interfacial condition during solidification

The existence of an interfacial barrier between casting and mould has long been recognised in the ingot casting of steel (50-53). The critical role of the interface has been highlighted in the development of continuous casting (54). Control of the continuous casting process has only been possible with a clear understanding of the changing condition in the moving casting-mould interface. Sully (16) and Pehlke (55) also recognised the existence of gap at the interface. They concluded that for accurate simulation of solidification of a casting freezing against a chill, formation of an air gap between the chill and the metal should be taken into account in numerical simulation.

Chills are used to remove latent heat rapidly for desired increase in properties. The effectiveness of chill is generally reduced by the formation of barrier to heat flow at the interface between the chill and casting (16).

Pehlke (55) emphasised in the review of interface that interfacial heat transfer rate must be known for an accurate simulation of the solidification of the castings.

For a properly designed casting, liquid metal can fill the entire mould cavity. Heat flow from the metal to the mould results in a skin of solidified metal which is initially in contact with mould. As solidification progresses, the thermal condition at the interface may change. Depending on the material properties of casting and mould and

12

the casting geometry the interface may reach any of the following states:

2.4.1.1 Conforming and non-conforming solid-solid contact

When the liquid metal first enters the mould the liquid metal conforms to the mould and macroscopically the contact is good (Fig. 2.1a). Microscopically, gap exists between the high spots. At the high spots, the high initial heat flux causes nucleation of the metal by local severe undercooling. The solid then spreads to cover most of the surface of the casting and contact changes to non-conforming state (Fig. 2.1b).

Prates and Biloni (37) proposed a mechanism for the initial contact based on work with aluminium alloys in permanent moulds to explain the relationship between mould micro-geometry and number of predendritic nuclei. The postulation is based on the fact that, on a microscopic scale, the surface of a mould or chill is not completely smooth and a small asperities protrudes from the surface profile. When liquid metal first approaches the mould surface, contact occurs at the peaks of the asperities. Rapid cooling at this peaks causes solidification of the liquid metal to nucleate from their sites. At the same time the surface tension of the liquid metal and subsequent rapid growth of solidification from the nucleation sites prevent solidifying metal from wetting the valleys on the surface profile of the mould. As a result, with the start of solidification a non-conforming contact is maintained at the interface.

2.4.1.2 Gap formation

An interfacial gap, separating the metal and mould, may gradually develop due to the movements of the mould and metal walls relative to each other during the later stage of solidification (Fig. 2.1c). After initial formation of the solidified skin, the metal-mould interfacial condition becomes dynamic in nature. As the surface of a mould or chill is not completely smooth and generally contain small or large ridges, when the cast metals first solidifies, its surface profiles conforms to these ridges. However, subsequent contraction of the metal skin upon cooling causes misalignment parallel to the interface. As a result, interfacial gaps develop between the ridges. The early investigators (21, 32, 33, 56, 57) of solidification in metallic moulds found that an air gap forms between a casting and its mould in the initial stage of solidification

and this gap continues to increase with time. Their efforts were directed towards finding the time, location and other factors relevant to this gap formation (20, 32, 33, 57). The variation in the size of the air gap during the solidification of the casting was monitored by some investigators (56, 58). Matuschka (58) investigated systematically the formation of air gap and concluded that the formation of an air gap between a casting and its mould is a result of the expansion of the mould due to absorption of heat and the contraction of the casting due to solidification and subsequent cooling.

2.4.2 Important factors for interfacial conditions

The interfacial condition, whether it is solid-solid contact or interfacial gap, may be affected by the following mechanism:

2.4.2.1 Surface interaction of metal and mould

Davies (47) proposed a mechanism in which surface interaction in a die casting is caused by the presence of relatively large ridges on the surface of the mould. When the cast metal first solidifies, its surface profiles of the casting conforms to those of mould ridges. However, subsequent contraction of the metal skin upon cooling causes misalignment parallel to the interface. As a result, interfacial gaps develop between the ridges of the mould and the surface of the casting.

2.4.2.2 Transformation of casting and mould materials

Volumetric changes accompanying phase transformation of the casting material and the mould material may also affect the gap formation at the interface. Engler et al. (59) found that in the case of gray cast iron of near eutectic composition, volumetric expansion associated with graphite segregation in the solidified shell has forced the metal to come in contact with the mould, showing no measurable gap up to the end of solidification.

2.4.2.3 Casting geometry

Several cast examples in the literature showed the effect of geometry on gap formation (60, 61). When the mould surface is concave towards the casting, contraction of the

solidified metal upon cooling and outward movement of mould upon heating result in an interfacial gap. In this case, thermal expansion within the mould causes the mould surface to detach from the metal (Fig.2.1c).

Inward movement may happen when the mould surface is convex towards the casting which favours solid-solid contact (60). Cylindrical moulds expand away from the casting. whereas for flat casting the mould expands towards the casting, maintaining contact under pressure during the early stage of cooling (61) (Fig. 2.2) .

2.4.2.4 Contact pressure

The effect of gravity could favour solid contact on one part of casting but gap in another part (50). Nishida and Matsubara (62) have studied the effect of applied pressure on the heat transfer. They found that heat transfer coefficient under loading is always higher than that of no-load condition. They also found that the heat transfer coefficient decreases sharply from the maximum value under loading. The abrupt change was explained by Ho and Pehlke (10) by the hypothesis that the shell of the solidified metal. in going from a plastic to an elastic state, has gained sufficient strength to overcome the applied pressure and begin to recede away from the mould. In general, raising the interfacial contact pressure will lead to an overall increase in the heat transfer coefficient. Two mechanisms are responsible for this behaviour. For non-conforming contact at low interfacial contact pressure, there are relatively few solid contacts. Consequently, heat will be transferred mostly by means of gas conduction across the interfacial voids. Raising the contact pressure will cause a reduction in void spacing and a resultant increase in HTC_g according to equation [2.10.1]. At the same time, number of solid contact spots will be increased. On the other hand, at sufficiently high contact pressure, the degree of solid contact approaches the theoretical limit given by equation [2.9]. Under this condition the relative contributions of HTC_s as well as overall heat transfer coefficient itself is much higher. Further increase in contact pressure will not cause any appreciable decrease in void spacing, but the softer material around each contact spot will deform plastically. As a result, the area of sold contact will increase, causing a corresponding increase in solid conductance, HTC_s (63).

15

2.4.3 Heat flow under various conditions

2.4.3.1 Metal and mould in solid-solid contact (conforming and non-conforming)

In a solid-solid contact, the casting is in contact with asperities in some places, whereas, at the other places it makes contacts through gas with the mould (Fig.2.1a-b). The number of contact points decreases when contact changes from conforming to non-conforming. According to Ho and Pehlke (10) the total heat transfer, HF, will be the sum of the three components, namely HF_s, heat flow through cast-metal solid contact, HF_c, heat flow by gas conduction and HF_r, heat flow by radiation.

$$HF = HF_s + HF_c + HF_r \qquad\qquad [2.8.1]$$

The total heat flow can also be represented by the product of overall heat transfer coefficient and temperature difference between casting and mould surface, as follows

$$HF = HTC * (Tc - Tm) \qquad\qquad [2.8.2]$$

Here, $HTC = HTC_s + HTC_c + HTC_r$, overall heat transfer coefficient $\qquad [2.8.3]$

HTC_s = heat transfer coefficient due to metal-mould contact,

HTC_c = heat transfer coefficient due to gas conduction,

HTC_r = heat transfer coefficient due to radiation.

As the conforming contact changes to non-conforming contact the contribution of HF_s on HF decreases.

According to Rapier et al. (63),

$$HTC_s \propto \frac{K_{hm}}{C} \sqrt{\frac{P}{HN}}, \text{ where} \qquad\qquad [2.9]$$

P is the interfacial contact pressure, HN the hardness of the softer solid in the contacting interface, K_{hm} the harmonic mean of thermal conductivities of the contacting surfaces, and C the wave length of surface roughness for the rougher surface. The proportionality constant is a geometry-dependent factor.

$$HTC_c = \frac{K_g}{x_g} \text{ (when the gap is relatively large with respect to mean free path of the gas)} \quad [2.10.1]$$

$$HTC_c = \frac{K_g}{x_g + g_1 + g_2} \text{ (when the gap is sufficiently small gap with respect to mean free path of the gas)} \quad [2.10.2]$$

Where, K_g is thermal conductivity of the gas, x_g void spacing, g_1, g_2 are temperature jump distances for both the contacting surface.

$$HTC_r = \sigma \frac{\left(Tc^4 - Tm^4\right)}{(Tc - Tm)\left(\dfrac{1}{\varepsilon_1} + \dfrac{1}{\varepsilon_2} - 1\right)} \quad [2.11]$$

Here, σ is the Stefan-Boltzman constant, Tc and Tm are the surface temperatures and ε_1 and ε_2 are the emissivity for casting and mould, respectively.

2.4.3.2 The heat flow at metal-mould interface in the presence of a gap :

When gap forms (Fig. 2.1c) the heat is transferred partly by gas conduction and partly by radiation due to the temperature difference. The total heat flow,

$$HF = HF_c + HF_r \quad [2.12]$$

$$HF = HTC * (Tc - Tm) \quad [2.13.1]$$

$$HTC = HTC_c + HTC_r \quad [2.13.2]$$

With the formation of interfacial gap, HTC_c decreases as x_g increases and the heat transfer by radiation is more prominent.

The significance of heat transfer by radiation at high temperature was demonstrated by Jaccobi (64). His experiments were involved with the solidification of pure iron in a water-cooled copper mould with controlled atmosphere of various gases as well as in vacuum. It was found that the heat transfer coefficient measured under vacuum condition is a significant fraction of that measured under various gases at atmospheric pressure.

2.4.4 Representation of the interfacial condition for the analysis of heat flow.

The interface between a casting and a metal mould or chill is a controlling factor in the heat flow (16). A coefficient of heat transfer is used to describe the degree of the interfacial thermal resistance. Traditionally, a constant value of the heat transfer coefficient between casting and mould has been used for such situation as in ingot mould casting or chills in sand moulding. Studies on continuous casting processes reported in the literature have revealed the dynamic nature of the interface. Various types of representation of interface heat transfer found in literature were either assumed or experimentally found. They are summarised as follows :

2.4.4.1 Infinite HTC

In the early stage of numerical analysis of phase change problem, several numerical analyses assumed perfect contact at the cast-mould interface (65-67). They assumed zero resistance due to lack of any viable physical model of gap formation and heat transfer characteristics across narrow gaps at metallurgical temperature. Jeyarajan and Pehlke (68) considered perfect contact between casting and mould in their simulation of Al and Si brass in sand moulds. The assumption of considering interface as perfect is not justified. Perfect contact can be achieved when the molten metal is welded with the mould. It is justified only to neglect the resistance at the interface between core and casting (69) when the casting solidifies around a central core. Marrone's simulation disagreed to some extent with the measured thermal profiles which was adjusted by adjusting the thermal properties of sand. But the disagreement may lead from the limitation of assuming perfect contact which was felt by them (67).

2.4.4.2 Constant HTC

Durham and Berry (13) introduced an air gap conductance, HTC, constant for each run which can be varied for different run to simulate the pure lead and Al-5% Cu alloy. They assumed the value of 4178.86 W/m^{2}C for HTC to match the estimated curves with the experimental curves of pure lead with brass chill for low superheat. The value is in between 4178.86 and 8357.72 W/m^{2}C for high superheat. The simulated solidified thickness-time curves mismatch in some places may be due to the assumption of constant HTC.

Hou and Pehlke (69) assumed constant HTC (1983 W/m^2C) in the simulation of medium carbon steel in sand mould. Experimental thermal profiles showed that solidification time increases with the decrease of mould thickness. But, the simulated results depicted that the solidification was delayed with increased mould thickness. They reasoned it as they assumed higher mould wall heat transfer coefficient for lower mould thickness.

2.4.4.3 Time averaged HTC

Prates and Biloni (37) estimated heat transfer coefficient using fluidity test of different Al-Cu (0-5%Cu) alloys for different mould material (copper, mild-steel, and 18/8 stainless steel) and found the highest HTC (~5000W/m^2C) for copper mould and the lowest (~3000W/m^2 C) for stainless steel mould. HTC increases with the increase of copper content significantly for without coating condition. The investigators recognised that the HTC might be varied as the contact between the liquid and the mould varied from point to point. However, they used this value as reference in order to find the effect of different substrate and micro-geometry of the mould surface.

2.4.4.4 Step function HTC

Hou and Pehlke (70) assumed different heat transfer coefficient in the form of step function for different mould wall thicknesses to simulate medium carbon steel in gray cast iron mould. The initial constant value of HTC is higher for thicker mould. Experimental and simulated thermal profiles showed that solidification time increases with the decrease of mould thickness. But the heat transfer coefficient at the external surface is reverse to the previous one (69). They assumed lower heat transfer coefficient at the external surface for lower mould thickness (70).

2.4.4.5 Linearly varying HTC

Sun (71) used an empirical relation in the form of a + bt (a, b are empirical constants and t is time) in a finite difference analysis to fit the experimentally measured temperature profile of metal rod dipped into a molten metal bath. The surface conductance value increases with metal-mould contact time was believed due to an increase of contact pressure at the interface resulting from mould expansion (convex

shape) and contraction of solidified metal (concave shape) for uncoated mould. The investigator found same HTC for uncoated copper rod and cast iron in molten aluminium and Hastaloy X and HTC does not depend significantly on casting surface temperature. The fluidity/welability of the casting materials (aluminium and Hastolloy X) may be similar to yield same HTC value. The matching technique may have some error in finding HTC.

2.4.4.6 Non-linearly varying HTC

Ho and Pehlke (10) found HTC to decrease from a higher value (1800 W/m^2C) to a lower value (1300 W/m^2C) at about 25 sec and then it was increased to a maximum value (2000 W/m^2C) at 80 sec, after which it was found to decrease continuously for Al casting water cooled copper chill on the top. The fluctuation at 60 sec was happened due to assuming a uniform initial temperature in the casting for the estimation of HTC.

Jacobi (64) carried out experiments with pure iron with a water cooled mould wall. The HTC varied both in magnitude and shape with time for different interfacial gas environments. For vacuum, N_2, and CO, the HTC found to decrease continuously as time elapsed. But for H_2 and H_2S, there were double peak value for HTC and after the second peak it was found to decrease.

Tillman and Berry (14) worked on Al-4.5% Cn in graphite mould with water cooled copper chill at bottom and found HTC to increase with time. They could not found reliable HTC value just after filling. It may be due to slower rate of data acquisition.

Ho and Pehlke (12) used two types of casting-mould configurations for pure aluminium and Cu-5%Al castings. First type favoured the gap formation where water cooled copper chill is on the top of the casting, whereas, the second type of chill does not favour the gap formation. For both the casting configurations, HTC was found to decrease from a peak value and then it was decreased continuously or remained constant. There was a sudden drop in HTC for the first type of casting where gap

20

formation started to set. But for the second type casting the HTC remained constant after the initial period as gap formation did not occur.

2.4.4.7 HTC as a function of interface temperature

Sully (16) found HTC to depend only on casting surface temperature for tin and lead casting. But for aluminium, it was observed to be a function of both the casting and mould surface temperature. The probable cause of the early rise in HTC was the oxide formation on aluminium casting. But oxide formation changes the contact from conforming to non-conforming.

Jeyarajan and Pehlke (53) found HTC as to be step function of casting surface temperature. They concluded that heat transfer across the interface can be accurately described in terms of an interfacial heat transfer coefficient which is a function of metal-side interface temperature. They used a constant ($H1=17000$ W/m^2C) value for liquid casting surface and $H2= 2550$ W/m^2C for solid surface.

2.4.4.8 Non-linear time varying HF

Jacobi (64) carried out experiments using pure iron with water cooled copper mould wall and found HF to increase to peak value and then decrease as a function of time, $HF = at^b$, where a and b are constants.

Kumar and Prabhu (37) estimated a time varying heat flux working on aluminium alloys for various type of coating and chills. They observed that the peak value of HF-time curves was obtained shortly after pouring. They explained the occurrence of the peak - as the casting started solidifying, the contact became less and less perfect, resulting in a reduction of the heat flux across the interface and the peak could be associated with the start of solidification. They also found that the occurrence of the peak value was around 20 sec for most of the experiments. The pouring temperature and mould temperature were taken 750 C and 150 C, respectively. The start of solidification should differ as the heat flux from the interface differ and the of the peak value of HF might related to some other variables.

Kumar and Prabhu (37) developed an empirical relationship,

$$\frac{HF}{HF_{max}} * \alpha^{0.5} = Ct^{D}$$
[2.14.1]

where, $HF_{max} = A\left(\frac{d}{\alpha}\right)^{B}$; A, B, C and D are constants which varied with the casting-mould systems. HF increases with time to a maximum value and then decreases. B has a negative value and the equation depicts that HFmax increases as the chill thickness decreases. The chilling power denoted by heat diffusivity (ρCV) is not fully utilised when the chill is saturated. With the decreases of chill thickness, the chill is saturated earlier and the peak may be affected.

Alalem et al. (72) carried out experiment with aluminium in steel for 2-D heat flow. The interface was divided into 4 regions, and the heat flow in the 4 regions is considered to be uniform having values HF1, HF2, HF3, and HF4. They used 4 temperatures to estimate 4 heat flux without taking boundary condition. HF1 is at the centre and HF4 is at the corner of the casting. The HF2 and HF3 are in between them. They found heat decreases from a maximum value continuously. The HF1 > HF1 and HF4 > HF3. Without boundary the results might have some error.

2.4.5 Effect of different variables on HTC
Sully (16) studied the effect of casting size, casting materials, mould materials and geometry on the heat transfer coefficient at the casting-mould interface. The effect of geometry has been an overriding factor in determining the HTC. HTC decreases from a maximum to a steady value if the casting contracts away from the mould. A high value of HTC is maintained if the geometry causes the casting to remain in an intimate contact with the mould. Casting size governs the time frame of the transient interface properties. The use of a steady value for HTC is only valid where the time to reach steady value is small compared to the total freezing time of casting. The HTC was found to be strongly related to the casting surface temperature but independent of mould surface temperature.

22

2.4.5.1 Casting material

Sully (16) experimentally showed the effect of casting material on heat transfer coefficient. He worked on Al, Sn, Pb, Gray CI and Steel in CI and Steel moulds and found HTC to increase from smaller to a maximum value and then to decrease sharply to a constant value. The peak value of HTC varied with the variation of cast-mould combination. HTCmax was attained at about the end of pouring. For example, the maximum value of HTC for Pb in CI is about 2270.8 W/m^2 C, but for Sn in CI it was about 1845.025 W/m^2 C.

2.4.5.2 Mould material

Sully's (16) experiments revealed strong effect of mould material on HTC. For the same casting material, the HTC-time curves differed both in shape and magnitude for different mould materials. Sn-steel yielded the highest value of HTC and Sn-Brass gave the lowest value of HTC. Sn-CI was found in between the above two values.

2.4.5.3 Wash or Coating

Sully (16) also found a distinct effect of wash used on chill for steel casting. For example, in the early stage of solidification, HTC is higher for graphite wash than for zircon wash, used for graphite chill. As a result, zircon wash reduced the effectiveness of chill.

2.4.5.4 Mould-metal surface reaction

Interfacial reaction markedly change the interfacial heat transfer coefficient. Sully (16) concluded that the oxide formation of Al casting caused a lower value of HTC.

2.4.5.5 Casting size

Sully(16) pointed out that casting size affects the value of HTC. Thin castings solidify in a short time during which the value of HTC is high. Thick castings do not solidify completely until HTC reaches a low steady state value which implies a low overall value of HTC. Similar results were observed by Sharma et al. (73). The delay in gap formation due to plastic deformation in thick castings can lead to a high

initial value of HTC which persists for a long duration (74). Thamban and Panchnathan (26) on the other hand stated that, for a given volume ratio, HTC remains nearly the same for different casting thickness for long freezing alloys. They also found that HTC varied with variation of volume ratio. Issac et al. (15) found that, for aluminium casting in cast iron mould without coating, the initial value (maximum) of HTC was the highest (3558.95 W/m^2 C) for volume ratio 1, and the lowest (2512.2W/m^2C) for volume ratio 2. But for volume ratio of 3 it was in between the volume ratios 1 and 2. The rate of decreasing HTC was the highest for the lowest volume ratio of 1 and lowest for volume ratio of 2. Again, for volume ratio of 3, the rate was in between volume ratios of 1 and 2. They reasoned that the highest rate of decreasing HTC for the lowest volume ratio is due to higher gap size for lower volume ratio.

2.4.6 Effect of different variables on HF

Heat flux is the product of heat transfer coefficient and difference of temperature of the mould and casting surface. So, heat flux is expected to vary with the variation of the heat transfer coefficient.

Das and Paul (75) acknowledged the effects of (1) imperfect contact at the interface resulting in discontinuity of temperature , (2) releasing agent, often sprayed on the die walls to ensure proper release of the solidified casting from the die, and (3) formation of air gap between the interface to cause resistance, on the heat flux.

2.4.7 Effect of HTC on solidification pattern

Durham and Berry (13) in their experiments with various material (metal and alloy) in various type of mould found distinct effect of HTC on solidification pattern. In their theoretical work, using constant HTC, it was found that the rate of solidification, R, increases with increase of heat transfer coefficient, HTC. During early stage of solidification, R decreases with the decrease of HTC. As the time elapsed the effect of HTC on R diminishes.

24

Ho and Pehlke (12) carried out purely theoretical investigation on the effect of HTC on solidification time for Al casting in various types of mould (steel, cooper. dry sand mould) and found that the solidification time decreases with the increase of HTC, hyparabolically.

2.5 INVERSE HEAT CONDUCTION PROBLEM (IHCP)

2.5.1 The direct and the inverse problem

The direct problem of the heat flow refers to the situation in which the boundary conditions in the form of temperatures or heat fluxes are known and the temperature distribution inside the body is to be obtained from the known initial and boundary conditions. Analytical and numerical methods are available for solving the partial differential equation of the direct problem satisfactorily. However, the direct problem has drawbacks because of the difficulties in determining the actual boundary conditions. For example, it may not be possible to attach a sensor and measure the surface temperature accurately due to physical limitation imposed by the configuration.

The inverse conduction problem (IHCP), on the other hand, is related to the estimation of the surface heat flux history or surface temperature history of a body given one or more measured temperature history in side the conducting body (76). The word estimation is used here because in measuring the internal temperatures, errors are always present to some extent. Besides, the IHCP is an ill-posed problem and hence the heat flux can not be calculated accurately. A comparison of the direct and inverse heat conduction problems is shown in the Fig.2.3.

2.5.2 Inverse heat conduction -an ill-posed problem

The solution of a well posed problem should satisfy the condition of existence, uniqueness, and stability. The solution of the inverse heat conduction problem does not satisfy these conditions (76) and hence it is an ill-posed problem. The IHCP is difficult to solve analytically because the temperature response at an interior location in a body due to given stimulus at the surface is both delayed and

diminished in amplitude. Measurements of temperatures at discrete time intervals provides incomplete information for obtaining an accurate solution.

For the one dimensional IHCP, when discrete values of HF are estimated at various points of time i, maximising the amount of information implies small time steps between HF_i values. However, the use of small time steps frequently introduces instabilities in the solution of the IHCP (77).

The direct problem suffers from inaccuracies in the measurement of boundary temperature or heat fluxes while the IHCP poses a difficult analytical problem. According to Beck (76) an accurate and tractable solution to the inverse problem would minimise both the disadvantages, simultaneously.

2.5.3 Estimation of HF and HTC

Both HF and HTC can be found by analysing the experimental data of temperature. Among methods described in the literature the main four methods are: (1) purely analytical methods, (2) semi-analytical and empirical methods, (3) quasi-steady-state approximation -gap measuring technique, and (4) numerical technique.

In purely analytical techniques, a constant heat transfer coefficient is assumed to obtain the solution of the Fourier heat conduction equation (78-80).

In contrast, the semi-analytical or empirical techniques do not attempt to solve rigorously the Fourier heat conduction equation, but involve analysing the experimental data by means of semi-analytical formulae (37, 81) or by curve fitting techniques (14).

Quasi-steady state approximation-gap measuring process is only suitable when a clear gap develops at the interface. Two linear traducers continuously record the movements of the metal and mould. Using the difference in displacement as an indication of the average gap size, the transient interfacial heat transfer coefficient may be derived from the thermal conduction and radiation across a static gap

(assuming the validity of the quasi steady state approximation (77)). In addition to this, the exact time of onset of gap formation is detected by monitoring the electrical continuity across the metal-mould interface. As soon as a clearance gap develops, the break in electrical continuity is revealed as a sudden increase in the recorded voltage.

In spite of the advantage of relative simplicity, the approaches of the data analysing become unsuitable when dynamic changes occur at the metal-mould interface. Such changes can occur, for example, when the interface changes from a state of initial contact to a clear gap, accompanied by a drop of heat transfer coefficient and also of heat flux.

The **numerical techniques** are generally used as the method of solving the inverse conduction problem. Difficulties arise in the solution of the inverse conduction problem as a consequence of the delayed and diminished thermal response in the interior of the body. Errors associated with the use of truncated temperature data at an exterior point are numerically amplified during the determination of the time varying thermal conditions at the surface (12). Moreover, since the solidification of a casting involves a change of phase and temperature variable thermal properties, the inverse problem is non-linear.

The numerical techniques is based on the statistical estimation procedure. Statistical estimation procedures solve the IHCP by maximising (or minimising) an objective function F(HF) is given as (82), given as,

$$F(HF) = \sum_{j=1}^{n_s} w_j \sum_{i=1}^{n_f} \left(T_{i,j} - Y_{i,j}\right)^2 + w_0 \sum_{k=1}^{n_r} \beta_k^2 + w_1 \sum_{k=1}^{n_r-1} \left(\beta_{k+1}^2 - \beta_k\right)^2 \qquad [2.15]$$

where,

F(HF) = objective function,

n_s = number of sensors,

w_j = weighing constant for the temperature measurements from the jth sensor,

n_f = number of future measurements,

27

✓

Y = measured temperature,

T = calculated temperature,

w_0 = the zeroth order regularisation constant,

n_p = number of parameters,

β = parameter (W/m^2). and

w_1 = the first order regularisation constant.

By putting w_j = 1 and w_0. w_1 = 0, a simplified form of the objective function is obtained which is the least square estimator based on the minimisation of

$$F(HF) = \sum_{i=1}^{i=mr}\left(T_{\eta-i} - Y_{\eta+i}\right)^2 \qquad [2.16]$$

where,

F(HF) = object function,

I = mr (m is small integer),

r-1 = number of future temperatures,

$T_{\eta+1}$ = estimated temperature obtained with assumed HF,

$Y_{\eta+1}$ = experimentally measured temperature.

2.5.4 Beck's Non-linear estimation procedure (77) for HF

Beck's non-linear estimation technique utilises the numerical approach for estimating surface heat flux from a knowledge of measured temperature inside a heat conducting solid body. The configuration in Fig. 2.4 can be used to describe Beck's method. It is necessary to estimate HF at the surface S with known temperature Y3 (T3) at point C and Y4 (T4) at point D. The analysis in the region C to D is a direct problem but, in the region S to C, the problem is an inverse one. Beck's solution procedure consists in minimising the function F(HF), defined by the equation [2.16]. The heat flux HF and the surface temperature Tm at S have to be determined from the measured temperature T3 at C as in Fig. 2.4.

2.5.5.1 Mathematical development for the solutions of inverse problem (Beck's method)

The following steps are followed in obtaining the solution:

(1). Discretisation values of temperature at time interval, Δt are known i.e.

$$T(X1,t)=Y3(t)=T3(t)$$

$$T(X2,t)= Y4(t)=T4(t)$$

The heat flux across the interface is constant during any time interval, $\Delta\theta$, where, $\Delta\theta$ is an integral multiple of Δt, that is

$$\Delta\theta = m\Delta t$$

where m is a small integer. If 0_M and t_η refer to the same point of time, then the subscripts M and η are related by the relation:

$$mM = \eta$$

The relation between M, η and the discretisation of HF are shown in Fig. 2.5 (where m=2).

(2). To take into account the delayed temperature response of an interior location, 'future temperatures' are used in estimating HF. Thus, if r intervals of $\Delta\theta$ are used in estimating HF, it is assumed that the same heat flux HF flows during these (r-1) future intervals, that is,

$$HF_{M+2} = HF_{M+3}\ldots\ldots\ldots\ldots= HF_{M+r}= HF_{M+1}$$

where, HF_{M+1} is to be estimated.

The non-linear estimation procedure determines the value of HF which minimises $F(HF)$ given in equation [2.16], form,

$$\sum_{i=1}^{I=mr}\left(T_{\eta+i}-Y_{\eta-i}\right)\frac{\partial T_{\eta+i}}{\partial HF} = 0 \tag{2.17}$$

Here, $\dfrac{\partial T_{\eta+1}}{\partial HF}$ is the sensitivity coefficient $\phi_{\eta+1}$. The above equation can be solved by a Taylor series expansion. For the lth iteration, the Taylor series approximation is

$$T_{\eta+i}^{l} \approx T_{\eta+i}^{l-1} + \frac{\partial T_{\eta+i}^{l-1}}{\partial HF_{M+1}^{l-1}}\left(HF_{M+1}^{l} - HF_{M+1}^{l-1}\right) \tag{2.18}$$

29

$$\phi_i^{l-1} \equiv \frac{\partial T_{\eta+i}^{l-1}}{\partial HF_{M+1}^l} \approx \frac{T_{\eta+i}(HF_{M+1}^{l-1}(1+\varepsilon)) - T_{\eta+1}(HF_{M+1}^{l-1})}{\varepsilon HF_{M+1}^{l-1}} \qquad [2.19]$$

Now from equations [2.17] and [2.19] the correction can be obtained as,

$$\nabla HF_{M+1}^l = \frac{\sum_{i=1}^{i=mr}(Y_{\eta+i} - T_{\eta+i})\phi_i^{l-1}}{\sum_{i=1}^{l}(\phi_i^{l-1})^2} \qquad [2\ 20]$$

So, the new value of HF is

$$HF_{M+1}^l = HF_{M+1}^{l-1} + \nabla HF_{M+1}^l \qquad [2\ 21]$$

For m = 2 and r = 2; l = 4 (as in Fig 2 5)

$$\phi_1^{l-1} \equiv \frac{T_{\eta+1}(HF_{M+1}^{l-1}(1+\varepsilon)) - T_{\eta+1}(HF_{M-1}^{l-1})}{\varepsilon HF_{M+1}^{l-1}} \qquad [2.22.1]$$

$$\phi_2^{l-1} \equiv \frac{T_{\eta+2}(HF_{M+1}^{l-1}(1+\varepsilon)) - T_{\eta+2}(HF_{M+1}^{l-1})}{\varepsilon HF_{M+1}^{l-1}} \qquad [2.22.2]$$

$$\phi_3^{l-1} \equiv \frac{T_{\eta+3}(HF_{M+1}^{l-1}(1+\varepsilon)) - T_{\eta+3}(HF_{M+1}^{l-1})}{\varepsilon HF_{M+1}^{l-1}} \qquad [2.22.3]$$

$$\phi_4^{l-1} \equiv \frac{T_{\eta+4}(HF_{M+1}^{l-1}(1+\varepsilon)) - T_{\eta+4}(HF_{M+1}^{l-1})}{\varepsilon HF_{M+1}^{l-1}} \qquad [2.22.4]$$

$$\nabla HF_{M+1}^l = \frac{\left(Y_{\eta+1} - T_{\eta+1}^{l-1}\right)\phi_1^{l-1} + \left(Y_{\eta+2} - T_{\eta+2}^{l-1}\right)\phi_2^{l-1} + \left(Y_{\eta+3} - T_{\eta+3}^{l-1}\right)\phi_3^{l-1} + \left(Y_{\eta+4} - T_{\eta+4}^{l-1}\right)\phi_4^{l-1}}{(\phi_1^{l-1})^2 + (\phi_2^{l-1})^2 + (\phi_3^{l-1})^2 + (\phi_4^{l-1})^2}$$

$$[2.23.1]$$

For convenient representation, if l and l-1 are replaced by new and old respectively. then

$$\nabla HF_{M+1}^{new} = \frac{\left(Y_{\eta+1} - T_{\eta+1}^{old}\right)\phi_1^{old} + \left(Y_{\eta+2} - T_{\eta+2}^{old}\right)\phi_2^{old} + \left(Y_{\eta+3} - T_{\eta+3}^{old}\right)\phi_3^{old} + \left(Y_{\eta+4} - T_{\eta+4}^{old}\right)\phi_4^{old}}{(\phi_1^{old})^2 + (\phi_2^{old})^2 + (\phi_3^{old})^2 + (\phi_4^{old})^2}$$

$$[2.23\ 2]$$

$$HF^{new} = HF^{old} + \nabla HF^{new} \qquad [2.24]$$

The procedure is repeated with HF^{new} in place of HF^{old} until : $\quad \dfrac{\nabla HF^{new}}{HF} < 0.005$

CHAPTER 3

A SEMI-INFINITE MOULD MODEL TO CALCULATE THE SOLIDIFICATION TIME AND THE EFFECT OF CASTING VARIABLES ON IT

3.1   INTRODUCTION

Literature survey indicates that solidification time plays an important role in obtaining sound casting. It yields good casting design and provides better conception about the casting structure. The survey of literature also depicts that the solidification process and solidification time are markedly affected by a number of variables such as casting thickness, interfacial heat transfer coefficient, superheat of the molten metal and mould temperature.

In this chapter an one dimensional numerical model has been developed to observe the effect of casting variables on the solidification process.

3.2   ONE DIMENSIONAL HEAT TRANSFER MODEL

As casting solidifies, heat transfer occurs in three ways: conduction, convection and radiation. These are defined by Fourier, Newton, and Stefan-Bolzman, respectively. Heat transfer through solidification, caused by phase change, differs from other heat transportation mode because it involves release of latent heat either at constant temperature (for pure or congruent materials) or at a range of temperature (for short or long freezing alloys). Beside these, solidification of casting is essentially a transient problem and, therefore, partial differential equations relating time, temperature and location must be solved. When the system undergoes no phase transformation, the governing equation for transient heat conduction can be expressed in vector notation as

$$\rho\left(\frac{\partial H}{\partial t}\right) = \nabla.(K\nabla T) \qquad\qquad [3.1]$$

where, mass density, ρ, is assumed to be independent of temperature and K is the thermal conductivity. When a solid phase is nucleated from liquid while cooling down, the associated latent heat acts as a heat source and the quantity of it evolved per unit time, L, is dependent on the fraction of solid that is formed. The heat flow equation is represented by

$$\rho\left(\frac{\partial H}{\partial t}\right) = \nabla.(K\nabla T) + L$$ [3.2]

In Cartesian co-ordinates, the expanded form of equation [3.2] in the three dimensions is given by

$$\rho\left(\frac{\partial H}{\partial t}\right) = K\left(\frac{\partial^2 T}{\partial x^2} + \frac{\partial^2 T}{\partial y^2} + \frac{\partial^2 T}{\partial z^2}\right) + \frac{\partial K}{\partial x}.\frac{\partial T}{\partial x} + \frac{\partial K}{\partial y}.\frac{\partial T}{\partial y} + \frac{\partial K}{\partial z}.\frac{\partial T}{\partial z} + L$$ [3.2.1]

For a casting having very large length and width compared to thickness, the end effect will not be observed in the central region of the plate. Heat transfer in this region of the casting may be considered as one-dimensional perpendicular to the plate surface) and the above equation can be simplified as

$$\rho\left(\frac{\partial H}{\partial t}\right) = K\left(\frac{\partial^2 T}{\partial x^2}\right) + \frac{\partial K}{\partial x}.\frac{\partial T}{\partial x} + L$$ [3.2.2]

$$\rho\left(\frac{\partial H}{\partial t}\right) = K\left(\frac{\partial^2 T}{\partial x^2}\right) + \frac{\partial K}{\partial T}*\left(\frac{\partial T}{\partial x}\right)^2 + L$$ [3.2.3

3.2.1 Boundary conditions

There are three characterised boundary conditions in this study.

3.2.1.1 Casting-mould interface

There is a discontinuity of heat flux across the mould-casting interface which can be treated as a contact resistance, leading to the interfacial condition,

$$-K\left(\frac{\partial T}{\partial x}\right) = HTC*\Delta T$$ [3.3]

The heat flux across the mould-casting interface is considered to be equal to the product of a heat transfer coefficient, HTC, at the interface and the temperature drop, ΔT, across the interface.

3.2.1.2 Centre of the casting

The mid-surface of a plate casting will behave like an insulating surface across which there will be no heat flux. Thus, from Fourier law,

$$\frac{\partial T}{\partial x} = 0 \tag{3.4}$$

3.2.13 Outside surface of the mould

The outside wall of the mould is considered to transfer heat by convection and radiation, satisfying,

$$-K\left(\frac{\partial T}{\partial x}\right) = HTC_e (Tw - Ta) \tag{3.5}$$

Here, Ta is the ambient temperature, Tw the mould temperature, K the thermal conductivity and HTC_e the total heat transfer coefficient at the surface of mould due to convection and radiation.

The explicit FDA representation of enthalpy method for rectangular and cylindrical casting is given in APPENDIX-A. The thermophysical properties of casting and mould materials are given in APPENDIX-B.

The enthalpy-temperature relations are as follows:

$H = C_s T$	for $T < T_f$	(solid)
$H = L + C_s T_f$	for $T = T_f$	(phase change)
$H = L + C_s T_f + C_l(T - T_f)$	for $T > T_f$	(liquid)

3.2.2 Computation

The following sequence are performed for the numerical study.

- choosing of casting material
- choosing of mould material
- input pouring temperature, mould temperature, ambient temperature
- input casting thickness, mould thickness
- nodal representation
- initialisation of enthalpy and temperatures of the nodes in casing and mould

33

- calculation of new enthalpy after each time step from finite difference equations

- transformation of enthalpy to temperature

-assigning newer temperature to each node

- continuing the procedure until the centre temperature is sufficiently lesser than the melting point of the casting metal

Fig. 3.1 shows the flow chart for the temperature distribution in casting and mould.

3.3 RESULTS AND DISCUSSION

3.3.1 Effect of casting variables on solidification time

3.3.1.1 Effect of mould thickness

Fig. 3.1a shows the effect of mould thickness on solidification time for a 0.014m thick plate shaped aluminium casting at various interfacial heat transfer coefficients (1000, 2000 and 4000) W/m^2 C. for 0 C superheat in the cast iron mould initially at an ambient temperature of 25 C. It reveals that the solidification time decreases with the increase of mould thickness to a minimum value and then remains constant for higher mould thickness. By observing the thermal profiles in the casting and the mould regions for various mould thickness it is found that a certain value of mould thickness (0.03m for 1000 W/m^2C, 0.02m for 2000 W/m^2 C and 0.01m for 4000 W/m^2C) is reached for which the casting either solidifies completely before the heat reaches the external surface of the mould or even when the heat reaches the external surface of the mould but the effect of surroundings does not affect the heat flow at the casting-mould interface. The thermal profiles in the casting up to the time of completion of solidification are the same for any mould thickness above this value. Therefore, the solidification time remains constant. In case of lower mould thickness heat reaches the mould surface before the completion of solidification. Heat flow is then controlled by the heat removal from the external surface of the mould. The influence of this surface effect on solidification time is more for lower mould thickness because the heat reaches the surface earlier and the volumetric heat capacity of the mould is lower. This is why the solidification time is higher for lower mould thickness. Fig. 3.1a also shows the solidification time is higher for lower interfacial heat transfer coefficient. It

34

can be explained in the following way: the lower is the interfacial heat transfer coefficient the greater is the resistance to the heat flow path which takes longer time to release the heat from the casting. As a result longer solidification time was found for lower heat transfer coefficient.

Similarly, the effect of mould thickness on the solidification time is found for the Al-Sand, Cu-CI and Zn-CI casting- mould combinations are shown in Figs. 3.1b, 3.1c and 3.1d, respectively, for a plate shaped 0.014m thick casting at various interfacial thermal resistance (100, 2000 and 4000) W/m^2 C, for 0 C superheat and 25 C initial mould temperature.

It has been observed (83) that, in general, the semi -infinite mould thickness is increased with the increase of casting thickness, superheat of the molten metal, and mould temperature.

To find semi-infinite mould thickness, the following steps are performed:

1. Finding of the solidification time for maximum casting thickness, highest superheat and highest mould temperature and for lowest interfacial heat transfer coefficient for a minimum mould thickness.

2. Performing step 1 repeatedly by increasing the mould thickness until the solidification time is constant. When the solidification time becomes constant the semi-infinite mould thickness is obtained.

3. Finding of the solidification time for variation of casting thickness, superheat, and mould temperature, using semi-infinite mould thickness.

Using semi-infinite mould thickness, the effects of interfacial thermal resistance, superheat of molten metal, initial mould temperature and casting thickness on the solidification time have been analysed. The variables are: casting materials- Al, Zn and Cu, mould materials- Sand and CI, superheat ranging from 0 to 60 C, mould

35

temperature ranging from 0 to 100 C and interfacial heat transfer coefficient (100, 2000 and 4000) W/m^2 C.

3.3.2 Effect of interfacial heat transfer coefficient (HTC), casting thickness, superheat, and mould temperature on solidification time

Fig. 3.2a shows the effect of heat transfer coefficient on solidification time for aluminium casting in cast iron semi-infinite mould at variable casting thickness (from 0.002m to 0.03m), 0 C superheat and 25 C initial mould temperature. It is found that, for any casting thickness, the solidification time, t_f, increases linearly with the increase of interfacial thermal resistance (ITR=1/HTC). The equations obtained from the graph are:

$t_f = 0.02 + 1305.85$ (ITR)	for CT= 0.002 m	[3.6.1]
$t_f = 0.17 + 3049.85$(ITR)	for CT= 0.006 m	[3.6.2]
$t_f = 0.40 + 4851.08$(ITR)	for CT= 0.010 m	[3.6.3]
$t_f = 0.72 + 6670.77$(ITR)	for CT= 0.014 m	[3.6.4]
$t_f = 1.57 + 10449.85$(ITR)	for CT= 0.022 m	[3.6.5]
$t_f = 2.76 + 14304.00$(ITR)	for CT= 0.030 m	[3.6.6]

Using statistical curve fitting package the above equations are obtained. The average correlation coefficient is 0.99995.

Similar graphical representation was also found by Ohtuska et al. (84). Ho and Pehlke (12) obtained rectangular hyperbolic graphical representation.

The first term of the equations is the solidification time for perfect contact and the second term is the additional term for imperfect contact. It is found that both the intercept and slope terms increase with increase of casting thickness. The first term can be replaced by $[0.11 + 51.88(CT)]^2$ having a correlation coefficient of 0.9998. The slope term can also be replaced by $300962.87(CT)^{0.89}$ having a correlation coefficient of 0.99995. The combined equation is

$$t_f = [0.11 + 51.88(CT)]^2 + 300962.87(CT)^{0.89} (ITR)$$

$$\text{for SH=0 C; MT=25 C} \qquad [3.6]$$

For perfect contact, the equation becomes

$t_f = [0.11 + 51.88(CT)]^2$

The above equation shows that the solidification time increases quadraticaly with casting thickness for perfect contact. Similar expressions of solidified skin as a function of time based on experimental work have been shown by many authors (18, 85). Solidification time increases with the increase of casting thickness due to the fact that with the increase of casting thickness the heat content increases and consequently the solidification time increases. The intercept is found not to depend on the casting thickness. It shows that when the casting thickness is zero, t_f is equal to 0.0121. This has been explained elsewhere (18) that initially the solidification rate is linear and a parabolic relationship develops after the formation of a sufficient casting thickness.

The additional term in equation [3.6] is $300963(CT)^{0.89}$(ITR)

This term shows that additional solidification time increases more or less linearly with the increase of casting thickness with a slope of 300963 (ITR).

The effect of interfacial thermal resistance on solidification time for various casting thickness, for superheat 20 C, 40C and 60 C and for constant mould temperature (25 C) are shown in Figs. 3.2b, 3.2c and 3.2d, respectively. And the developed equations from the figures are :

$t_f = [0.10 + 52.90(CT)]^2 + 354006(CT)^{0.90}$(ITR)

$$\text{for } SH=20 \text{ C}; MT=25 \text{ C} \qquad [3.7]$$

$t_f = [0.11 + 54.65(CT)]^2 + 409921(CT)^{0.91}](ITR)$

$$\text{for } SH=40 \text{ C}; MT=25 \text{ C} \qquad [3.8]$$

$t_f = [0.11 + 56.90(CT)]^2 + 45466CT)^{0.92}$(ITR)

$$\text{for } SH=60 \text{ C}; MT=25 \text{ C} \qquad [3.9]$$

It is found that the intercepts of the first term are more or less constant, so this term can be replaced by the average of the terms. But the slope term of the first term increases with the increase of superheat heat linearly and it can be replaced by [51.56+

37

0.084(SH)] having correlation coefficient of 0.9997 and the second term can be replaced by $[550.62 + 2.15(SH)]^2$ having correlation coefficient of 0.9701.

So the combined equation is

$$t_f=[0.11+\{51.56+0.084(SH)\}CT]^2+[550.62+2.15(SH)]^2(CT)^{0.90}(ITR)$$

for MT= 25 C   [3.10.1]

For perfect contact, (ITR = 0), the equation becomes-

$$t_f = [0.11+\{51.56+0.08(SH)\}CT]^2$$

This equation reveals that solidification time increases quadratically with the increase of superheat for perfect contact. Here, the intercept term is the sum of constant term, 0.11 and 51.56CT and for a given casting thickness this term is constant. So, for a specific casting thickness and casting-mould perfect contact, solidification time increases with the increase of superheat and it is a quadratic function. Similar expression was also found by Gafur and Haque (83).

For additional term in equation [3.10.1] is $550.62+2.15 (SH)]^2(CT)^{0.90}(ITR)$. It is also found that for constant ITR and CT, the additional part of solidification time is a quadratic function of time.

Similarly, for mould temperatures of 50 C (Figs. 3.3a, 3.3b, 3.3c and 3d), 75 C (Figs.3.4a, 3.4b, 3.4c and 3.4d), and 100 C (Figs. 3.5a, 3.5b, 3.5c and 3.5d). the equations are,

$$t_f=[0.12+\{52.04+0.086(SH)\}CT]^2+[556.07+2.31(SH)]^2(CT)^{0.90}(ITR)$$

for MT= 50 C   [3.10.2]

$$t_f=[0.12+\{53.05+0.090(SH)\}CT]^2+[579.18+1.61 (SH)]^2(CT)^{0.90} (ITR)$$

for MT= 75 C   [3.10.3]

$$t_f=[0.12+\{54.23+0.094(SH)\}CT]^2+[584.36+2.43 (SH)]^2(CT)^{0.90} (ITR)$$

for MT= 100 C   [3.10.4]

Combining the equations [3.10.1-4]

$$t_f = [0.12 + \{50.51e^{0.0007(MT)} + 0.08e^{0.0016(MT)}(SH)\}(CT)]^2$$
$$+ [537.13e^{0.0009(MT)} + 2.13(SH)]^2(CT)^{0.90}(ITR) \qquad [3.11.1]$$

or,

$$t_f = [0.12 + \{50.47 + 0.036(MT) + \{0.08 + 0.00014(MT)\}(SH)\}(CT)]^2$$
$$+ [537.17e^{0.0009(MT)} + 2.13(SH)]^2(CT))^{0.90}(ITR) \qquad [3.11.2]$$

The correlation coefficients for the replacement of constants in terms of MT are in the range of 0.98-0.90.

For perfect contact the above equation becomes,

$$t_f = [0.12 + \{50.51e^{0.0007(MT)} + 0.08e^{0.0016(MT)}(SH)\}(CT)]^2$$

or,

$$t_f = [0.12 + \{50.47 + 0.036(MT) + \{0.08 + 0.00014(MT)\}(SH)\}(CT)]^2$$

These equations reveal that, for a specific casting thickness, solidification time increase exponentially or quadratically with the increase of mould temperature. Similar result was found by Gafur and Haque (83).

Similarly, from Figs. 3.6, 3.7, 3.8 and 3.9 the combined equation (86) for aluminium - sand casting combination is

$$t_f = [0.47 + \{277.60e^{0.0013(MT)} + 1.42e^{0.0013(MT)}(SH)\}(CT)]^2 + [1121.25e^{0.0008(MT)}$$
$$+ 7.46(SH)]^2(CT)^{1.09}(ITR) \qquad [3.12.1]$$

or,

$$t_f = [0.47 + \{276.95 + 0.38(MT) + \{1.42 + 0.0020(MT)\}(SH)\}(CT)]^2$$
$$+ [1121.25e^{0.0008(MT)} + 7.46(SH)]^2(CT)^{1.09}(ITR) \qquad [3.12.2]$$

The equations can be written as:

$$t_f = [A + \{Be^{C(MT)} + De^{E(MT)}(SH)\}(CT)]^2 + [Fe^{G(MT)} + h(SH)]^2(CT)^I(ITR)$$
$$\qquad [3.12.3]$$

or,

$$t_f=[A+\{B+C(MT)+\{D+E(MT)\}(SH)\}(CT)]^2+[Fe^{G(MT)}+h(SH)]^2(CT)^I(ITR)$$

[3.12.4]

TABLE I: CONSTANTS FROM EQUATIONS [3.11.1], and [3.12.1]

	A	B	C	D	E	F	G	h	I
Sand	0 47	277.06	0.0013	1.42	0.0013	1121.25	0.0008	7.46	1.09
CI	0.12	50.51	0.0007	0.08	0.0016	537.13	0.0009	2.13	0.90

TABALE II: CONSTANTS FROM EQUATIONS [3.11.2] and [3.12.2]

	A	B	C	D	E	F	G	h	I
Sand	0.47	276.95	0 38	1.42	0.0020	1121.25	0.0008	7.46	1.09
CI	0.12	50.47	0.036	0.08	0.00014	537.13	0.0009	2.13	0.90

Tables I and II show that the constant terms designated by B, C, D, F and h have higher value for sand mould because of lower thermal diffusivity of sand and are affected by mould characteristics. The value of G is more or less the same for both the moulds and the values of E and I are more or less similar for the moulds and they are not affected by the mould characteristics. The value of A appears due to the fact that that initially the solidification rate is linear and a parabolic relationship develops after the formation of a sufficient casting thickness.

From Figs. 3.10, 4.11, 4.12 and 4.13, the combined equations for copper- cast iron combination (87) are

$$t = [0.13+\{72.68e^{0.00048(MT)}+0.11e^{0.0017(MT)}(SH)\}(CT)]^2+[998.44e^{0.00066(MT)}$$
$$\div 1.22(SH)]^2(CT)^{1.04}(ITR)$$

[3.13.1]

or,

$$t=[0.13+72.65+0.036(MT)+\{0.11+0.0002(MT)(SH)\}(CT)]^2+[998.44e^{0.00066(MT)}$$
$$+1.222(SH)]^2(CT)^{1.04}(ITR)$$

[3.13.2]

Similarly, the combined equations from Figs. 3.14, 3.15, 3.16 and 3.17 for zinc- cast

iron combination (88) are

$$t = [\, 0.083 + \{\, 115.31\, e^{0.0021\,(MT)} + 0.46\, e^{0.0023\,(MT)}(SH)\} \,(CT)]^2 +$$
$$[1278.77e^{\,0.0015\,(MT)} + 1.53(SH)]^2\,(CT)^{\,1.06}\,(ITR) \qquad\qquad [3.14.1]$$

or,

$$t = [\, 0.083 + \{\, 114.40 + 0.28\,(MT) + \{\, 0.45 + 0.0012\,(MT)\,\}\,(SH)\,\}\,(CT)\,]^2 +$$
$$[1278.77e^{\,0.0015\,(MT)} + 1.53(SH)]^2\,(CT)^{\,1.06}\,(ITR) \qquad\qquad [3.14.2]$$

TABLE III: CONSTANTS FROM EQUATIONS [3.11.1], [3.13.1] and [3.14.1]

	A	B	C	D	E	F	G	h	I
Al- CI	0.12	50 51	0.0007	0.08	0.0016	537.13	0.0009	2.13	0.90
Cu -CI	0.13	72.68	0.00048	0.11	0.0017	998.44	0.00066	1 22	1.04
Zn-CI	0.083	115.31	0.0021	0.46	0.0023	1278.77	.0015	1.53	1.06

TABALE IV: CONSTANTS FROM EQUATIONS [3.11.2], [3.13.2] and [3.14.2]

	A	B	C	D	E	F	G	h	I
Al-CI	0.12	50.47	0.036	0.08	0.00014	537 13	0.0009	2.13	0.90
Cu-CI	.13	72.65	0.036	0.11	0.0002	998.44	0.00066	1.22	1.04
Zn-CI	0.083	114.40	0 28	0.45	0.0012	1278.77	0.0015	1.53	1.06

Tables III and IV show that the value of the constants B, C, D, E, F and G   have the highest value for zinc and the lowest for aluminium. The value of I is similar for all metals. The value of A is similar for all metals and it appears due to the fact that the solidification rate is linear initially and parabolic after the formation of sufficient thickness. Zinc has the highest solidification time and aluminium has the lowest solidification time. Copper solidifies ahead of zinc due to its higher melting point and higher thermal diffusivity. Aluminium solidifies ahead of copper due to its lower latent heat per unit volume.

3.3.3   Validation of the model

For validating the theoretical model, plate shaped aluminium castings were cast in sand mould. The mould is a one part and it is in the sand bed. The mould can be considered as   semi-infinite mould. The mould cavity is 0.13 x 0.13m with a

thickness of 0.022m. A photograph of casting is shown in Fig. 3.18. The Fig. 3.19 shows transient HF and HTC for one of the castings for a casting having pouring temperature 700 C and mould temperature 30 C . The procedure of the estimation of HF and HTC are discussed in chapter 5. The figure shows the HF increases from lower value to peak heat flux at the end of filling and then it decreases continuously. The figure also shows that HTC increases from a minimum value to a maximum ($550W/m^2C$) at the end of filling due to the maximum metallostatic pressure. After that it decreases sharply to a more or less constant value (~400 W/m^2C) and remains constant. As the HTC remains more or less constant for a longer period of time, it can be averaged. Taking the average value of HTC (404 W/m^2 C) the temperature distribution in casting and mould is obtained. The experimental and estimated temperature-time profiles of the casting at different locations are given in Figs. 3.20-23. The temperature-time profiles are well matched.

The experimental and estimated solidification time of the casting are 183 sec and 184 sec respectively. The solidification time calculated using equation [3.12.1] is 180 sec. The errors are 0.5% and 1.6% for the estimated solidification time using model and developed equations.

So, it can be concluded that the semi-infinite mould model and the developed equations are good enough to estimate the temperature-time profile and solidification time for metal castings. The model can be used to estimate the solidification pattern if the experimentally validated data of HTC or HF is known.

CHAPTER 4

EXPERIMENTAL PROCEDURE

4.1 GENERAL FEATURE

This chapter describes the experimental details for finding the effects of casting variables. such as superheat of molten metal, casting thickness, mould thickness, chill thickness, and mould temperature on solidification process. More attention has been given on the interfacial heat transfer at casting-mould interface.

Three shapes of castings, (a) Bar shape in the sand mould with chill at the end, (b) Plate shape in metal mould, and (c) Cylindrical shape in metal mould, are used for the investigation.

The effects of superheat and chill thickness are investigated for bar shaped castings. The effects of superheat and casting thickness are investigated for plate shaped casting. To investigate the effects of superheat and mould temperature, cylindrical shaped castings are used.

Common features of these experiments such as casting materials, crucible, degasser, flux, mould/chill materials, preparation of thermocouples, melting and pouring and data acquisition system are briefly described here.

Gray cast iron is used as chill or mould. A pair of glass lined chromel-alumel thermocouple of 24 SWG is used. They are bared first, then twisted by a pair of pliers and then gas welded. This type of thermocouples are used to obtain the mould/chill temperature. A different type of thermocouple of 24 SWG is used to obtain the casting temperature. In this type both the wires are bared to a sufficient length and then they are passed through the bores of twin bore porcelain beads having an OD of 3mm and a length of 50mm. Then both the wires are twisted and welded as above.

Commercially pure aluminium ingot is selected for all the sets of the experiments. The metal is melted in a gas fired pit furnace. The ingots are cut by power saw into small pieces and then charged in a crucible placed in the pit furnace. Clay-graphite crucibles of different sizes are used for melting the metal. When the metal is melted completely and has attained the required temperature, the crucible is removed from the furnace and placed in a suitable holder for pouring. A suitable preheated tool is used to skim off the dross. An immersion thermometer is used to check the temperature of the liquid metal. At a suitable temperature the liquid metal is skimmed for degassing. Foseco degasser -190 is used for degassing the molten aluminium. Before pouring, the molten metal is degassed in the ladle using Fousecos's degasser. The degasser is kept in a heated tong to keep it in the molten metal and stirred in the molten metal. Ammonium chloride is used as fluxing material. After reaching the required pouring temperature, the pre-started data logger is used by the software to collect the temperature. The data is recorded for a period of at least 5 minutes.

The data acquisition system consists mainly of Casting setup, Data Logger, IEEE 488 Card. and Computer. Simplified representation is shown in Fig. 4.1. A number of thermocouples are set in the casting setup. Then they are connected to the Data Logger- Keithly 740 System Scanning Thermometer. The data logger is connected to the PC via a IEE488 interfacing card. The values of temperature were acquired by a software 740 Data Logger. A maximum of 9 channels were used for the experimentation. The scanning rate is 9 channels per second.

4.1.1 Bar shaped castings

4.1.1.1 1-Bar castings

To find out the effects of superheat and chill thickness, bar shaped castings were cast using a 1-Bar mould. Fig. 4.2 shows the sand mould with square chill at one end. The cross-section of the Bar is 50mm X 50mm. The chill thickness used are 24mm, 47mm and 70mm. The location of thermocouples at the mid height of chill and casting are shown in Fig. 4.2 (SECTION-RR). The superheats are in the rage of 100-300 C. The position of the thermocouples are shown in Table 4.1.

Table 4.1: THERMOCOUPLE POSITION IN THE CHILLS

Chill Dimension	Thermocouple Position from the interface (mm)			
	In Casting		in Mould	
	Thermocouple 1 (A)	Thermocouple 2 (B)	Thermocouple 3 (C)	Thermocouple 4 (D)
50x50x24	30	4	4	20
50x50x47	30	4	4	43
50x50x70	30	4	4	66

The sand mould is first dried naturally and, before pouring the molten metal in it, dried by gas flame. The chill is dried at a temperature of 110 C to remove the moisture especially from the holes of thermocouple and then cooled to room temperature.

Three chills are prepared from a gray cast iron bar. The surface were machined by shaper and then polished by emery paper (GRIT 4).

The sand bed is used for drag portion of the mould, that is, the chills and main part of the casting are in the sand bed. The pouring basin, sprue and feeder are in the cope. There are also two holes in the cope to introduce thermocouple (the porcelain beads type) into the cavity of the mould.

The chills are placed first in the cavity. Then the thermocouples are set in the chill. The casting's thermocouples are introduced in the cope's hole and lowered down to 25 mm from the parting line so that the tips of thermocouples are at the mid level. After that the cope is placed on the mould cavity.

4.1.1.2 3-Bar castings

For 1-Bar casting it was quite tough to maintain the same superheat and same filling time for different chill thickness. To investigate the effect of chill thickness at the same superheat and same pouring time 3-Bar casting are cast. Fig. 4.3 show

the sand mould with three square bar chill at the end for each. A photograph of the set up consisting of mould assembly, the thermocouples, the data logger and computer is shown in Fig. 4.4. The superheats are in the range of 40-140 C.

The locations of thermocouples at the mid height of chill and casting are shown in Fig. 4.3 (SECTION-PP & RHS VIEW). The position of thermocouples are the same as given in the Table 4.1 except that of thermocouple 1 at A. Since the scanning thermometer can read a maximum of 9 channels, the thermocouple 1 is omitted in 3-Bar casting.

4.1.2 Plate shaped castings

To find out the effects of superheat and casting thickness, plate shaped castings were cast using plate mould (Fig. 4.5). The mould cavity is 300mm X 300mm with variable thickness. The casting thickness used for this study are 68 mm, 52 mm and 36 mm. The mould wall is 26mm thick. The width (300mm) and height (300mm) of the mould are enough compared to the thickness to consider the heat flow as one dimensional at the centre of the casting face. The thermocouples are placed at the mid level as shown in Fig. 4.6. A photograph of the set up consisting of mould assembly, the thermocouples, the data logger and computer is shown in Fig. 4.7. The superheats are varied in the range of 40-290 C.

The distances of thermocouples in castings are 0, 8, 16, 24 and 30mm respectively from the centre of the castings for 68mm casting. For 52mm thick casting, the distances of the thermocouples in the casting are 0, 8, 16 and 22mm from the centre of casting. The thermocouples in castings are at distances of 0, 8 and 14mm for 36mm thick casting. The thermocouples in the mould wall are at distances of 3, 8, 16 and 22mm from the interface. Molten metal is poured from the top in one corner of the mould. The plate shaped metal mould is prepared from five plate-shaped gray cast iron plates. They are machined by shaper and polished by polishing paper. For every casting the inside of vertical plates are polished by emery paper (GRIT 4).

4 holes of 2mm diameter are made at the side wall at the periphery of a circle having 5mm radius. The holes are at different depth so that 4 temperatures at different distances from the interface are obtained. A 6mm stainless steel pipe is introduced through two holes of the two large plates. The two holes are 50mm below the mid level of the mould. There are five 3mm-holes through which the porcelain beads containing thermocouples are introduced. The thermocouple tips are at the mid level of the mould.

The stainless steel pipe containing five thermocouples is set at the fixed large plate's holes. Then the moving large plate are set to the stainless steel pipe. The thermocouples are set vertically. This arrangement is made to minimise disturbance in the 1-D heat flow path.

4.1.3 Cylindrical shaped castings

To find the effects of superheat and mould temperature on interfacial heat transfer, cylindrical castings are cast using vertical cylindrical bottom-gated cast iron mould (Fig. 4.8). A photograph of the set up consisting of mould assembly, the thermocouples, the data logger and computer is shown in Fig. 4.9. The average initial mould temperatures used are 82 C and 107 C. The internal dimensions of the mould are 76mm in diameter and 430mm in height. The mould thickness is 26mm. The height of the casting was sufficient to consider the heat transfer at the mid level of the casting as one-dimensional. Thermocouples are placed radialy at the mid level as shown in Fig. 4.6. Thermocouple 1 is placed at centre of the casting, the thermocouple 2 in casting at a distance of 4mm from the interface, the thermocouple 3 in mould at a distance of 3mm from the interface and the thermocouple 4 is at a distance of 4mm from the outer surface of the mould. The temperature of the positions A, B, C and D are designated by T1, T2, T3 and T4 respectively. The superheats are varied from 10 C to 300 C.

Two-parts split type moulds were used. They were made from gray cast iron and machined by lathe. 4 bolts were used to attach them.

The pouring basin and sprue were made first using sand in a 4-inch diameter steel pipe. Then the runner was made in the sand bed. One part of core box was used to make two holes. One was used by sprue and the other by mould. This part was set on the sand bed where the sprue and runner are produced. The sprue and mould were set on this mould box. They were weighed down by two weights.

CHAPTER 5

ANALYSIS OF EXPERIMETAL DATA

5.1 INTRODUCTION

The estimation of the heat flow rate per unit area, HF, from the casting into the chill or mould across the casting-mould/chill interface as a function of time are carried out using the time temperature data obtained from the experiments described in chapter 4. The temperatures T1, T2, T3 and T4 at the positions A, B, C and D respectively are measured for every second. The time temperature data of a typical experiment is shown in Fig. 5.1. The first column shows time in sec and the remaining columns are the temperatures T1, T2, T3 and T4. During the estimation of HF, the temperature of mould at the interface, Tm, is also estimated. Using the value of HF as boundary condition at the casting surface, the casting surface temperature, Tc, is found. The values of HF, Tm and Tc are used to calculate HTC as a function of time. The determination of HF at the interface from the temperatures measured inside a body requires to solve the 'Inverse heat conduction problem' (IHCP). Fig. 5.2 shows the inverse conduction problem for 1-D heat flow in the case of plate and bar shaped casting. The unknown heat flux from casting to the mould or chill, HF, and the surface temperature, Tm, at S are to be determined from the measured temperature, T3 and T4.

5.2 STATEMENT OF THE INVERSE PROBLEM

Referring to Fig. 5.2 the heat flux, HF, and the temperature, Tm, at S have to be determined by comparing measured temperature, T3 (=Y), at C with the estimated temperature. The temperature, T4, at D is taken as boundary condition. The estimated temperatures are obtained by solving the 1-D heat conduction equation:

$$\frac{\partial}{\partial x}\left(K\frac{\partial T}{\partial x}\right) = \rho\frac{\partial H}{\partial t} \quad \text{(for plate and bar shaped castings)} \qquad [5.1]$$

$$\frac{1}{r}\frac{\partial}{\partial r}\left(rK\frac{\partial T}{\partial r}\right) = \rho\frac{\partial H}{\partial t} \quad \text{(for cylindrical casting)} \qquad [5.2]$$

49

The explicit finite difference approximation of the equations [5.1] and [5.2] are given in APPENDIX-A. The time step and space step are 0.001 sec and 1 mm, respectively.

5.3 SENSITIVITY COEFFICIENTS AND CORRECTION FACTOR

In the estimation of interfacial heat flux the Beck's (73) non-linear estimation procedure as described in 2.5.4 is used. For the present study, heat flux, HF is taken to be constant for 1 second that is $\Delta\theta = \Delta t$. For estimation of heat flux, one future temperature is also taken into the consideration. So, m=1, r=2 and I=mr=1,2=2 and from the equation [2.19] the following equations for sensitivity coefficients are obtained and used in the present study.

$$\phi_1^{old} = \frac{T_{\eta+1}(HF_{M+1}^{old}(1+\varepsilon)) - T_{\eta+1}(IIF_{M+1}^{old})}{\varepsilon HF_{M+1}^{old}} \qquad [5.3.1]$$

$$\phi_2^{old} = \frac{T_{\eta-2}(HF_{M+1}^{old}(1+\varepsilon)) - T_{\eta+2}(HF_{M+1}^{old}))}{\varepsilon HF_{M+1}^{old}} \qquad [5.3.2]$$

$$\nabla HF_{M+1}^{new} = \frac{\left(Y_{\eta+1} - T_{\eta+1}^{old}\right)\phi_1^{old} + \left(Y_{\eta+2} - T_{\eta+2}^{old}\right)\phi_2^{old}}{(\phi_1^{old})^2 + (\phi_2^{old})^2} \qquad [5.4]$$

5.4 PROCEDURE FOR DETERMINATION OF INTERFACIAL HEAT FLUX (IIF)

The initial temperature distribution in the chill / mould is obtained from the measured temperature as shown in data file (Fig. 5.1). A suitable initial value for IIF_1^0 (=10 W/m^2) is assumed and with this value, the temperature distribution from S to D are determined using FDA equations (APPENDIX -A). The thermophysical properties of casting and mould material are given in APPENDIX-B. The estimated temperatures for the value of HF_1^0, $T(HF_1^0)$, at location C are stored at the time of 1 sec and 2 sec. HF_1^0 is increased by a small value εHF_1^0 (where ε is 0.001) and using the new value of $HF_1^0(1+\varepsilon)$ the temperature from S to D are estimated. The

temperature at C, $T(HF_1^0(1+\varepsilon))$, for 1 sec and 2 sec are also saved. With these values, 'sensitivity coefficients' (ϕ_1 and ϕ_2) are calculated using the temperatures those are saved at time of 1 sec and 2 sec at the location, C. The new value of HF is obtained using the following equation

$$HF^{new} = HF^{old} + \nabla HF^{new} \qquad\qquad [5.5]$$

The procedure is repeated with HF^{new} in place of HF^{old} until:

$$\frac{\nabla HF^{new}}{HF^{new}} < 0.005 \qquad\qquad [5.6]$$

A flow chart for the determination of HF is given in Fig.5.3.

5.5 DETERMINATION OF INTERFACIAL HEAT TRANSFER COEFFICIENT (HTC)

In the present study, the inverse heat conduction problem on the chill/ mould side is solved using the known temperature T3 and T4. The estimation starts from the time of response of T3. The T4 is used as known boundary condition. The calculations are performed using explicit FDA. This yields the value of HF, interfacial heat flux per unit area, and also the temperature of mould at the interface, Tm (the mould/ chill surface temperature). The value of casting surface temperature. Tc. is calculated either using this estimated value of HF and T1 as known boundary conditions, the temperature distribution in the casting is obtained by the explicit FDA or by extrapolation. The interfacial heat transfer coefficient is obtained using the following equation:

$$HTC = \frac{HF}{Tm - Tc} \qquad\qquad [5.14]$$

CHAPTER 6

RESULTS AND DISCUSSION

6.1 BAR SHAPED CASTING WITH CHILL AT THE END

Fig. 6.1.1 shows a typical temperature-time profile of a bar shaped aluminium casting with 24mm CI chill at the end. The temperature-time profile is shown when the T3 begins to change. The top curve shows the cooling curve of casting (T2-t) at point B which is at a distance of 4mm from the casting-chill interface. The second one is the heating curve of the chill (T3-t) at a distance of 4mm from the interface and the bottom one is the heating curve of chill (T4-t) at a distance of 4mm from the external surface of the chill. The pouring temperature (PT) is 760 C. The maximum temperature recorded by the thermocouple at B is 674.1 C. Since B is only 4mm from the casting-chill interface, a remarkable holding time at the melting point is not observed in T2-t due to higher cooling rate. In plate shaped casting (art. 6.2) it is observed that the surface temperature of the plate decreases slowly until there remains molten metal at the centre of the plate which releases latent heat. When the last liquid solidifies and there is no more latent heat all the temperatures fall at a faster rate. The sudden change in slope in the temperature profile of thermocouple at B can therefore be considered as the end of total solidification of the bar. The temperatures T3 and T4 in the chill initially show a continuously increasing value, T3 increases at a faster rate since it is measured at a point closer to the casting chill interface. The thermocouple at D responds later than that at C and the difference between T3 and T4 increases with the increase of chill thickness, since more is the chill thickness more is the distance between C and D. The difference between T3 and T4 increases to a maximum and then it gradually decreases. And after sufficient time, the difference is negligible.

6.1.1 Heating curves of chills near the interface

6.1.1.1 Effect of superheat

Fig. 6.1.2a shows the effect of superheat on temperature-time (T3-t) profiles of 24mm chill near the interface of bar shaped aluminium castings. It reveals that the higher is the superheat, the steeper is the heating curve and also the higher is the

corresponding maximum chill temperature. The maximum chill temperatures are in the rage of 445-541 C for pouring temperatures in the range of 705-800 C. For 70mm chill, the corresponding maximum chill temperatures are in the range of 337-440 C. Higher superheat causes more heat to flow to chill because of high initial temperature difference and better casting-chill contact. The rate of heating of chill is higher at higher superheat than that at lower superheat. Bishop et al.(49) also found higher mould surface temperature for higher superheat of medium carbon steel in cast iron mould.

6.1.1.2 Effect of chill thickness

Fig. 6.1.2b and c show the effect of chill thickness on the heating curves (T3-t) near the interface for PT-705 C and PT-730 C, respectively. The curves reveal that initially all temperatures increase at a similar rate but after about 30sec the rate of increase of temperature of the thicker chill becomes lower than that of thinner one and the temperature of the thinner one always remains higher than that of thicker one. Then the temperature of thicker chill decreases, but temperature of thinner one remains more or less constant. The lower is the chill thickness, the higher is the maximum temperature and the longer is the time of attaining the maximum temperature. Initially the rates of heating of the chill are the same for all chill thicknesses. When the heat reaches the external surface of the chill, the heat transfer from the interface is controlled by the surroundings. For the thinner chill the heat reaches the outer surface ahead of thicker one. Due to the control of the surroundings, the heat is accumulated and the temperature increases continuously. It decreases the efficiency of chill by reducing the extraction of heat from the casting. The higher is the chill thickness, the higher is the volumetric heat capacity and the more is the heat absorbed by the thicker chill. Due to lower volumetric heat capacity, the temperature of chill, T3, near the interface of thinner chill increases at a faster rate. Hou and Pehlke (70) concluded that the different thickness of chill walls result in different thermal capacities, resulting in different temperature distributions in the chills. The thinnest chill showed an insufficient heat capacity which resulted in continued rapid heating throughout the entire wall. The intermediate chill wall had sufficient heat capacity to maintain an approximately

53

constant interface temperature, while the thicker one was more than sufficient so that the temperature continuously decreased after reaching the maximum.

6.1.2 Heating curves of chills near the external surface

6.1.2.1 Effect of superheat

Fig. 6.1.3a shows effect of superheat on the heating curves of chills near the external surface (T4-t) for bar shaped aluminium castings. The curves are similar to T3-t except at the initial stage. Initially there is no change in temperature because it requires time to reach heat to the external surface of chill.

6.1.2.2 Effect of chill thickness

Fig. 6.1.3b shows the effect of chill thickness on T4-t curves for bar shaped aluminium castings. Since it takes time to reach heat at D, the thermocouple of higher chill thickness takes longer time to respond. The time of remaining the external surface at the initial temperature has an effect on heat extraction from the interface. The heat extracted by the chill depends on the temperature gradient of the chill at the interface. When heat reaches the external surface, temperature gradient near the external surface of the chill decreases and this effect defuses gradually towards the casting-chill interface. As a result, the temperature of the inner surface increases due to higher rate of heat accumulation. Bishop et al.(49) observed that the temperature of external surface of 38mm chill instantaneously increases, whereas, that of 105mm chill remains at initial temperature unto about 40sec.

6.1.3 Cooling curves of castings near the interface

6.1.3.1 Effect of superheat

Fig. 6.1.4 shows the effect of superheat on temperature-time profiles (T2-t) of casting near the interface for bar shaped aluminium castings with 24mm CI chill at the end. The temperature, T2, measured at B is higher for higher pouring temperature. The maximum temperatures are 660 C and 666 C for the pouring temperature 705 C and 760 C, respectively. Since B is only 4mm away form the chill a considerable lower temperature is recorded by it. Bishop et al. (49) observed higher casting surface temperature for higher pouring temperature.

6.1.3.2 Effect of chill thickness

Fig. 6.1.5 shows the effect of chill thickness on the cooling curves, T2-t. of casting near the chill. Initially, for all chill thicknesses, the temperatures are same. The figure shows that upto about 30sec, the temperatures are the same and after that a slight lower temperature is observed for thicker chill. The thicker is the chill, the more is the heat absorbed, resulting in lower temperature of casting for thicker chill. Rao and Panchanathan (89), and Hou and Pehlke (70) found lower surface temperature of casting for thicker chill.

6.1.4 Heat Flux

6.1.4.1 Effect of superheat

Fig. 6.1.6a shows the effect of superheat on the transient interfacial heat flux of bar shaped aluminium castings with 24mm CI chill at the end. It reveals that the interfacial heat flux increases sharply with time from a minimum value to a peak at all superheats. Then it decreases very sharply within a few second and then slowly. The calculation of HF starts from the time when T3 starts increasing. The peak heat flux (HFmax) is obtained at the end of filling.

Jacobi (64) carried out experiments using pure iron with water cooled copper mould wall and found IIF to increase to peak value and then decrease as a function of time, $HF = at^b$, where a and b are constants.

Kumar and Prabhu (7) carried out experiments using bar shaped casting with 50 x 50 x 50mm copper chill at the end. They also found similar HF-time curves for different aluminium alloys. For LM13 alloy, the peak value was 2.0×10^6 W/m^2 for the pouring temperature of about 750 C. In the present study, the peak heat flux is - 1.02×10^6 W/m^2 when aluminium was cast with 50 X 50 X 47mm CI chill at the end. The lower value of HFmax obtained than the former may be due to difference in casting metal and chill material combination.

Kumer and Prabhu (7) has mentioned that the peak heat flux was obtained shortly after filling and suggested that as the casting started solidifying, the contact became

less and less perfect, resulting in a reduction of heat flux and the peak value was related with the start of solidification. In the present study, the peak value was obtained at the end of filling.

As the level of liquid metal rises upward the metallostatic pressure increases continuously. When it fills the feeder at the end of filling the metallostatic pressure is at its maximum. The contact is more intimate with increasing metallostatic pressure. As a result the HFmax is obtained at the end of filling. To verify whether the peak is associated with the start of solidification or with some other reasons, the pouring temperature were varied. At the end of filling, depending on the superheat of the molten metal, the casting surface was found to be liquid (Tc-771 C) as shown in 6.1.6b, or at melting point (Tc-660 C) as shown in Fig. 6.1.6c or may form solidified skin (Tc-615 C) as shown in 6.1.6d. The peak values were observed at the end of filling for each of the three conditions. Others investigators (35,36,37) have also observed that the heat extraction at the interface increases due to increase in pressure.

After the end of filling, as the liquid level decreases due to shrinkage, the contact pressure decreases gradually. In one hand, when the melt starts to solidify, the solidified skin may have sufficient strength to initiate gap after the end of filling and it gradually increases. On the other hand, when the melt is nearly at the melting point at the end of filling the solidification proceeds with non-conforming solid-solid contact. The lowering of pressure, the non-conforming contact and the initiation of gap are all possibly responsible for the sharp fall in heat flux after the end of filling. A number of investigators (7, 37) suggested that the start of solidification caused the sharp decrease in heat flux or heat transfer coefficient. The present study shows that the decrease in metallostatic pressure is also associated with the sharp decrease in HF. This sharp fall of heat flux changes the slopes of Tm. Figs. 6.1.6b, c and d show the slope change in Tm at HFmax.

After the sharp decrease in HF, the chill surface is sufficiently heated and the difference between the Tm and Tc becomes small and decreases very slowly with time as shown in Figs. 6.1.6b-d. As a result the heat flux decreases very slowly.

Fig. 6.1.6a shows that the difference in HF due to superheat is found to decrease with time from peak heat flux. It also shows that the higher is the superheat, higher is the HFmax. As HF is a product of (Tm-Tc) and HTC, the higher HFmax for higher superheat may be due to following reasons:

-the higher is the superheat, the higher is the initial temperature difference (Tm-Tc) between casting and chill surfaces
- the higher is the superheat, the better is the contact due to lower surface tension of the liquid metal causing higher HTC.

6.1.4.2 Effect of chill thickness

Figs. 6.1.7a and b show the effect of chill thickness on the transient interfacial heat flux for bar shaped aluminium castings with CI chill for PT-800 C, and PT-760 C. respectively. Initially HF increases in all cases in a similar manner from a low value to a maximum. The figures show a slight low value of HFmax for 24mm chill, but the value is the same for larger chill thickness (47mm and 70mm). Fig. 6.1.2b and c show that the effect of chill thickness on Tm is not observed upto certain time. Tm will differ when heat flow will be controlled by the outer surface of the chill. After reaching the external surface of the chill, the heat will take some time to create lower temperature gradient at the interface and from that time the conduction through chill is reduced. If the end of filling is before the time of reaching the effect of chill thickness at the interface, the peak heat flux, HFmax, will be the same as the conduction is not hampered. For higher chill thickness, the time responding the thermocouple at D is after the time of end of filling. It means that the heat does not reach at the end of the chill and the effect of chill thickness is not noticed at the end of filling. Consequently, the peak heat flux is the same for thicker chills. But for 24mm chill, heat reaches the outer surface before the end of filling and the heat flux

57

at the interface is also controlled by the surroundings. As a result, a slight lower HFmax is observed.

Kumar and Prabhu (7) found that the peak heat flux decreases with the increase of chill thickness for aluminium alloys. In the present study, the effect of chill thickness on HFmax is not observed for higher chill thickness. For lower chill thickness the value of the peak is slightly lower than that of thicker chill.

The figures show that HF for the thicker chills remain same even after HFmax. After that a slight difference in HF is observed when the effect of thickness is noticed at the interface. The time of responding thermocouple at D is longer for thicker chill and the volumetric heat capacity is also greater for the same.

6.1.4.3 Total heat flux

Fig. 6.1.8 shows the effect of superheat on the total heat flux for different chill thicknesses up to 275 sec. It shows that the higher is the superheat, the more is the total heat flux passes through interface. The higher is the superheat, the more is the temperature difference and the better is the contact and the more is the heat passes through the interface for the same span of time (275 sec). The figure also shows that the higher is the chill thickness, the more is the heat to pass through the interface. The higher is the chill thickness, the greater is the temperature difference near the interface which will remain for longer time, as a result more heat will flow through the interface. Fig. 6.1.8 also shows that the difference of total heat absorption due to chill thickness decreases with the decrease of superheat and nearly disappear for 45 C superheat. It shows that for 45 C superheat 47mm chill is enough to take same amount heat flux as 70mm chill. For higher superheat, thinner chill is not enough to take heat as much as thicker one.

6.1.5 Modelling

From the effect of superheat and chill thickness on heat flux, it has been found that the HFmax varied with the variation of superheats only and can be expressed as a function of superheat.

HFmax = 403600 + 6201 (SH)   (for 45-140 C superheats)

The initial rise in heat flux is more or less linear which can be represented in the following way :

$$\frac{HF}{HF\max} = \frac{1}{C_1} * t$$

C_1 = Time from responding the thermocouple at C to the end of filling

        = Filling time- time reqnired to respond thermoconple at C.

In the present study C_1 is in between 14 sec to 16 sec.

t   = time after responding thermocouple at C.

After reaching the peak heat flux ,the HF decreases logarithmically in the following way:

$$\frac{HF}{HF\max} = \left(1 - C_2 \ln(t - C_1)\right)$$

C_2 = 0.1693 - 0.4391*ChT + 0.0002*SH.

It is found that higher the superheat higher is the value of C_2 and thicker the chill lower is the value of C_2.

Using this model, the model temperature-time profiles of various casting experiments are obtained and shown in Fig. 6.1.9 (experimental and modelled side by side). They are all well matched.

6.1.6 Interfacial heat transfer coefficient (HTC)

6.1.6.1 Effect of superheat on HTC

Fig. 6.1.10a shows the effect of superheat on transient HTC with 47mm chill at the end. The heat transfer coefficient increases from a very small value to a peak value, from which it decreases sharply to a nearly steady valnc. The peak HTC were found at the end of filling because of maximum metallostatic pressure. Issac et al. (15) also found HTC to decrease from a maximum value to nearly steady value for

aluminium casting in CI mould. Davies (47), Nishida and Matsubara (62) found that HTC increases with contact pressure. Sully (16) observed the initial rise in HTC during filling due to increase in metallostatic pressure and the peak values of HTC curves were related with the end of filling.

The figure also reveals that higher is the superheat more is the heat transfer coefficient. The higher is the superheat. the lesser the surface tension, the more is the fluidity of the melt and the better is the contact yielding higher HTC. Durham and Berry (13) assumed higher constant HTC for higher superheat of lead casting upon lamp-black coated water cooled brass chill to match the estimated solidification front with that of experimental curves. In the present investigation, the peak heat transfer coefficient are in the range of 1535- 3679 W/m²C for the superheat in the range of 45-140 C and the steady values for present study are in the range of 900-2100 W/m²C.

6.1.6.2 Effect of chill thickness on HTC

Fig. 6.1.10b shows the effect of chill thickness on transient HTC having same superheat of 70 C. The maximum value attained at the end of pouring. No remarkable effect of chill thickness on HTC has been found. HTC depends on the contact between the casting and chill. Contact depends on surface condition and on the wetability of the melt on the chill surface. For same superheat the surface condition is same for any chill thickness. As a result the chill thickness has no effect on HTC.

6.2 PLATE SHAPED CASTING

Fig. 6.2.1 shows a typical temperature-time profile of a plate shaped aluminium casting (68mm thick) in 26 mm thick CI plate mould. The pouring temperature is 750 C. The maximum temperatures obtained at the centre (at A) and at a distance of 4mm from the interface (at B) of the casting are 686.5 C and 661.5 C, respectively. The temperatures T1, T2, T3, and T4 are at A, B, C, and D, respectively. The points C and D are in the mould at a distance of 3mm and 22mm from the casting interface.

The top two curves (T1-t and T2-t) are the cooling curves of casting. The bottom two curves (T3-t and T4-t) are the heating curves of mould.

The thermocouples 1 and 2 are located at the mid level of the mould cavity where the heat flow can be considered as 1-D flow. Initially, both the thermocouples respond very quickly. This is followed by sharp decrement of temperature to the melting point of aluminium.

T1 is always higher than T2, but the differences between them is very small as indicated by the cooling curves due to high thermal conductivity of aluminium. T2 remains very near to melting point as long as the centre is liquid with latent heat. After complete solidification, the temperatures falls at a faster rate and with time their difference become negligible. The faster rate of cooling is due to the fact that there is no more latent heat.

The temperatures in mould initially continuously increase. As time elapsed the difference between T3 and T4 increases to a maximum value and then decreases.

6.2.1 Heating curves near the interface
6.2.1.1 Effect of superheat
The Figs. 6.2.2a and b show the effect of superheat on the heating curves of the mould near the interface of 68mm and 52mm thick aluminium castings, respectively. The figures reveal that the higher is the superheat, the steeper is the initial heating curve and the higher is the maximum mould temperature as observed in bar shape casting with 24mm CI chill at the end.

6.2.1.2 Effect of casting thickness
Figs. 6.2.3a and b show the effect of casting thickness on the heating curves (T3-t) of the mould near the interface for pouring temperatures of 800 C and 850 C, respectively. The curves reveal that the rate of increase of mould temperatures near the interface are same for both casting thickness with same superheat up to 30 sec and 10 sec for the pouring temperatures of 800 C and 850 C, respectively. After

61

that the rate of increase of temperature of the mould for thicker casting is higher than that of thinner one and the temperature T3 for thicker casting always remains higher than that of thinner one.

The higher is the casting thickness, the higher is the maximum temperature (T3max) and the longer is the time to attain the maximum temperature. The higher is the casting thickness, the more is the heat content which enters the mould for longer period of time. As a result, after the initial period T3 increases at a higher rate and the time to reach the maximum temperature is longer for thicker casting than that for thinner casting. Initially, the contact pressure and (Tc-Tm) are similar for all the casting thickness, so T3 initially increases at a similar rate.

6.2.2 Heating curves near external surface

6.2.2.1 Effect of superheat

The Figs. 6.2.4a and b show the effect of superheat on heating curves, T4-t, of mould near the external surface of 68mm and 52mm thick plate aluminium castings, respectively. The time of increasing T4 at a same rate is longer than T3 (Figs. 6.2.4a-b). The thermocouple 4 is delayed respond and the T4-t curves are less steeper due to its position as mentioned earlier. The difference due to superheat is also lesser than that of T3. The time of attaining maximum temperature is also more than that of T3. The maximum temperature is lesser than that of T3 as point D is far away from the interface than from point C.

6.2.2.2 Effect of casting thickness

Fig. 6.2.5a and b show the effect of casting thickness on heating curves of mould near the external surface for pouring temperatures of 800 C and 850 C, respectively. The thermocouple 4 is delayed respond than the thermocouple 3. T4-t is less steeper than T3-t. The maximum temperature of thermoconple 4 is also lesser and more time to attain the maximum temperature than that of thermocouple 3 as mentioned earlier.

6.2.3 Cooling curves at the centre
6.2.3.1 Effect of casting thickness

Fig. 6.2.6 shows the effect of casting thickness on cooling curves of casting at the centre of casting (at A) for 850 C pouring temperature. The maximum temperature obtained at A are 777.6 C, 725.0 C and 685.0 C for casting thickness 68mm, 52mm, and 36mm, respectively. Thinner casting solidifies ahead of thicker one due to lower heat content of the thinner casting than that of thicker one.

6.2.4 Cooling curves near the interface
6.2.4.1 Effect of superheat

Fig. 6.2.7 shows the effect of pouring temperature on temperature-time profiles, T2-t. at B for plate shaped aluminium casting for 68mm thick casting. The T2max are 809.0 C and 759.1 C for pouring temperatures of 910.0 C and 875 C, respectively. It reveals that the higher is the pouring temperature, the higher is the T2max. Due to higher initial surface temperature of the casting for higher pouring temperature, the casting-mould interface contact is better. Therefore, the surface temperature of the casting with higher pouring temperature falls at a faster rate and becomes lower than that with lower pouring temperature. No holding time at the melting point is observed in T2-t. Upto the end of solidification, T2 is found to increases gradually from a minimum value towards the melting point due to increase in interface resistance.

6.2.4. 2 Effect of casting thickness

Fig. 6.2.8 shows the effect of casting thickness on T2-t for pouring temperature of 850 C. It revels that the higher is the casting thickness, the higher is the T2max. T2 always remains higher for higher casting thickness.

6.2.5 Heat flux

6.2.5.1 Effect of superheat

Figs.. 6.2.9a and b show the effect of superheat on the transient interfacial heat flux of 68mm, and 52mm thick plate shaped aluminium casting, respectively. Like bar shaped castings, heat flux increases with the increase of time to a peak value,

HFmax, at the end of filling and then it sharply decreases. After that it decreases slowly. The slight variation of peak position is due to the variation of filling time.

Like bar shaped castings, the surface temperature, Tc, of the casting at peak heat flux indicates that the surface remains either liquid (Tc-711 C, CT-68mm) as shown in 6.2.9c, or at melting point (Tc- 660 C, CT-52mm) as shown in Fig. 6.2.9d or may form solidified skin (Tc- 640 C, CT-36mm) as shown in Fig. 6.2.9e.

The nature of HF-time curves are similar as those of bar shapes casting and could be explained as earlier.

6.2.5.2 Effect of casting thickness

Fig. 6.2.10 shows the effect of casting thickness on transient interfacial heat flux for a pouring temperature of 850 C. Initially both of them increase in a similar manner from a very low value to peak value. The values of HFmax (690792 and 711608 W/m^2) are found to be nearly the same for both the casting thicknesses. For thinner casting, the amount of heat content is lesser than that for thicker casting. The casting surface temperature starts to decrease ahead of thicker one. As a result, the HF for thinner one decreases ahead of thicker one.

6.2.6 HFmax

Fig. 6.2.11 shows the effect of superheat on the HFmax for different casting thicknesses. The average linear relationship between HFmax and the superheat is:

HFmax = 986687 + 3488 (SH)

6.2.7 Solidification time

6.2.7.1 Effect of superheat

Fig. 6.2.12a shows the effect of superheat solidification time for different casting thicknesses. From the figure it is found that solidification time increases with the increase of superheat.

With the increase of superheat, the total heat content of casting increases and more time to be required to dissipate it to the mould, resulting in higher solidification

time. It can also be mentioned that with the increase of superheat the HTC also increases resulting in decrease in solidification time. Bishop et al. (49) carried out experiments with medium carbon steel in CI mould and found higher solidification time for higher pouring temperature. Din (90) also found higher solidification time for higher superheat for ZA27 alloy plate shape casting in cast iron mould and suggested that the solidification time increases with the increase in total heat content due to increase in superheat. Moreover, a high superheat of the molten metal may heat up the mould at high temperature and will, therefore, be expected to make an increase in solidification time.

Effect of superheat on solidification time, t_f can also be found from Ruddle's (91) formula given below:

$$t_f = \left[\left(\frac{V}{SA} \right) \left(\frac{\rho}{1.128\alpha(Ti - Tm)} \right) (L + SH) \right]^2$$

Here,

V= volume of casting ;

SA= cooling surface area of casting;

L = latent of fusion;

SH= superheat;

Ti = mould metal interface temperature;

Tm= initial mould temperature;

α= thermal diffusivity of the mould

ρ = density of metal.

The above equation shows that solidification time increases with the increase of superheat.

6.2.72 Effect of casting thickness

Fig. 6.2.12a also shows that the higher is the casting thickness, the higher is the solidification time. The rate of heat extraction from a given casting is a function of casting shape and size, heat content of casting, interfacial heat transfer coefficient,

65

mould temperature, and thermal properties of the casting and mould materials. Increasing the total amount of heat which must be removed during solidification has significant effect on solidification time. For castings having same superheat, the liquid metal density, specific heat and the heat content of casting will be proportion to its volume. Hence, solidification time increases with the increase of casting thickness.

Fig. 6.2.12b shows that the solidification time increases with the increase of modulus of casting (V/A) quadratically for plate shaped aluminium casting in cast iron mould for pouring temperature of 850 C. Din (90) found that the solidification time increases with increasing casting thickness for ZA27 alloy in Cl mould. The Ruddles's formula as given before also shows that the solidification time increases quadriticallly with the increase of modulus of casting. For plate shape casting, V/A represents the half of the casting thickness.

6.3   CYLINDRICAL SHAPED CASTING

Fig. 6.3.1 shows a typical temperature-time profile of 76mm diameter cylindrical shaped aluminium casting in a 26 mm thick cylindrical CI mould. For a pouring temperature of 950 C, the maximum temperature obtained at A and B are 823.0 C, and 808.8 C. respectively. The initial mean mould temperature is 107 C. The temperature-time profile is shown from the time when temperature of the thermocouple at C begins to increase. The top curve is the cooling curve. T1-t, at the centre of the casting (at A) and the second is the cooling curve, T2-t, in the casting 4mm away from the interface (at B).

The third one is the heating curve of the mould, T3-t, at a distance of 3mm from the interface (at C) and the lower one is the heating curve of the mould, T4-t, at a distance of 4mm from the external surface (at D).

Initially, the thermocouples at A and B, respond very quickly to maximum temperatures. This is followed by continuous fall of temperatures to melting point

66

of aluminium. The fluctuation in the cooling curves observed above melting point is due to the turbulence in the molten metal. The holding time of T2 at the melting point is very short compared to that of T1. After solidification, T2 decreases very slowly. The difference between T1 and T2 is appreciable up to the end of solidification. After the end of solidification, T1 is sharply decreased and this difference gradually decreases.

Temperatures T3 and T4 in mould continuously increase. Initially, T3 increases at a higher rate. As the time elapsed, the difference between them increases to a maximum value and then continuously decreases. T3 is always greater than T4 because of the location of thermocouples.

6.3.1 Effect of superheat and mould temperature

6.3.1.1 Heating curves of the mould

Fig. 6.3.2a and b show the effect of superheat on the temperature-time profiles, (T3-t) of mould at C for initial mean mould temperatures of 82 C and 107 C, respectively. Like bar shapes and plate shapes, the higher is the pouring temperature, the steeper is the heating curves and the higher is the maximum mould temperature.

The effect of superheat on temperature-time profiles of thermocouple at D (4mm from the external surface) for initial mean mould temperature 82 C is shown in Fig. 6.3.3a and for initial mean mould temperature 107 C is shown in Fig. 6.3.3b. The effect is similar to that of T3 except that the T4 starts increasing after some time and the initial rate of increasing is slower than that of the former.

The above figures show that the higher is the initial mould temperature, the higher and the steeper are the heating curves, which is more prominent near the interface as indicated by T3 (Fig. 6.3.2a and 2b).

67

6.3.1.2 Cooling curves of castings

Fig. 6.3.4a and b show the effect of pouring temperature on temperature-time profiles of thermocouple at A for initial mean mould temperatures of 82 C and 107 C, respectively. It reveals that the higher is the pouring temperature, the higher is the T1max. Solidification time as indicated by the cooling curves, T1-t, is higher for higher superheat.

Fig. 6.3.5a and b show the effect of pouring temperature on temperature-time profiles, T2-t, at B for initial mean mould temperatures of 82 C and 107 C, respectively. The curves show that the holding time of T2 at the melting point is very insignificant as B is only 4mm from casting mould interface.

6.3.1.3 Heat flux

Fig. 6.3.6a and b show effect of superheat on the transient interfacial heat flux for initial mean mould temperatures of 82 C and 107 C, respectively. The heat flux curves are similar in nature with that of bar shaped and plate shaped castings.

The position of the peak of heat flux curve is found to be related to the filling time. The peak heat flux is obtained at the end of filling. As in the case of bar and plate shaped castings the surface temperature, Tc, indicates that the casting surface may form solidified skin (as shown in Fig. 6.3.7, MT- 107 C, Tc- 657.6 C) or may remain liquid nearly at melting point (as in Fig. 6.3.8, MT-107 C, Tc- 670 C) at HFmax (end of filling). Fig. 6.3.9 shows that the slope change in Tm occurred at HFmax.

Fig. 6.3.10 shows the difference of Tc and Tm (Tc-Tm) with time. The difference falls sharply upto HTCmax, after that, it decreases slowly.

6.3.1.4 HFmax

Fig. 6.3.11 shows the effect of superheat on HFmax for different initial mould temperatures. It shows that HFmax increases with the increase of both superheat and mould temperature. Higher superheat yields higher HFmax due to higher difference

68

of Tc and Tm at the interface and may be due to better contact at the interface. Higher mould temperature yields higher HFmax because of better contact. HFmax can be related with SH as follows:

HFmax = 364956 + 1612(SH)   for 82 C MT

HFmax = 511929 + 1312(SH)   for 107 C MT

6.3.1.5 Heat transfer coefficient

Figs. 6.3.12a and b show the effect of superheat on HTC-time curves for 82 C and 107 C initial mean mould temperatures, respectively. The figures reveal that the HTC increases from a minimum value to a maximum value (HTCmax). The peak HTC correspond to the end of filling (at the time of occurrence of HFmax) due to maximum metallostatic pressure. After that it decreases rapidly and then very slowly. The sharp decrease from HTCmax might be due to decrease in metallostatic pressure, non-conforming contact and probably initiation of gap.

6.3.1.6 HTCmax

Fig. 6.3.13 shows the variation of HTCmax with the variation of superheats for different initial mean mould temperatures. It reveals that HTCmax increases with the increase of both the superheat and mould temperature. The cause of higher mould temperature yielding more HTCmax may be due to better contact at higher superheat and higher mould temperature. For the simulation of solidification of pure lead upon lamp-black coated water cooled brass, Durham and Berry (13) assumed higher constant HTC for higher superheat. HTCmax can be related to SH as follows:

HTCmax = 402.02 + 7.14 (SH)   for MT-82 C

HTCmax = 721.95 + 8.38 (SH)   for MT- 107 C

6.3.1.7 Solidification time

Fig. 6.3.14 shows the effect of superheat on solidification time at initial mean mould temperatures of 82 C and 107 C. Like plate shapes castings, the solidification time increases with the increase of superheat. The effect of mould temperature is not observed.

Theoretical calculation (art 3.3.2) shows that for a constant HTC the solidification time increases quadratically with the increase of superheat. But HTC increases with the increase of superheat (Fig. 6.3.12a and b) and therefore slope of t_f-time curve decreases gradually with the increase of superheat.

Assuming constant HTC throughout the solidification process it has been observed (art 3.3.2) that solidification time increases with the increase of initial mould temperature, but in practice, the estimated HTC has been found to be higher for higher initial mould temperature (Fig. 6.3.13), which tends to decrease solidification time. Therefore, for the initial mean mould temperature of 82 C and 107 C, the opposite effect balances each other showing no remarkable effect of initial mould temperature on solidification time. Mohan (33) found that the solidification time increases marginally with the increase of initial mould temperature for cast iron in cast iron mould. Din (90) carried out experiments with ZA27 alloy casting in cast iron mould and found solidification time to increase about 20% when mould temperature was increased from 150 C to 200 C and about 117% when mould temperature was increased from 200 C to 250 C.

Din's (90) graphical representation reveals that the effect of mould temperature on solidification may not be observed or may be insignificant for lower mould temperature as in the range of 82 to 107 C.

CHAPTER 7

CONCLUSIONS

The following conclusions may be drawn from the present theoretical and experimental investigations.

THEORITICAL INVESTIGATIONS

Based on the theoretical investigations, the following conclusions are drawn:

1. Solidification time decreases with the increasing mould thickness upto a critical value, called semi-infinite mould thickness, above which, the solidification time is not affected by the mould thickness.

2. Solidification time increases with the increase of interfacial thermal resistance.

3. Solidification time increases quadratically with the increase of casting thickness. superheat of molten metal, and initial mould temperatures.

4. Aluminium in CI mould solidifies ahead of Aluminium in sand mould due to higher thermal diffusivity of CI than that of sand.

5. The solidification time is the highest for zinc and the lowest for aluminium. The solidification time of copper is in between zinc and aluminium. Copper solidifies ahead of zinc, because of higher melting point and thermal diffusivity of copper.

8 Experimental and simulated results of Al castings in semi-infinite sand mould are in good agreement.

EXPERIMENTAL WORK

Based on the experimental investigations, the following conclusions are drawn:

Bar shaped casting

1. Initially the temperature of the inner surface of the chill increases at the same rate for all the chill thicknesses, but for higher superheat of molten metal, the rate becomes faster. The effect of chill thickness on heating curves is

observed after the heat reaches the external end, but the effect of superheat on it is felt from the early stage of heating.

2.   Interfacial heat flux increases from a low value to a peak value (HFmax). The HFmax is obtained at the end of filling due to maximum metallostatic pressure.

3.   The HFmax is not affected by the chill thickness when it is more than certain limiting value.

4.   HFmax increases with the increase of the superheat of molten metal. The effect of superheat on HF, diminishes with time after the occurrence of HFmax.

5.   The effect of chill thickness on HF-time curves is observed after some time from the occurrence of HFmax. It increases with the increases of chill thickness.

6.   The effect of chill thickness on total heat flux is significant for higher superheat, it decreases as the superheat decreases.

7.   HTC is higher for higher superheat of molten metal.

8.   No remarkable effect of chill thickness on HTC is observed.

Plate shaped casting

1.   The temperature of the inner surface of the mould initially increases at the same rate for all casting thicknesses, but the rate becomes faster at higher superheat of molten metal. The effect of casting thickness on heating curves is observed after an initial period, but the effect of superheat on it is felt from the early stage of heating.

2.   Superheat affects cooling curve initially, but casting thickness affects it after an initial period.

3.   HFmax occurs at the end of filling due to maximum metallostatic pressure.

4.   HFmax is not affected by the casting thickness.

5.   The higher is the superheat, the higher is the HFmax. The effect of superheat on HF, diminishes at later stage.

Cylindrical shaped casting

1. The higher are the superheat and initial mould temperature, the higher and steeper are the heating curves.

2. The higher are the superheat and initial mould temperature, the higher are the HFmax and HTCmax.

3. The higher is the superheat, the higher is the solidification time. The slope of the solidification time-superheat decreases with the increase of superheat.

4. There is no significant effect of initial mould temperature on the solidification time in the range of 82 to 107 C of initial mould temperature.

SUGGESTIONS FOR FUTURE WORK

The following suggestions can be made for better understanding:

1. A semi-infinite mould model with different mould-metal combinations should be developed using transient heat transfer coefficient and should be verified experimentally.

2. The effect of filling time on HF and HTC should be studied.

3. The effect of very thin mould on solidification of castings should be studied.

4. The effect of initial mould temperature on solidification of casting should be thoroughly studied.

5. The effect of cooling at the external surface of mould on interfacial heat transfer, structure and surface texture of casting should be studied.

6. The effect of organic coating at the mould/chill surface on interfacial heat transfer and solidification of casting should be studied.

7. The interfacial heat transfer for 3-D object at various locations should be evaluated.

8. By applying pressure after the end of filling, the occurrence of HFmax and HTCmax for different superheat of molten metal should be studied.

REFERRENCES

1. Chvorinov, R., "Theory of Solidification of Castings", Giesserei, p.177, (1940).

2. Berry, J. T. , Effects of Solidification Conditions on Mechanical Behaviour of Aluminium Cast Iron, AFS Trans. vol. 78, p.421, (1970).

3. Sirilertworakul, N., Webstar, P.D. and Dean, T. A., Computer prediction of location of heat centres in casting, Materials Sci. and Tech., vol. 9, p.923, (October 1993).

4. Darwish, S.M. H., Computer assisted riser design and Placement, Int. J. Mater. Prod. Techol., vol. 1, p. 43, (1997).

5. Chiesa, F., Mammen, J., and Smiely, L.E., Use of solidification modelling to predict porosity, distribution in Al A356 industrial casting, 102nd Annual Meeting of AFS, Atlanta, GA, USA, (10-13 May 1998)

6. Prabhu, K.N., Madheswaran, D., Kumar, T.S.P, and Venkataraman, N., Computer Modelling of Heat Flow and Microstructure Fineness in Chill-Cast Aluminium alloy LM-24, AFS Trans,. vol. 100, p. 611, (1992).

7. Kumar, T.S.P and Prabhu, N.K., "Heat Flux Transient at the Casting /Chill Interface during Solidification of Aluminium Base Alloy, Met. Trans. B, vol. 22B, p.717, (October 1991).

8. Prabhu, K.N., Srinivas, and Venkataraman, N.. Effect of Casting/Mould Wall/Casting thickness on Heat Transfer and Solidification of Al-Cu-Si Alloy (LM21) in Cast Iron Moulds, . AFS Trans,. vol.102, p. 94, (1994).

9. Prabhu, K.N., Srinivas, and Venkataraman, N., Effect of Mold Parameters on Solidification Behaviour of Al-Cu-Si alloy (LM21) Cast Iron Molds, 41st Indian Foundry congress, The institute of Indian Foundryman, New Delhi, p. 337, (Feb., 1993).

10. Ho, K. and Pehlke, R. D., Mechanism of Heat Transfer at a Metal-   Mould Interface, v. 92, p.587, (1984).

11. Ho, K. and Pehlke, R. D., Transient methods for Determination   of Metal- Mould Interfacial Heat Transfer, AFS Transaaactions, vol. 91, p. 689, (1983).

12. Ho K. and Pehlke, R. D., Metal-Mould Interfacial Heat transfer, Met. Trans., vol.16B, p. 585, (1985).

13. Durham D. R. and Berry, J.T. , Role of the Mould-Metal Interface During Solidification of A Pure Metal Against a Chill, AFS Transactions, vol. 82, p. 101, (1974).

14. Tillman, E. S., and Berry, J.T., Influence of Thermal Conduct Resistance on the Solidification of Long Freezing Range alloys, AFS Cast Metals Research Journal, p.1, (Mar 1973).

15. Issac, J. Reddy G.P. and Sharma, G. K., "Variations of Heat Transfer Coefficients during Solidification of castings in Metallic Moulds", The Britishman, p. 465, (November 1985).

16. Sully L. J. D., The Thermal Interface Between Casting and Chill Moulds, AFS Transactions, vol. 84, p. 735, (1976).

17. Flemings, M.C., Solidification Processing, McGraw-Hill, USA, (1974).

18. Cambell, J., Castings, Butterworth-Hienmann Ltd., Oxford, p.126, (1991).

19. Askeland, D.R., The Science and Engineering of Materials, 2nd SI ed.. Chapman and Hall, London, p. 226, (1990).

20. Irani D. R. and Kondic V., Casting and Mould Design Effect on Shrinkage porosity in Light Alloys, AFS Trans., vol. 77, p.208, (1969).

21. Srinivasan, M.N, Seshardi, M.R. and Ramachndran, A., " Studies on solidification of Non-ferrous castings in metal in metal Moulds", AFS Cast Metals Research Journal, p.23, (March1971).

22. Srinivasan, M.N, Seshardi, M.R. and Ramachndran, A., "Thermal Aspect of Metallic Moulds". AFS Trans., vol. 78, p. 395, (1970).

23. Issac, J., Reddy G.P. and Sharma, G. K., "Experimental Investigation of the influence of casting Parameters on the Formation and Distribution of Airgap during the Solidification of Castings in Metallic Moulds", AFS Trans., vol. 93, p.29, (1985).

24. Nehru, KVK, Seshadri M.R., and Ramchndran, E.G., Influence of Insulating Mould Coatings on the solidification of Copper Castings in Metallic Moulds and Thermal Behaviour of Moulds", AFS Cast Metals Research Journal., p.111. (September 1974).

25. Issac, J. Reddy G.P. and Sharma, G. K., "Numerical Simulation of Solidification of Castings in Metallic Moulds", AFS Trans., Vol. 93, p. 123, (1985).

26. Thamban M.I. and Panchanathan V., "Numerical Simulation of Solidification of Al Alloys in Cast Iron Moulds", AFS Trans., vol. 88. p. 167, (1980).

27. Kuttamba, R.G.V. and K. Panchanathan V., "End Chills Influence on Solidification Soundness of Al-Cu-Si (LM4) Alloy Castings", AFS Cast Metals Research Journal., p.135, (September 1973).

28. Thamban, M.I., Gopalakrishna, S. and Panchanathan V., "Thermal Behaviour of Cast Iron Moulds with Long Freezing Range Aluminium Alloy, AFS Trans., vol. 87, p. 171, (1979).

29. Prabakar K.V. and Seshardi M.R., " Influence of Chills on the Soundness of Al-12%Si Alloy Castings", AFS Trans., vol. 87, p. 377, (1979).

30. Shrinivasan, M.N., "Heat Transfer Coefficient at the Casting Mould Interface During Solidification of Flake Graphite Cast Iron in Metallic Moulds", Indian Journal of Technology, vol. 20, p. 123, (April, 1982).

31. Mohan V. and Senoy, R. N., " Prediction of Solidification Time of Iron Castings in Metallic Moulds", AFS Trans., vol. 90, p.435, (1982).

32. Nehru, K.V.K., "Studies on the influence of Mould Coats on Solidification of Copper and Gunmetal castings in Metallic Mould", Ph.D Thesis, IIT, Madras-36, (July 1974).

33. Mohan, V., "Studies on Some Aspect of Permanent Moulding (Gravity Die Casting of Cast Iron", IIT, Madras-36, (September 1981).

34. Chinnathambi K., "Feeding Aluminium Base Alloy in Metallic Mould", Ph.D, Thesis, IIT Madras-36, (1979).

35. Pathak S.D., Feeding Efficiency Parameters and Feeding Range for Aluminum Base Alloys Cast in Metallic Moulds', Ph.D, Thesis, IIT Madras-36, (1984).

36. Veinik, A. I., Thermodynamics for Foundrymen MaClaren, London, (1968).

37. Prates, M. and Biloni, H., Variables Affecting the Nature of the Chill-Zone, Met. Transactions 3A, p. 1501, (1972).

38. Morales, A., Glicksman M.E. and Biloni H., "Influence of Mould Wall Micrgeometry on Casting Structure", Solidification and Casting Metals, The Metal Society, London, p.184, (1979).

39. Assar, A. M., "Mould Surface Roughness and Interfacial heat transfer using hcay flow model", Materials Science and Tech., vol. 13, p.702,(August 1997).

40. Prabakar K.V., Seshardi M.R., and Srinivasan, M.N, "Studies on Solidification of Al-Cu Castings in Coated Dies and Thermal Behaviour of the Dies", AFS Trans. vol. 82, p.387, (1974).

41. Gafur. M. A. and Haque, N, "Effect of Process Variable on Solidification Time of Zinc and Copper," Proceedings, The First APM'94, BIT Khulna, October 26-29. p. 384, (1994).

42. Patterson W., Engler S., and Dietz G., " Solidification of Copper Tin Alloys", Giesserei Tech. Beih. GiesserWelt. Metallurgia, p. 1617, (1960).

43. Durham , D.R., Verma D. and Berry J.T., "Some Further Observation on freezing From Chills". AFS Trans. vol. 84, p.787, (1976).

44. Srinivasan, M.N, Seshardi, M.R. and Ramachndran, A., " Solidification of Simple Shaped Castings in Metallic Moulds", British Foundryman Society. vol. 59, p.314, (July 1966).

45. Chatterjee, S. and Das, A. A., "Effect of Pressure on the Solidification of Some Commercial Aluminium-Base Casting Alloys", British Foundryman, vol. 65 (11), p.420, (November 1972).

46. Chatterjee. S. and Das, A. A., "Some observations on the Effect of Pressure on the Solidification of Al-Si Eutectic Alloys", British Foundryman, vol. 66 (4), p.118, (April 1973).

47. Davies, V. de L., Heat Transfer in Gravity Die Casting. British Foundryman 73, p. 331, (1980).

48. Ayyampernumal, M.. "Feeding Bar and Cylindrical Castings of Aluminium Base Alloys in Metallic Moulds", Ph. D Thesis, IIT Madras-36, (1984).

49. Bishop, H.F., Barant, F.A., and Pellini, W.S., "Solidification of Steel Against Sand and Chill Walls," AFS Trans.m vol. 59, p.435, (1951).

50. Bishop, H. F., Barant, F.A., and Pellini, W.S ., Solidification Mechanism of Steel Ingots, J. of Metals,   p.45, (Jan 1952).

51. Savage, L. H. W. and Fowler, R. T., Ingot Heat Conservation. JISI, p. 119, (Feb 1953).

52. Fisher, G. A., Solidification and Soundness Prediction for   Larger Steel Ingot, Proc. ASTM, p. 1137. (1962).

53. Jeyarjan, A. and Pehlke, R. D., Computer Simulation of   Solidification of a Casting with a Chill, AFS Transactions.   vol.   84, p. 647, (1976).

54. Watanabe, S. et al., Heat Transfer in a Continuous Casting   Mould, Testu Hagane,   vol.   58, No. 11, lectures 109 and 110,   p. 5393, Bruchter Translation   No. 8906, (1972).

55. Pehlke, R. D.. The interface in Computer Simulation of Heat Transfer in Metallurgical Process, Metals Engr. Quaterly, p. 9, (1971).

56. Hanzel, J.G., and Keverian J., Gap Formation in Permanent Mould Casting, AFS Trans. Vol. 68, p373, (1960).

57. Deras, Rev. de Metall., p. 137, (June 1946).

58. Matuschka, B., Archiv f., Eisenhuttenwesen, vol. 2, p. 405, (January 1929).

59. Engler, S.. Boenisch, and Kohler, B., Metal and Mould Wall Movements During the Solidification of Cast   iron, AFS Cast Metal Research Journal, p. 20, (Mar 1973).

60. Levelink, H. G., Julien, F.P.M.A., AFS Cast Metal Research J., p. 56, (1973).

61. Campbell, J., Casting, BUTTERWORIH HEINEMANN Ltd, p. 90, (1991).

62. Nishida, Y., and Matsubara, H., Effect of Pressure on Heat Transfer at the Metal Mould-   Casting Interface, British Foundryman '69,   p. 274, (1976).

63. Rapier, A.C., Jones, T.M. and McIntosh, J.E., The Thermal Conduction of Uranium   Dioxide/Stainless   Steel   Interfaces, Int. J. Heat Mass Trans., vol. 6, p. 397, (1963).

64. Jacobbi, H., Influence of Different Gas Atmosphere in the   Gap in the Heat Transfer between Ingot and Water Cooled   Mould, Arch.   Eisenhuttenwes, 47, no. 6, p. 441, (1976).

65. Marrone, R. E., Wilkes, J.O. and Pehlke, R.D., Numerical Simulation of solidification, AFS Cast Metal Research J., vol. 6 (4), p. 184, (Dec. 1970).

66. R. D. Pehlke, Kirt, M.J., Marrone, R. E., and Cook, D. J., Numerical Simulation of Casting Solidification, AFS Cast Metal J., Vol. 9 (2), p. 49, (1973).

67. Marrone, R. E., Wilkes, J.O. and Pehlke, R.D., Numerical Simulation of solidification, AFS Cast Metal Research J., vol. 6 (4), p. 188, (Dec. 1970).

68. Jeyarjan A. and Pehlke R. D., Casting Design by Computer, AFS Transactions, vol. 83, p. 405, (1975).

69. Hou, T. X. and Pehlke, R.D , Computation of Solidification of a Steel Casting in a Sand Mould, AFS Transaction, vol. 95, p.477, (1986).

70. Hou, T. X. and Pehlke, R.D., Computation of Solidification of a Steel Casting Against a Chill Mould Wall, AFS Transaction, vol. 97, p.151, (1988).

71. Sun, R. C., Simulation and Smdy of Surface Conductance for Heat Flow in the Early Stage of Casting, AFS Cast Metals Research Journal, p. 117, (Sep 1973).

72. Alalem, K. A. T., Sharma. D.G.R. and Rahmat, A., Simulation of Casting Solidification in Metal, Int., Conference of RAMM. Parkroyal Penang, Malaysia, p. 111, (3-5 May,1994).

73. Sharma, D.G.R, Prabhakar, O., "Computer Simulation of Solidification With Feed Metal Transfer", Trans. Iim, vol. 38, p. 320. (August 1985).

74. Linacre, E.T., BISRA Report, Pe/A/2651, (August 1951).

75. Das, S. and Paul, A.J.. Determination of Interfacial Heat Transfer Coefficient in Casting and Quenching Using Solution Technique for Inversae Problems Based on the Boundary Element Method, Met. Trans B, vol. 24B, p. 1077, (1993).

76. Beck, J.V, Blackwell, B., and Charles R. St. Clair, Jr., Inverse Heat Conduction -Ill-posed Problems, Wiley Interscience, (1985).

77. Beck, J.V., Non-linear Estimation Applied to the Non-linear Inverse Heat Conduction Problem, Int. J. Heat Mass Trans., vol. 13, p. 703 (1970).

78.   Robertson, S.R. and Fascetts, Metall. Trans., B. 1997, vol. 8B, p. 619, (1997).

79.   Garcia, A., Clyne, T. W. and Parets, Metall. Trans., Vol. 10B, pp.85, (1972).

80.   Clyne, T. W. and Garcia, A., Int. J. Heat Mass Transfer, vol. 23, pp.773, (1985).

81.   Levy, S. A., Lipson, S. and Rosenthal; AFS Cast Metal Journal, vol. 8, p.1 (1972).

82.   Tu, J.S. , Inverse Heat Conduction Solution Using Two Dimensional Finite Element Solver, Proceedings of Winter Annual Session, p. 47, (1988).

83.   Gafur, M.A., and Haque, M.N., Computation of Solidification Time of Aluminium In Cast Iron Semi-infinite Mould Considering Perfect Contact between Casting and Mould, J. of IEB. vol. ME25-26, p. 44, (Dec. 1996-June 1997).

84.   Ohtusaka, Y., Mizuno and Yamada, J., Application of Computer Simulation System to Aluminium Permanent Castings, AFS Trans., vol. 89, p. 635, (1982).

85.   Heine, W.R. , Loper, C.R and Rosenthal, P.C., Principle of Metal Casting, Tata McGraw-Hill Publishing Co. LTD., New Delhi, TMH ed., p.180, (1976).

86.   Gafur, M. A., Haque, M.N. and Ferdous, D., Computation of Solidification Time of Aluminium in Semi-Infinite Sand Mould Considering Imperfect Contact between Casting and Mould, accepted for publication in the J. of Scientific and Industrial Research, Dhaka, Bangladesh.

87.   Gafur, M. A., and Haque, M.N. Computation Of Solidification Time of Copper in Semi-Infinite CI Mould Considering Imperfect Contact between Casting and Mould, accepted for publication in the J. of Scientific and Industrial Research, Dhaka, Bangladesh.

88.   Gafur, M. A., and Haque, M.N., Computation Of Solidification Time of Zinc in Semi-Infinite CI Mould Considering Imperfect Contact between Casting and Mould, accepted for publication in the J. of Science and Technology, BCSIR, Dhaka, Bangladesh.

89.   Rao, G.V.K. and Pannchanathan, V., Cast Metal Res. J., vol. 19 (3), p. 135, (1973).

90. Din, T.U., The effect of composition and Process variables on the microstructure, soundness and mechanical properties of Zn-27Al Alloy, Ph. D., Thesis, School of Metallurgy an Materials, University of Birminghum, p.59, (May 1991).

91. Ruddle, R.W., "The Solidification of Casting", 2nd. Ed, Ins. of Metal, London, 1957.
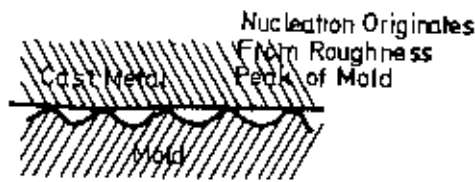
(a)
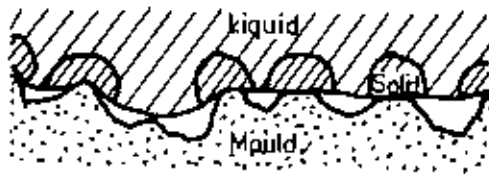
(b)
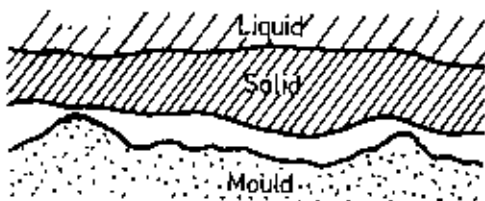
(c)
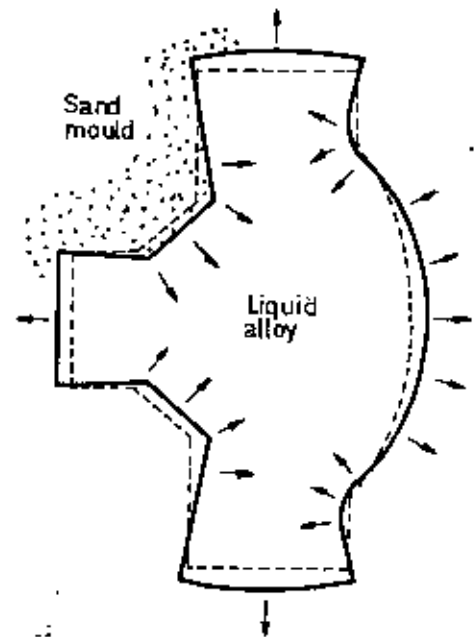
FIG. 2.1 INTERFACIAL CONDITION DURING SOLIDIFICATION OF CASTING : a) CONFORMING CONTACT, b) NON CONFORMING CONTACT, c) INTERFACIAL GAP (10)

FIG. 2.2 MOVEMENT OF MOULD WALLS, ILLUSTRATING THE PRICIPLE OF INWARD MOVEMENT IN CONVEX REGION AND OUTWARD MOVEMENT IN CONCAVE REGION (61)

Direct Problem

HF(0,t)

T(o,t)

Known B.C

BODY

L

HF(L,t)

T(L,t)

Known B.C.

Inverse Problem

HF(0,t)

T(0,t)

Unknown B.C.

BODY

HF(L,t)

T(L,t)

Known B.C.
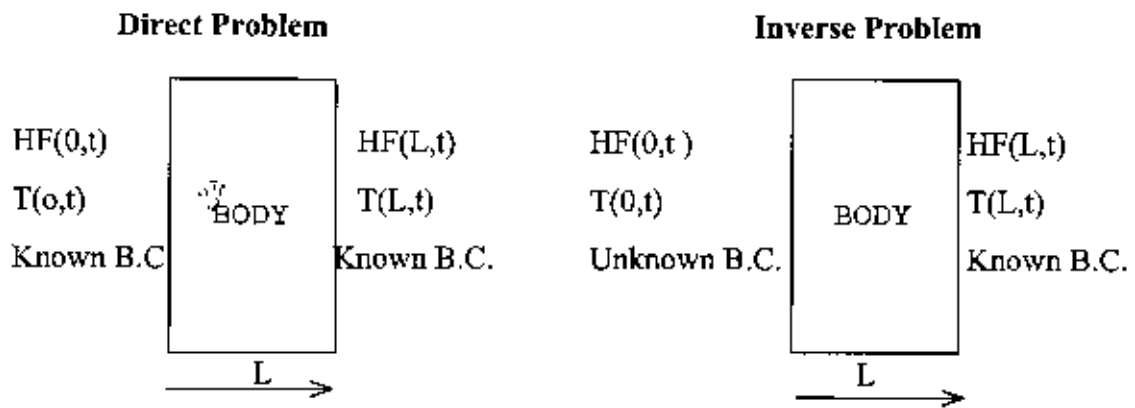
FIG. 2.3 COMPARISON OF DIRECT AND INVERSE PROBLEM

Tm (unknown)   Y3 (Known) Y4 (Known)

S   • C   •D

HF

Unknown

X1

X2

CASTING   MOULD /CHILL
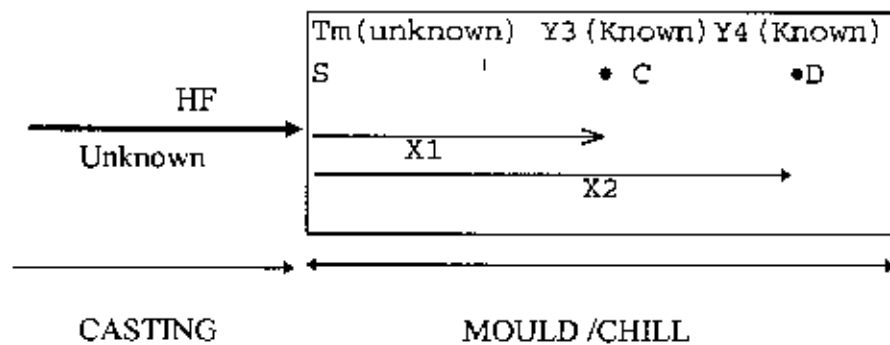
FIG. 2.4 INVERSE HEAT CONDUCTION PROBLEM IN 1-D HEAT FLOW
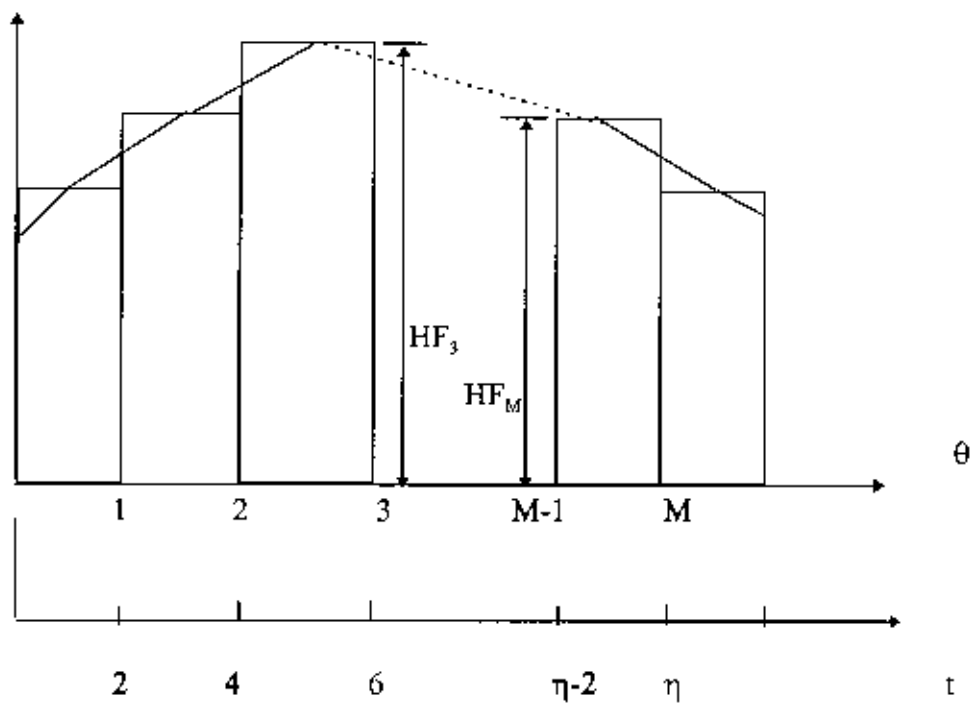
FIG. 2.5 APPROXIMATION OF HEAT FLUX BY DISCRETE VALUE
OF HF(77)

FIG. 3.1 FLOW CHART FOR TEMPERETAURE DISTRIBUTION IN CASTING AND MOULD

BEGIN

CM,MT, PT, AT, MT MMT CT ?

INPUT DX/DR, DT

CALCULATE NO OF NODES IN CASTING AND MOULD

ASSIGN ENTHALPY AND TEMP. FOR ALL NODES IN CASTING AND MOULD

CALCULATE NEW ENTHALPY FOR ALL NODES IN CASTING AND MOULD

CONVERT ENTHALPY TO TEMPERATURE AND ASSIGN TEMPERATURE FOR ALL NODES IIN CASTING AND MOULD

IS T1<(T₁-200 C)

NO

YES

STOP
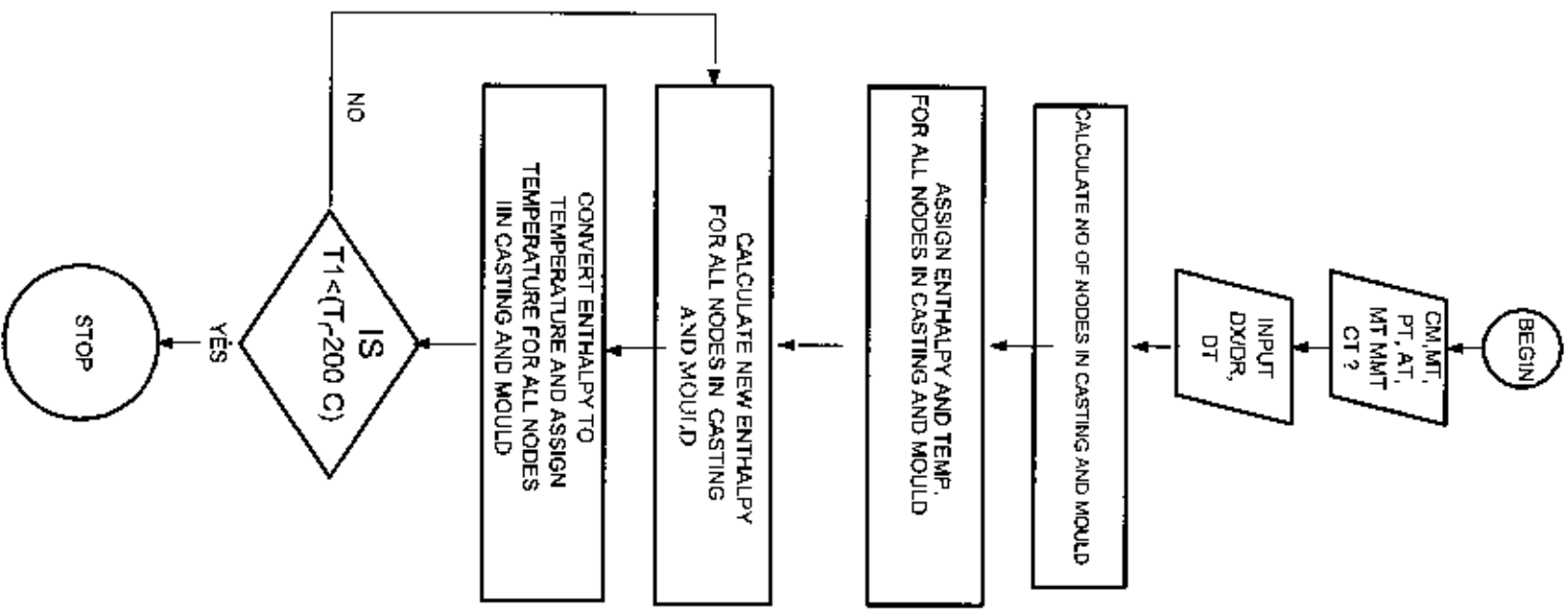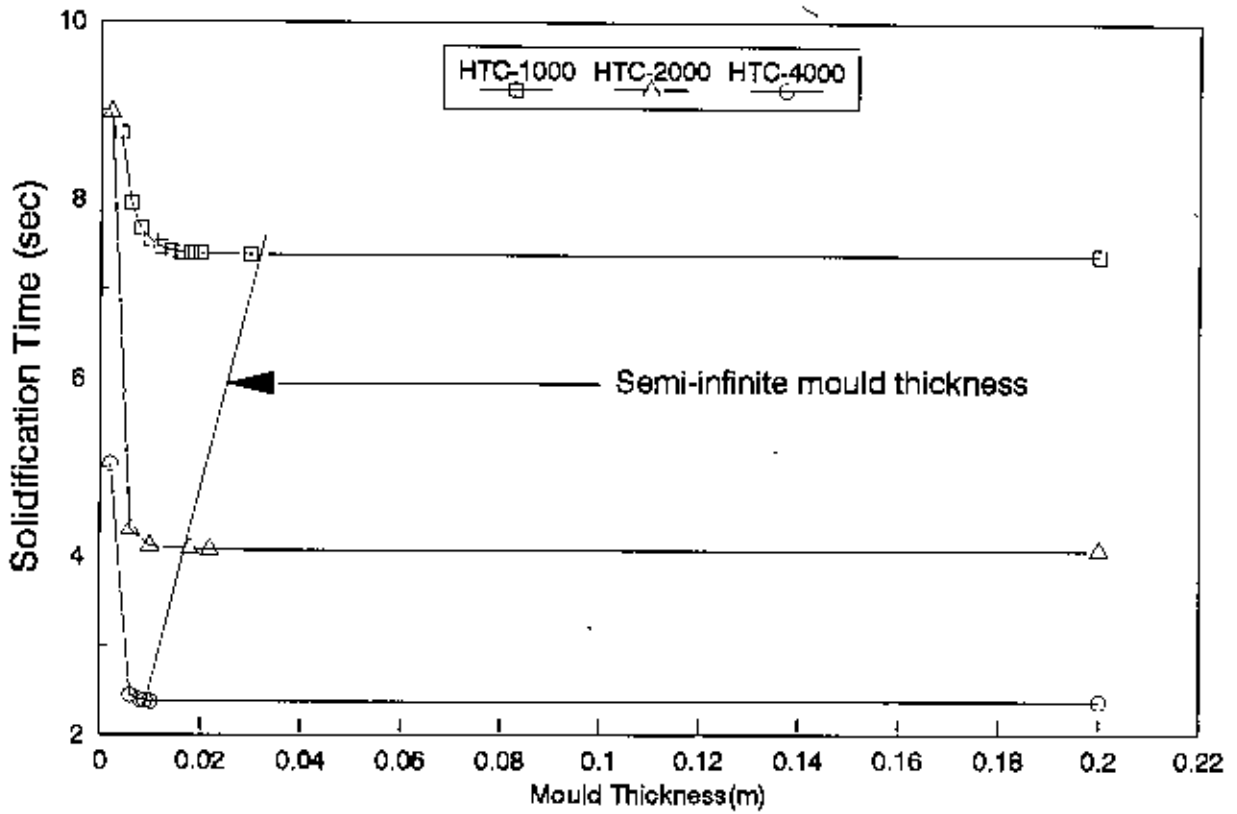
FIG. 3.1a EFFECT OF MOULD THICKNESS ON SOLIDIFICATION TIME

SHOWING SEMI-INFINITE MOULD THICKNESS FOR AI CASITNG IN CI MOULD
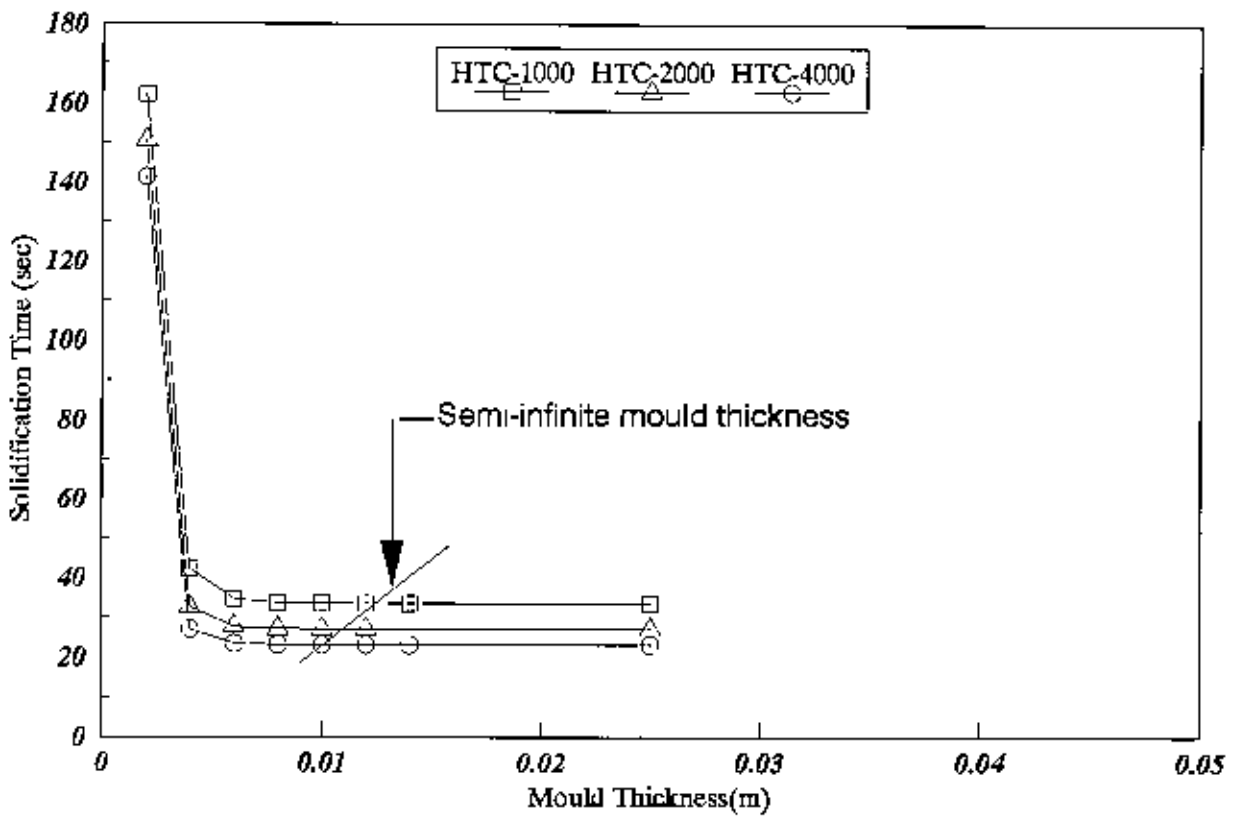
FIG. 3.1b EFFECT OF MOULD THICKNESS ON SOLIDIFICATION TIME
SHOWING SEMI-INFINITE MOULD THICKNESS FOR Al CASTING IN SAND MOULD
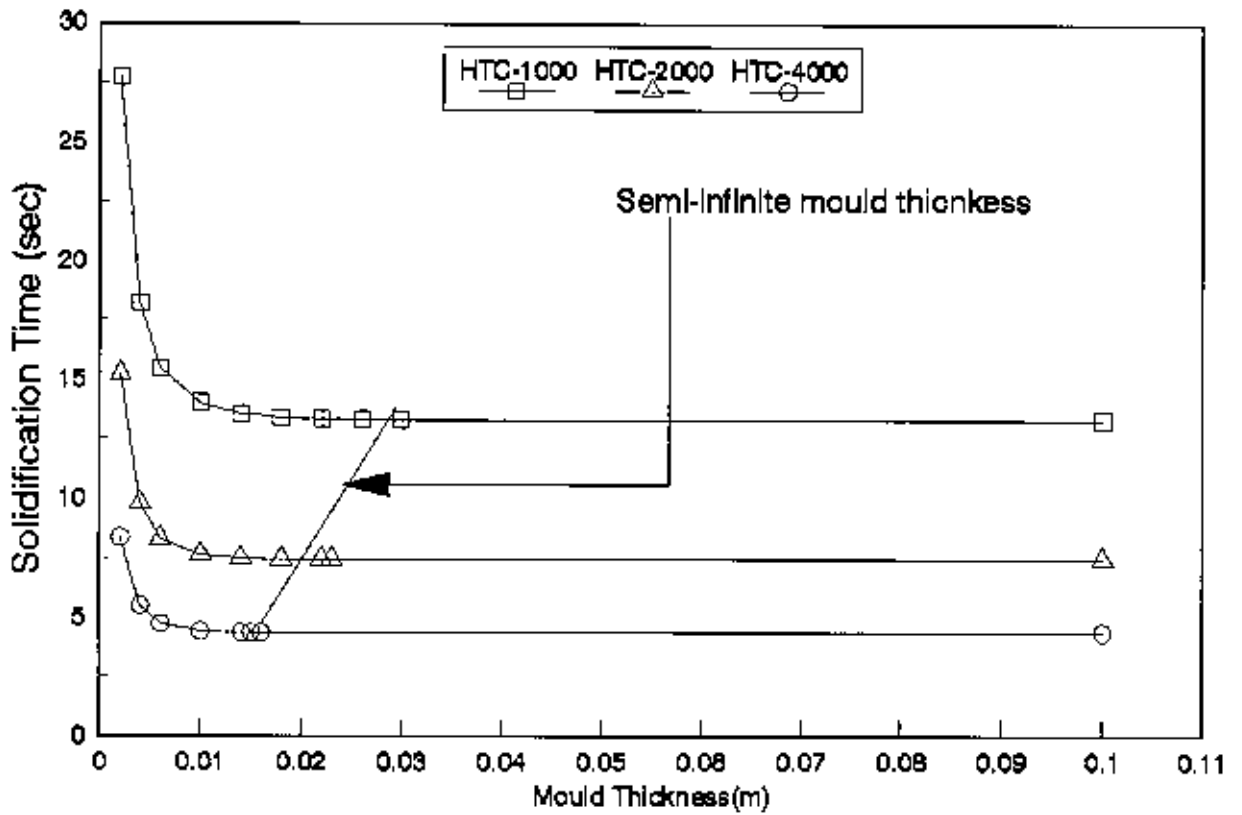
FIG. 3.1c EFFECT OF MOULD THICKNESS ON SOLIDIFICATION TIME
SHOWING SEMI-INFINITE MOULD THICKNESS for Cu CASTINGS IN CI MOULD
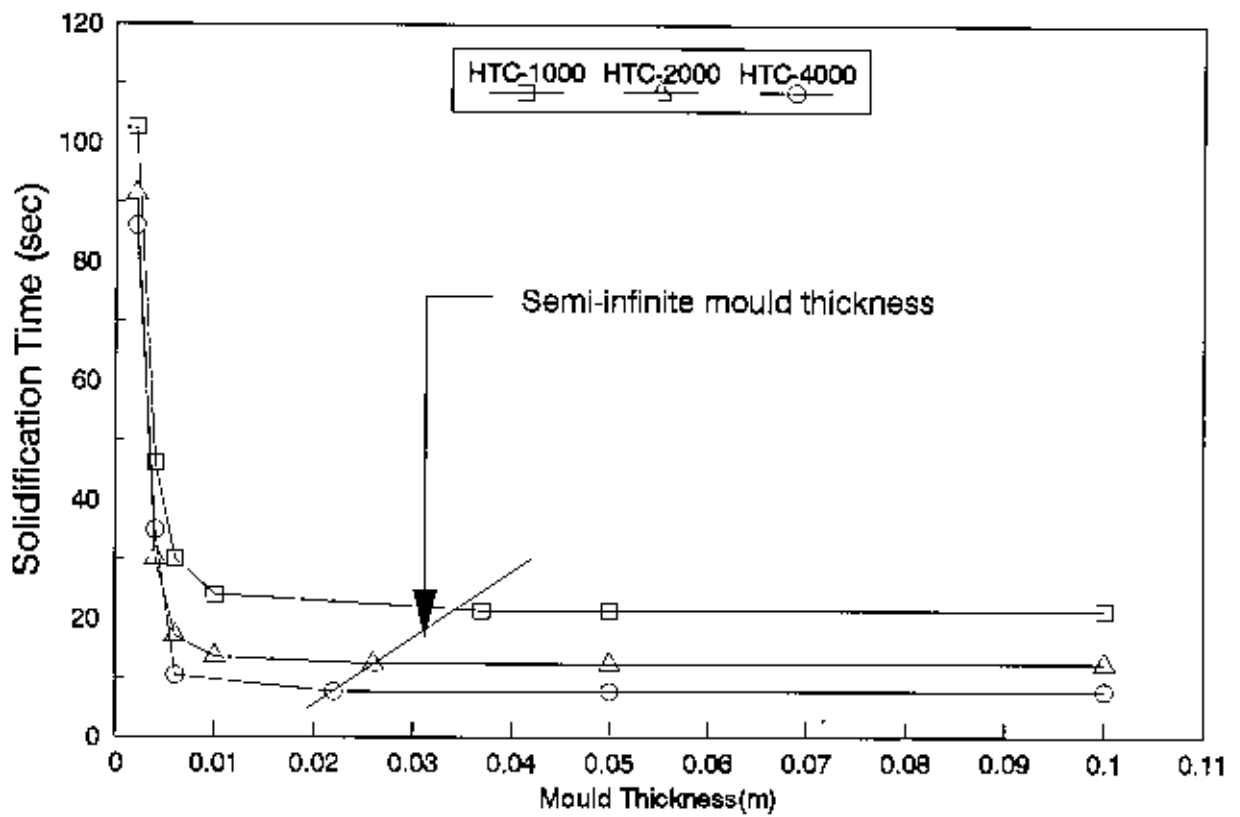
FIG. 3.1d EFFECT OF MOULD THICKNESS ON SOLIDIFICATION TIME
SHOWING SEMI-INFIMITE MOULD THICKNESS FOR Zn CASTINGS IN CI MOULD
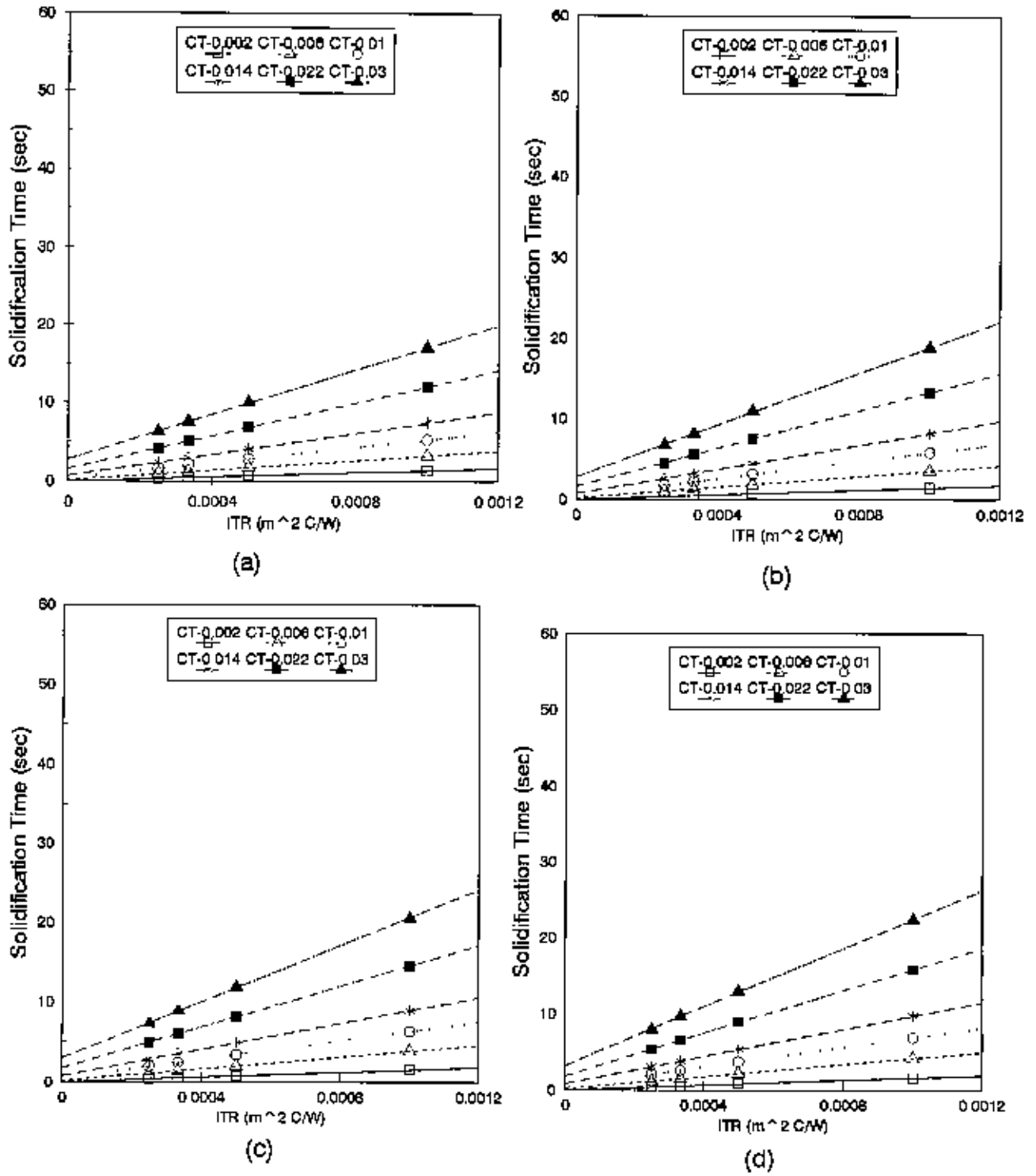
FIG. 3.2 EFFECT OF HEAT TRANSFER COEFFICIENT ON SOLIDIFICATION
TIME FOR 25 C MOULD TEMP. (a) SH=0 C, (b) SH=20 C,
(c) SH=40 C, (d) SH=60 C for Al CASTING IN CI MOULD
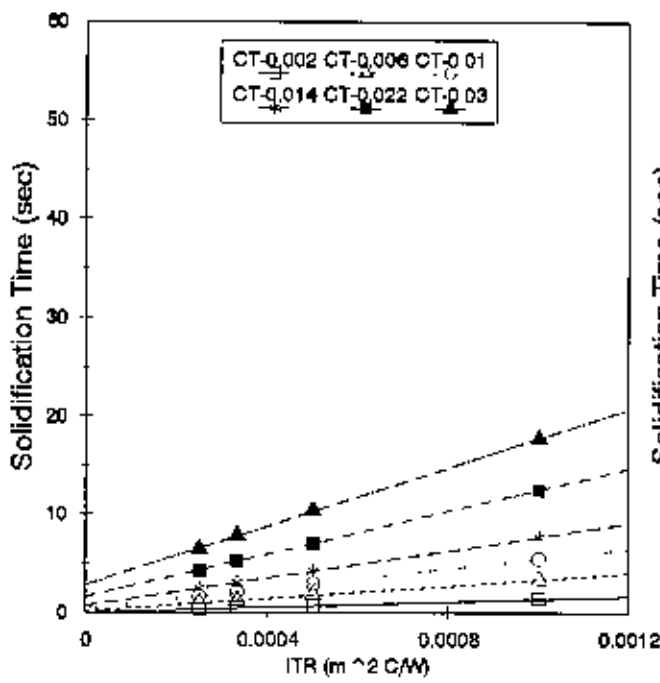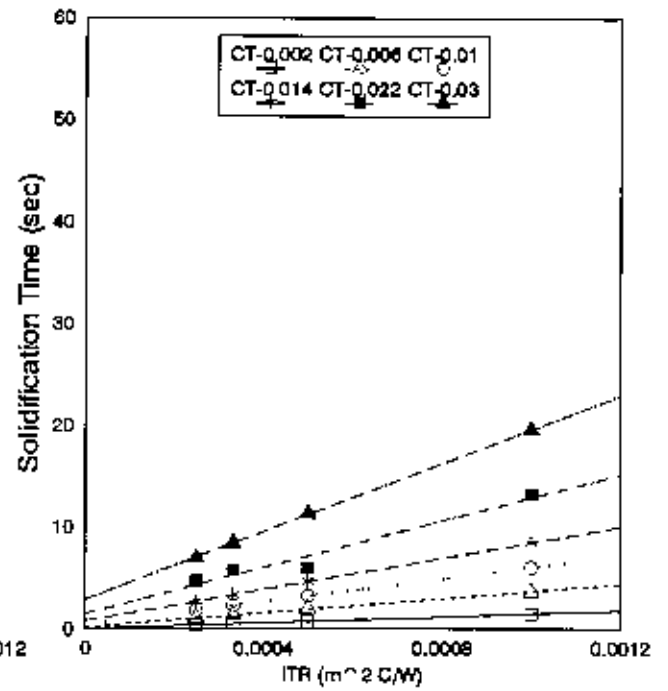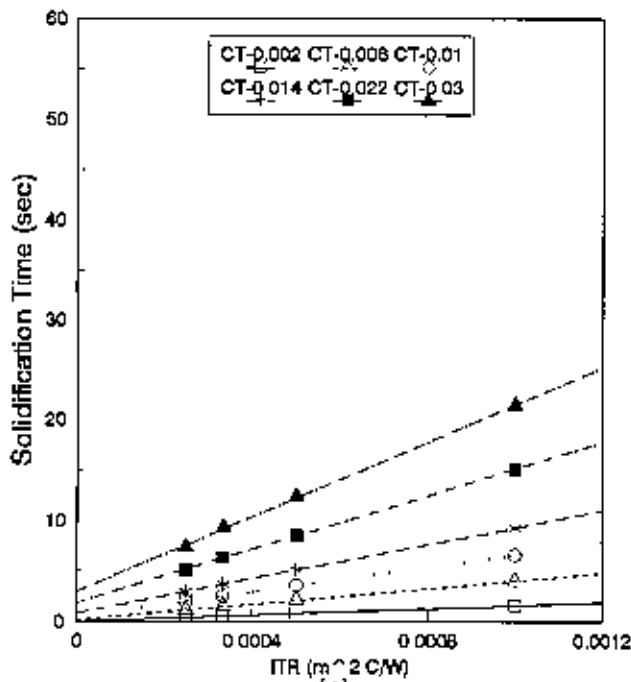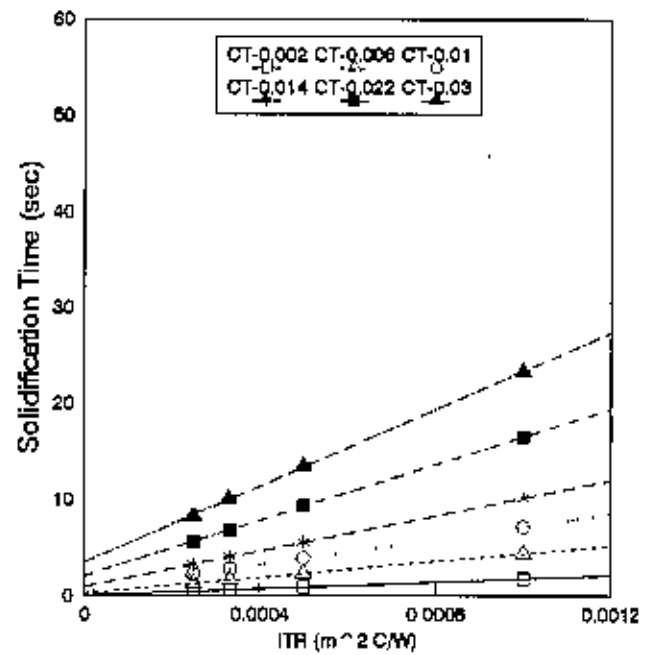
FIG. 3.3 EFFECT OF HEAT TRANSFER COEFFICIENT ON SOLIDIFICATION
TIME FOR 50 C MOULD TEMP (a) SH=0 C, (b) SH=20 C,
(c) SH=40 C, (d) SH=60 C FOR Al CASTING IN CI MOULD
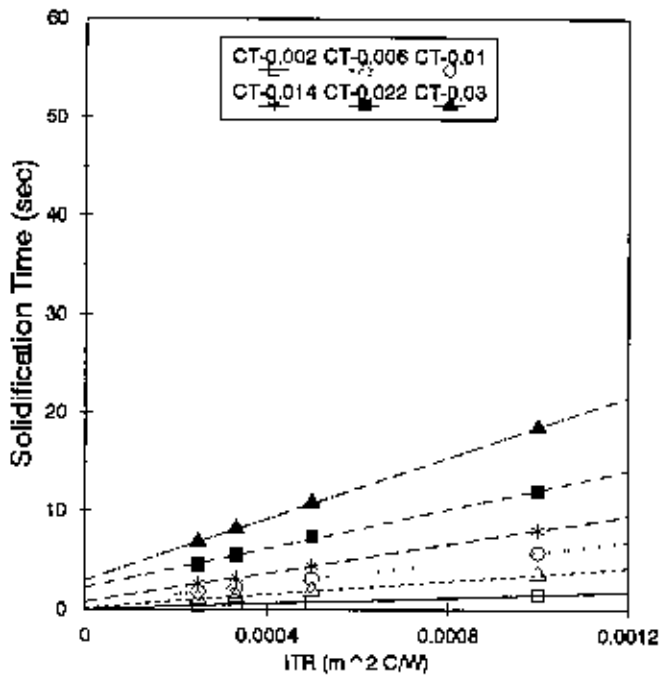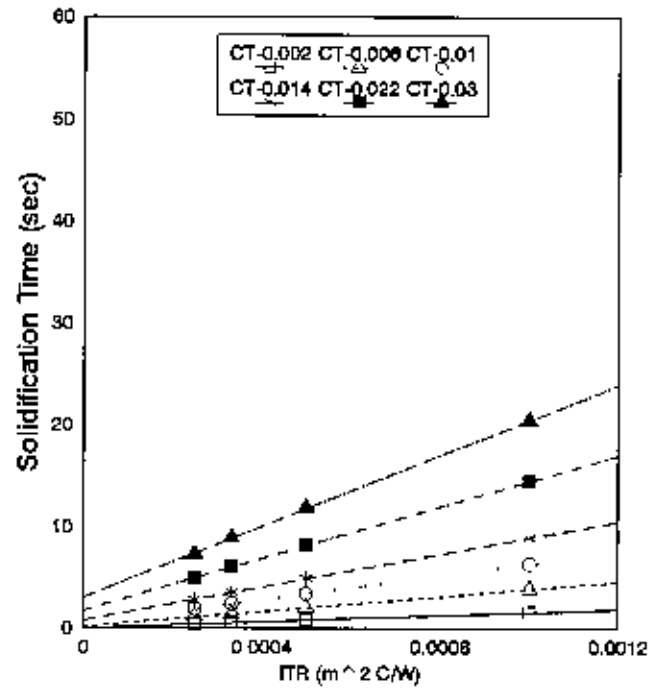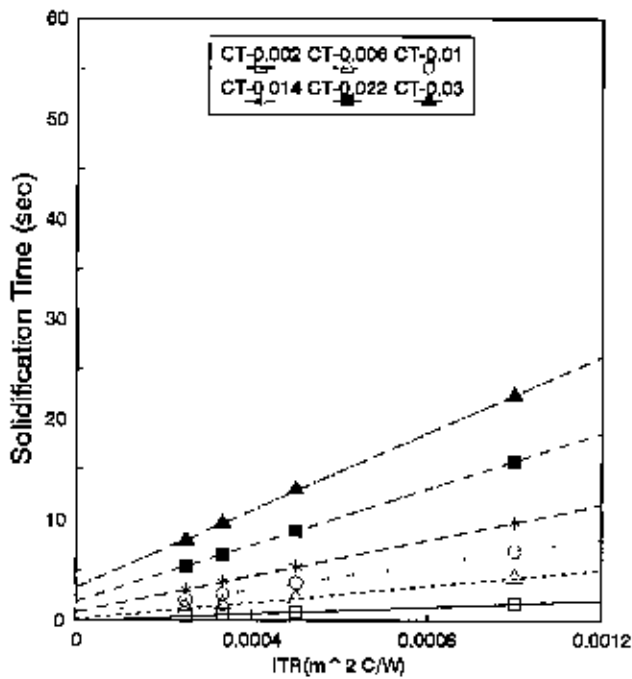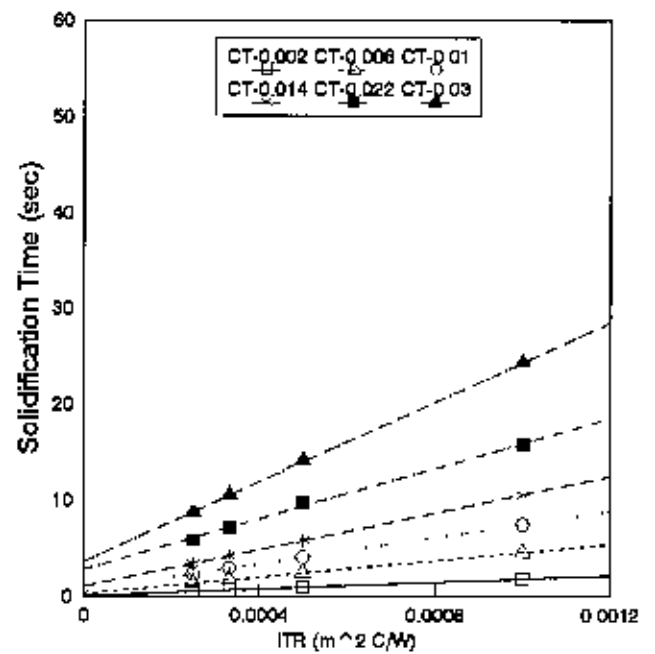
FIG. 3.4 EFFECT OF HEAT TRANSFER COEFFICIENT ON SOLIDIFICATION
TIME FOR 75 C MOULD TEMP. (a) SH=0 C, (b) SH=20 C,
(c) SH=40 C, (d) SH=60 C FOR Al CASTING IN CI MOULD
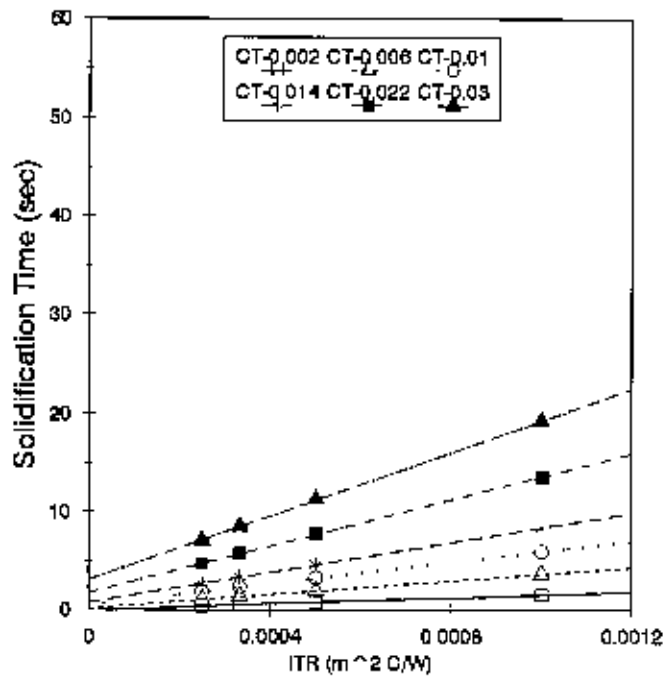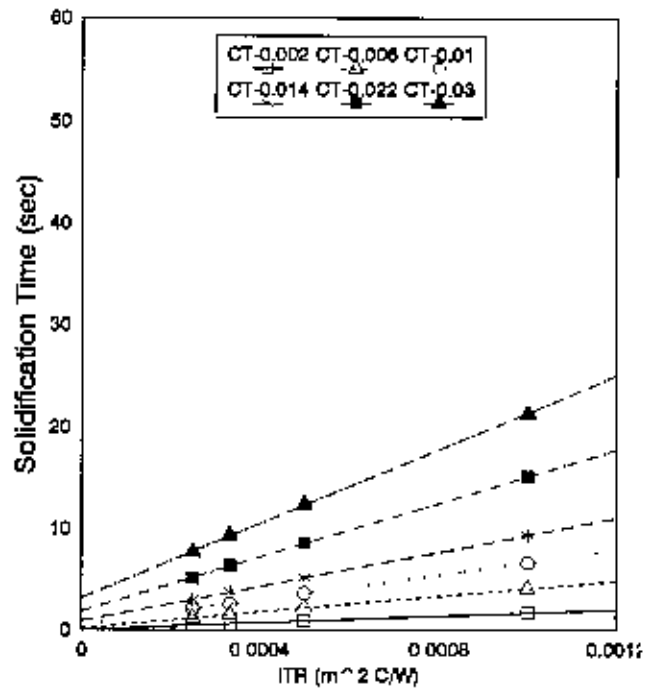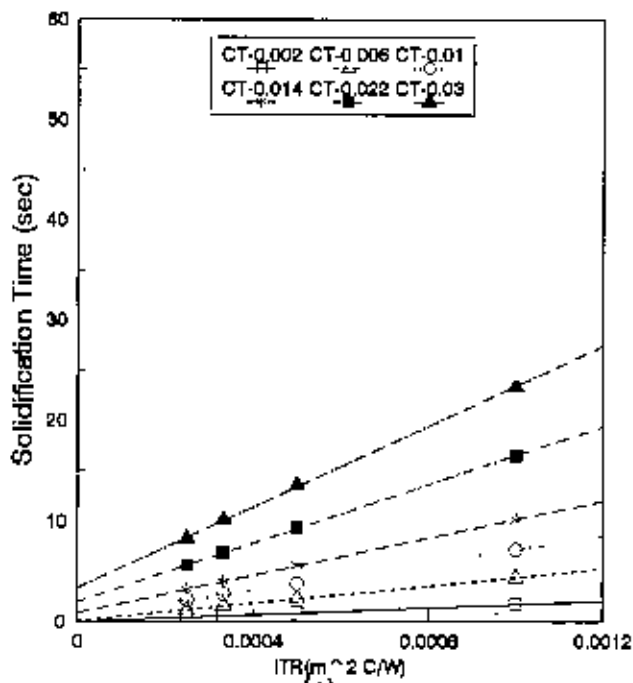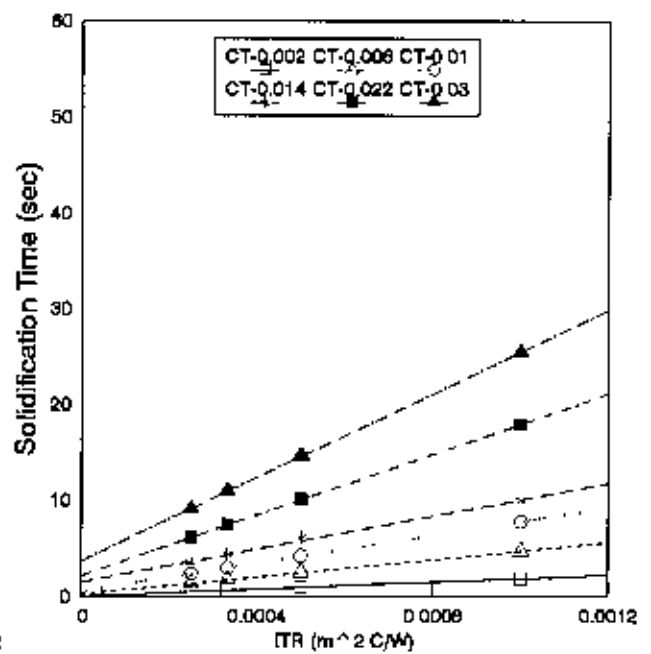
FIG. 3.5 EFFECT OF HEAT TRANSFER COEFFICIENT ON SOLIDIFICATION
TIME FOR 100 C MOULD TEMP. (a) SH=0 C, (b) SH=20 C,
(c) SH=40 C, (d) SH=60 C FOR Al CASTING IN CI MOULD
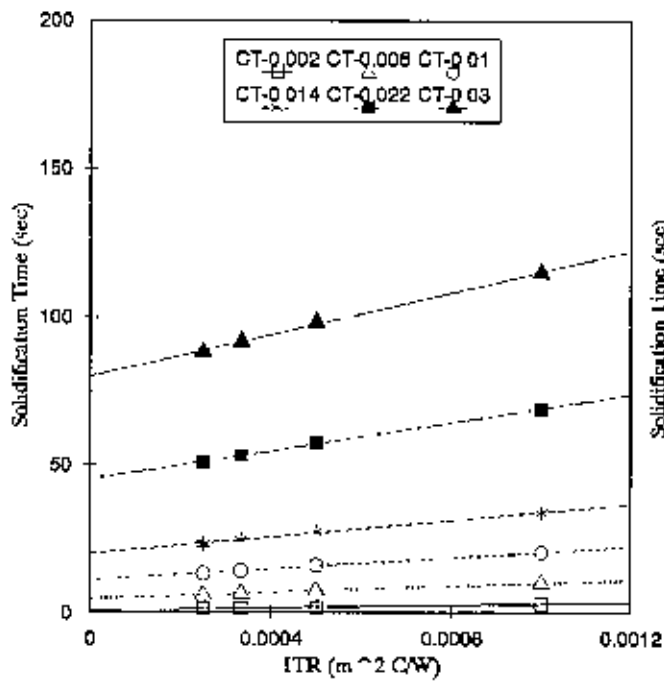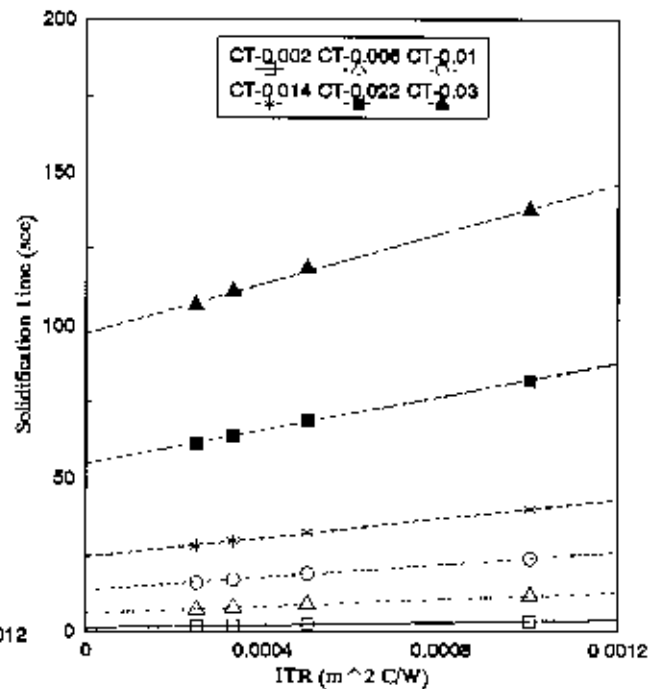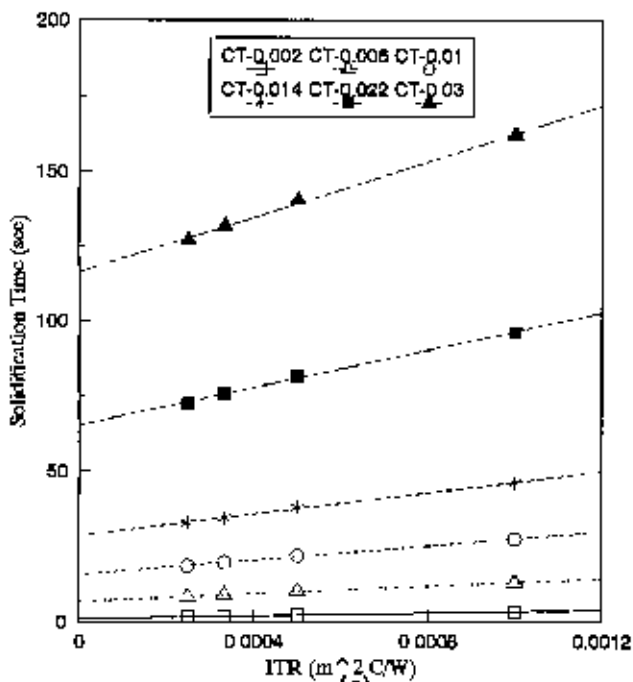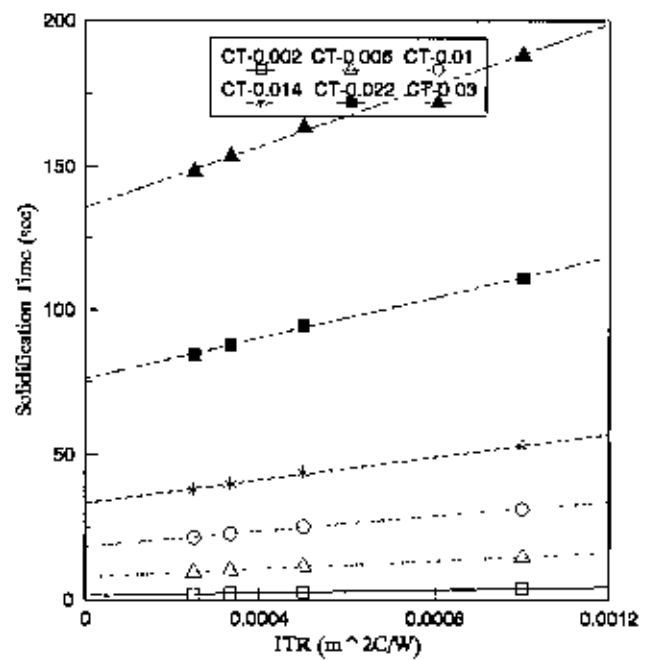
FIG. 3.6 EFFECT OF HEAT TRANSFER COEFFICIENT ON SOLIDIFICATION TIME
FOR 25 C MOULD TEMP.(a) SH = 0 C, (b) SH = 20 C, (c) SH = 40 C,
(d) SH=60 C FOR Al CASTING IN SAND MOULD
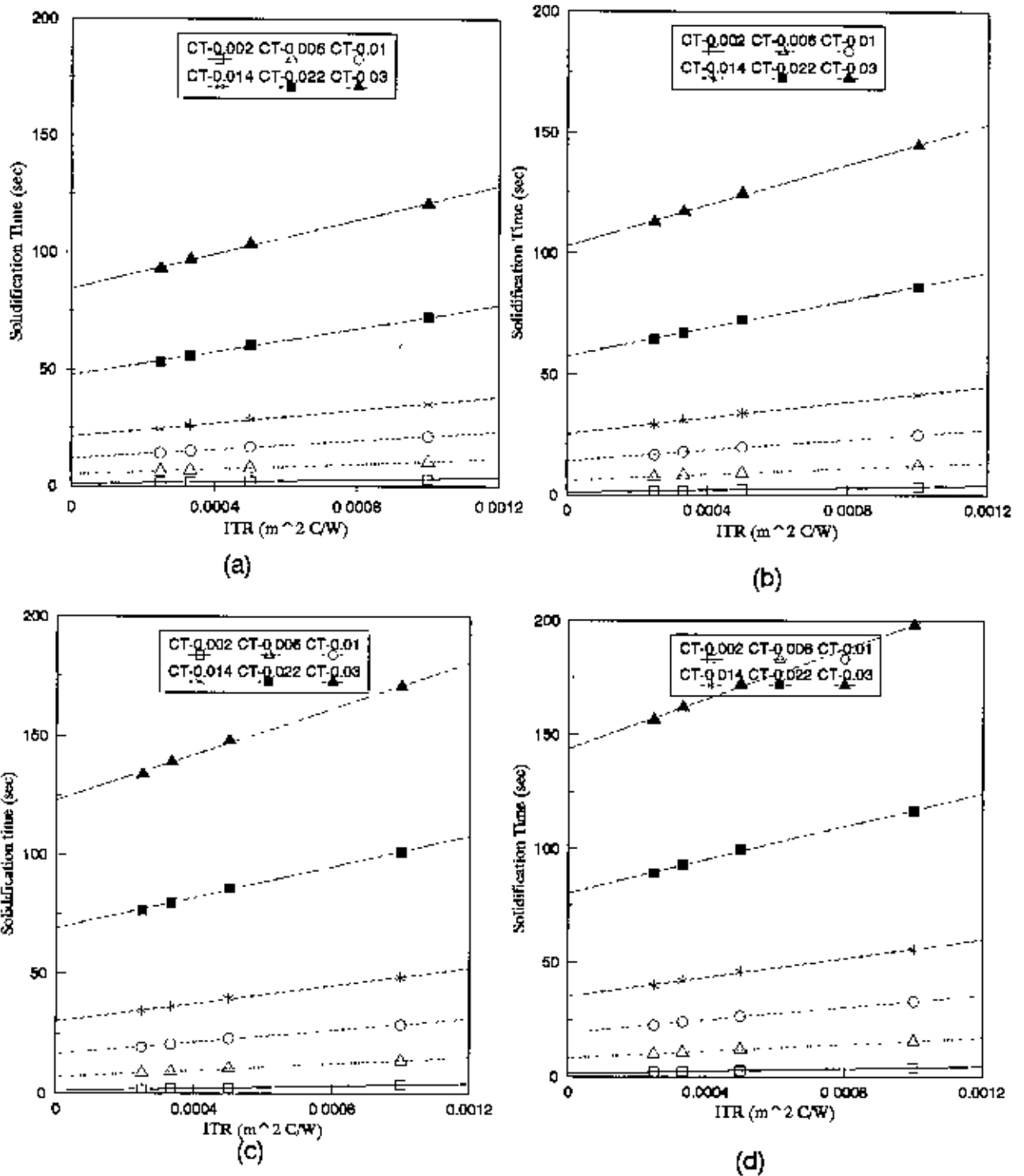
FIG. 3.7 EFFECT OF HEAT TRANSFER COFFICIENT ON SOLIDIFICATION TIME
FOR 50 C MOULD TEMP. (a) SH = 0 C, (b) SH = 20 C, (c) SH = 40 C, (d) SH = 60 C
FOR Al CASTINGS ON SAND MOULD
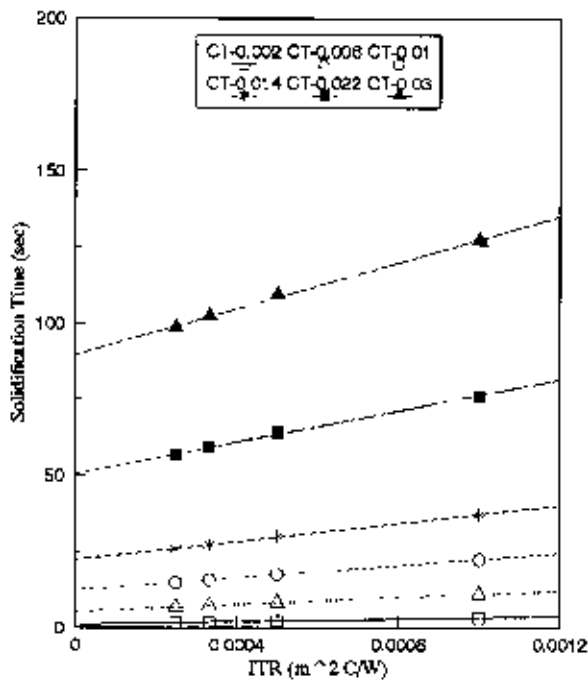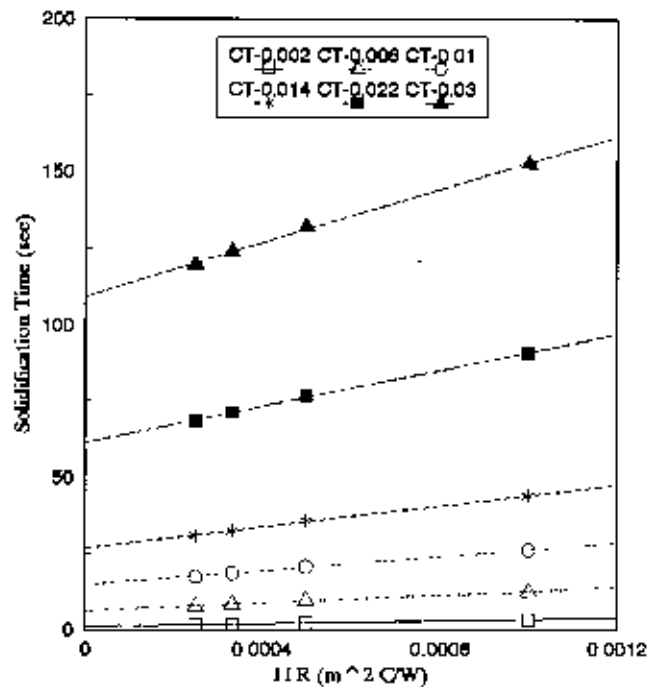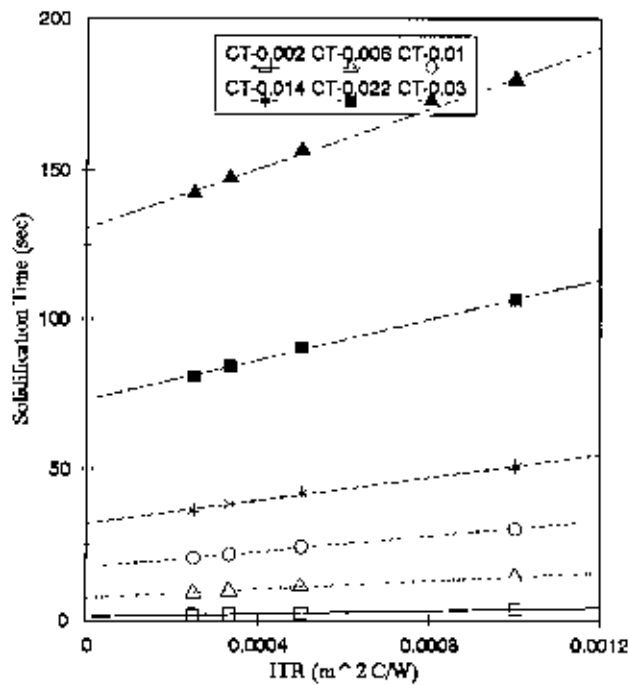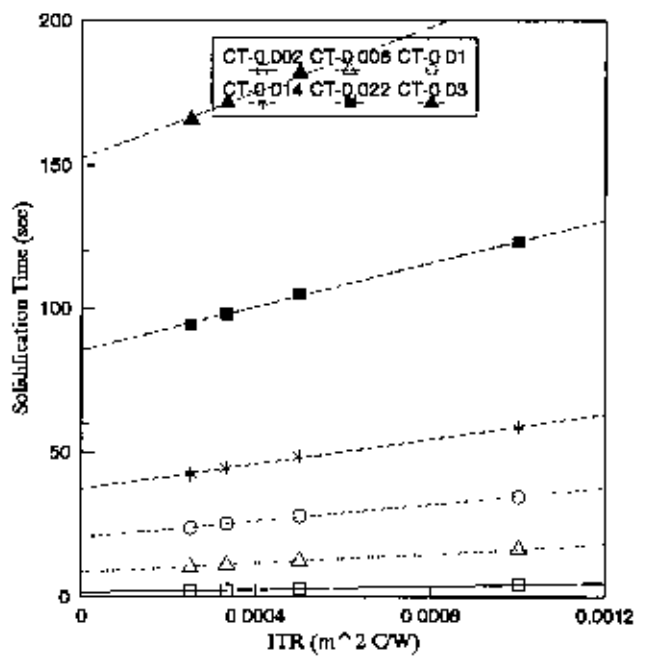
FIG. 3.8 EFFECT OF HEAT TRANSFER COEFFICIENT ON SOLIDIFICATION TIME
FOR 75 C MOULD TEMP. (a) SH = 0 C, (b) SH = 20 C, (c) SH = 40 C, (d) SH = 60 C
FOR Al CASTING IN SAND MOULD
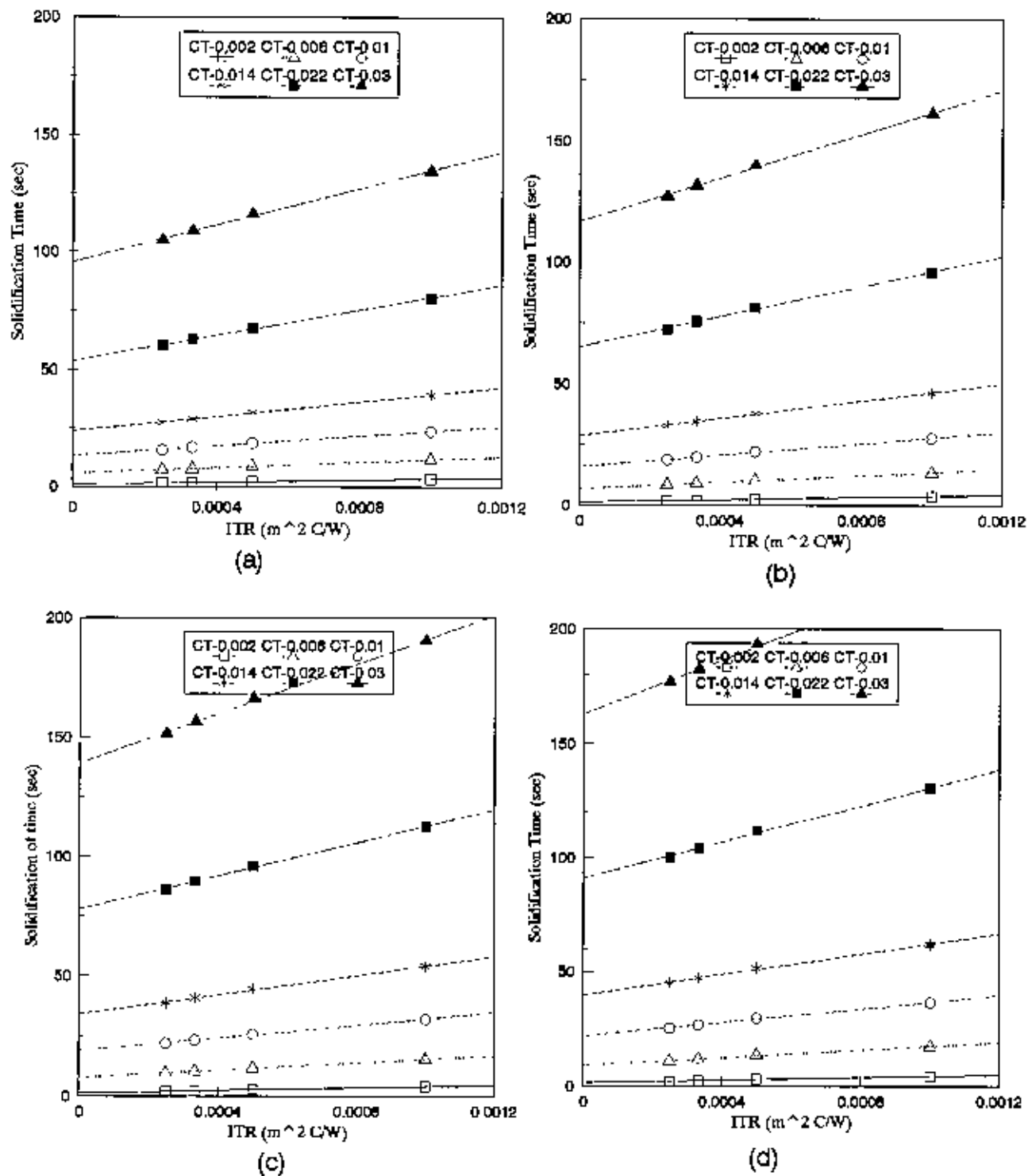
FIG. 3.9 EFFECT OF HEAT TRANSFER COEFFICIENT ON SOLIDIFICATION TIME
100 C MOULD TEMP. (a) SH = 0 C, (b) SH = 20 C, (c) SH = 40 C (d) SH = 60 C
FOR Al CASTINGS IN SAND MOULD
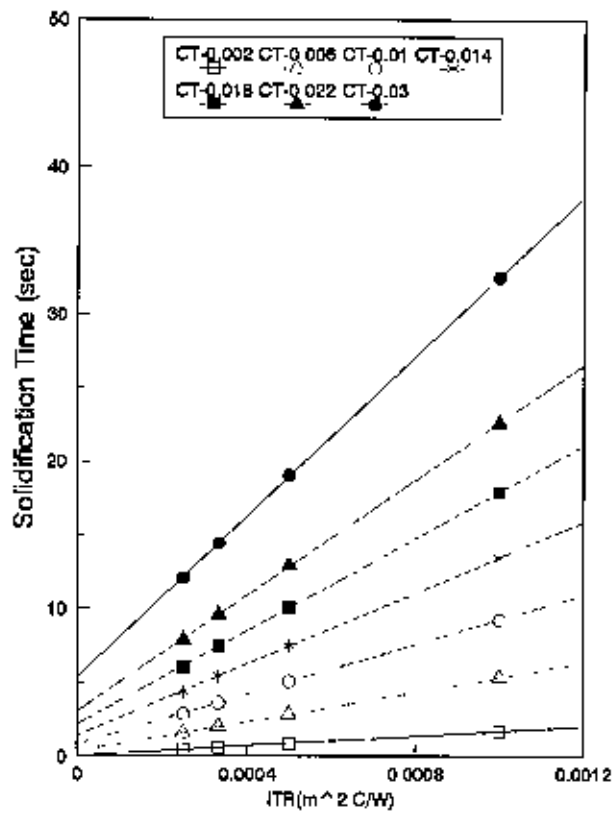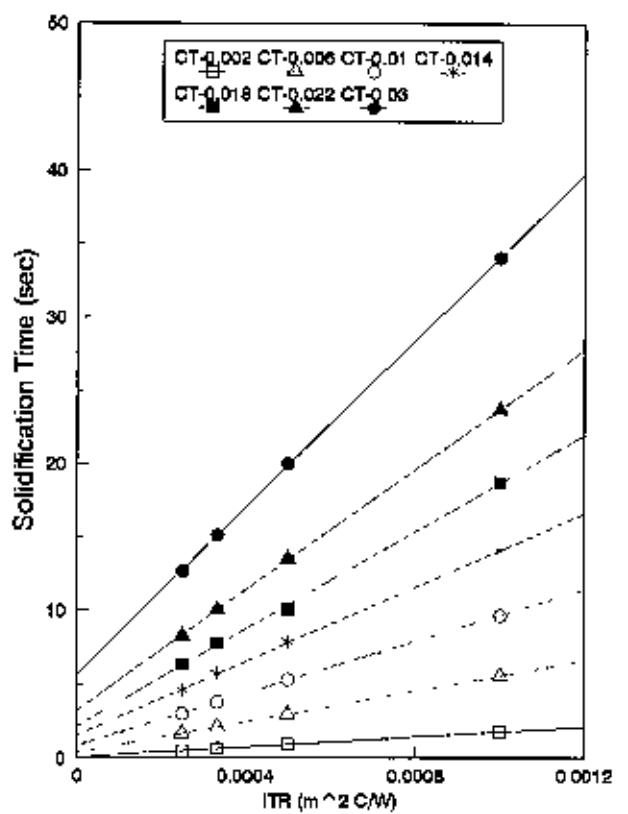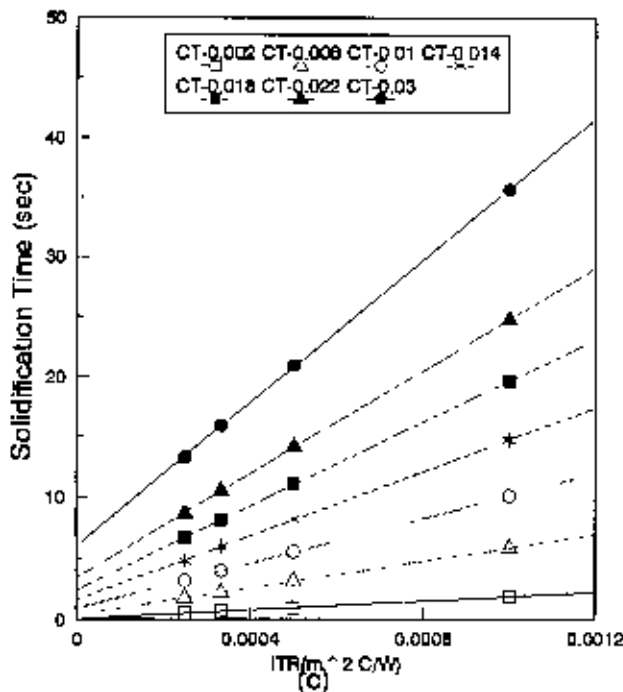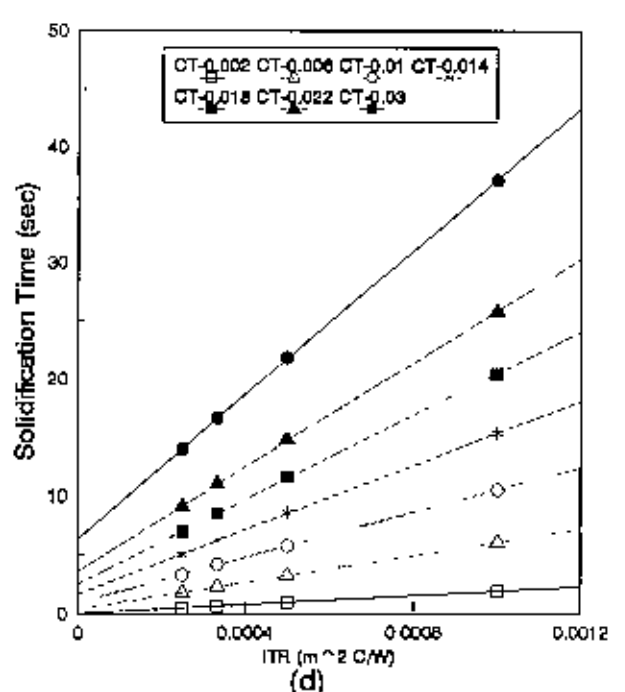
FIG. 3.10 EFFECT OF HEAT TRANSFER COEFFICINT ON SOLIDIFICATION TIME
FOR 25 C MOULD TEMP. (a) SH=0 C, (b) SH=20 C, (c) SH=40 C, (d) SH=60 C
FOR Cu CASTINGS CI MOULD
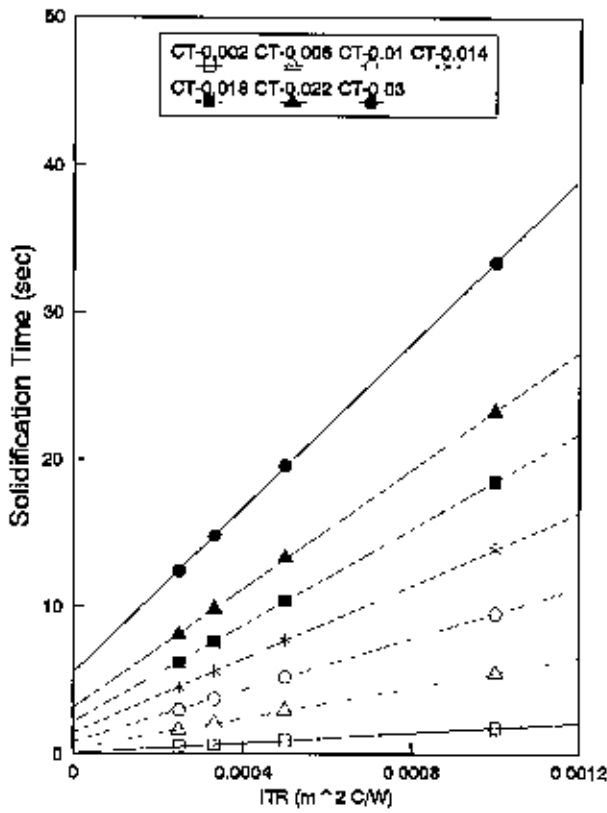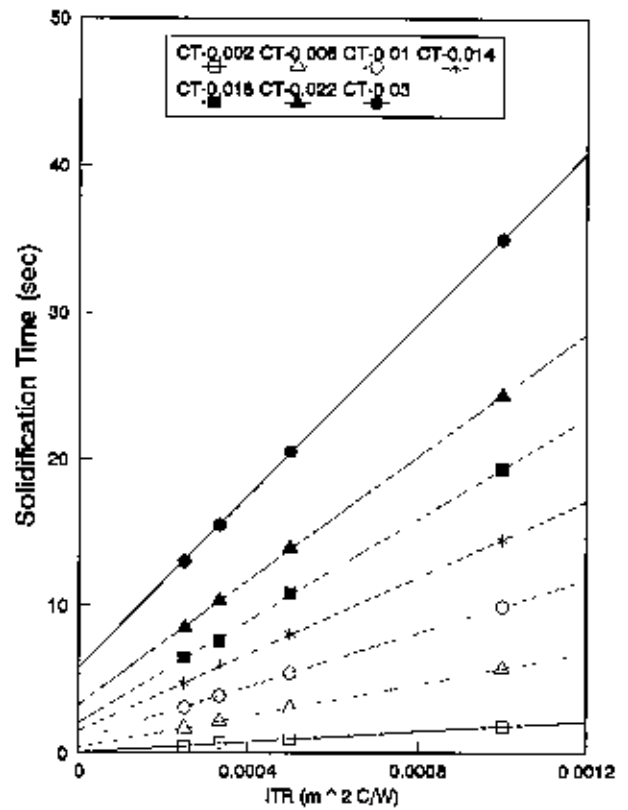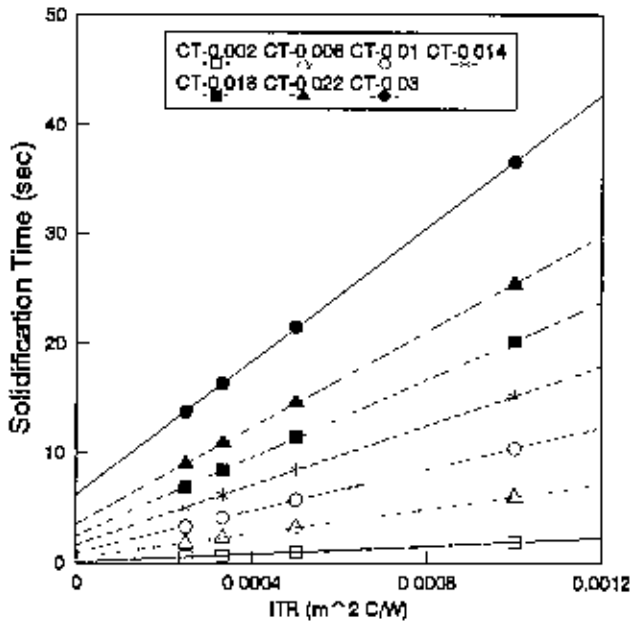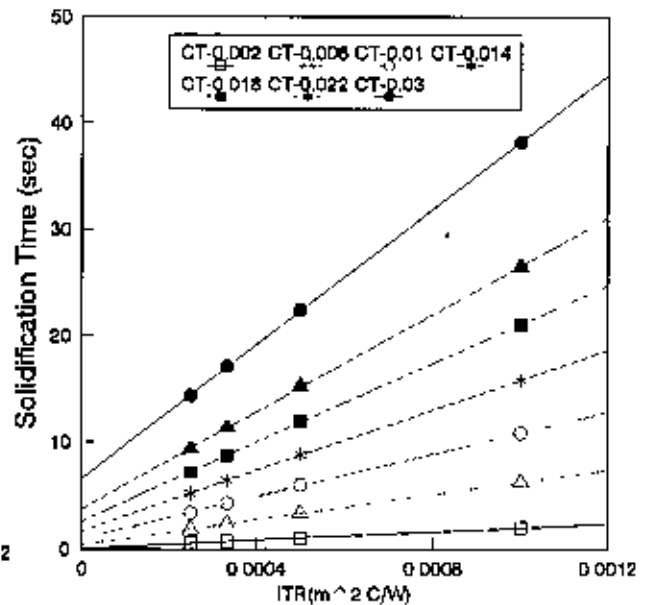
FIG. 3.11 EFFECT OF HEAT TRANSFER COEFFICIENT ON SOLIDIFICATION TIME
50 C MOULD TEMP. (a) SH=0 C, (b) SH=20 C, (c) SH=40 C, (d) SH=60 C
FOR Cu CASTINGS IN CI MOULD
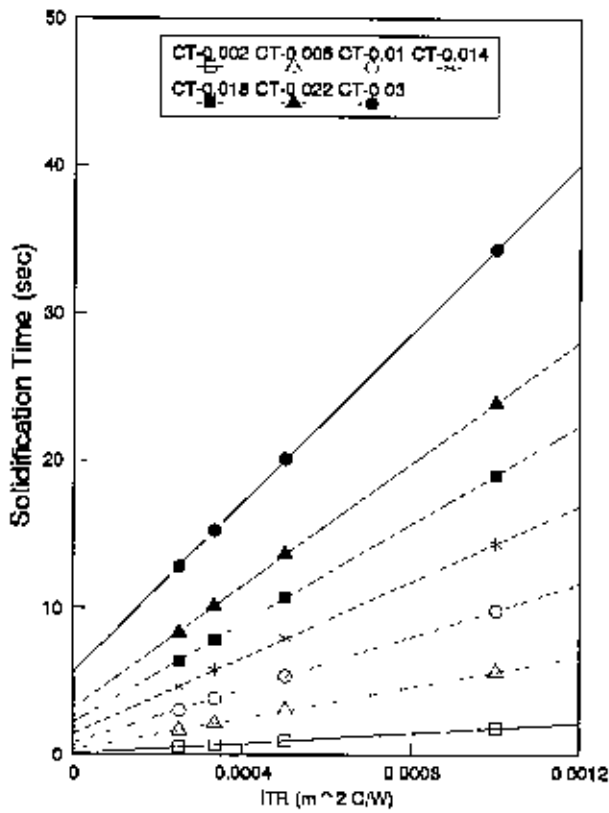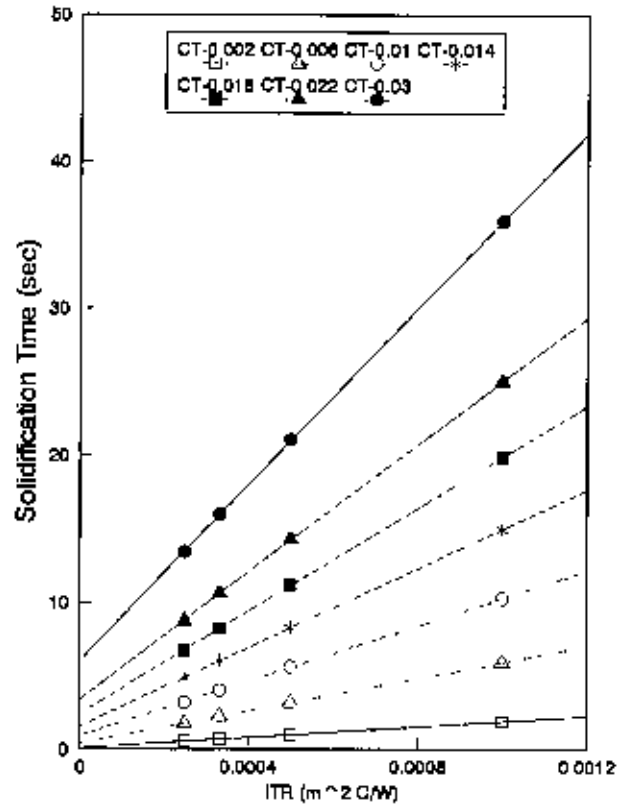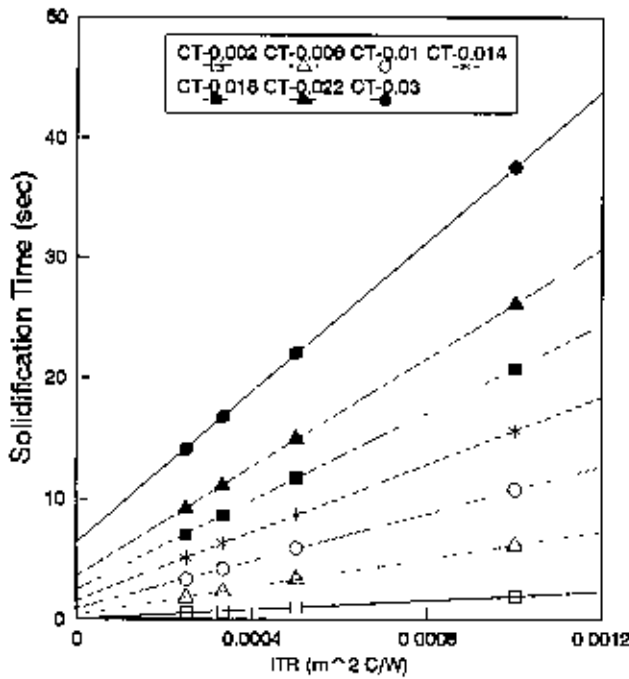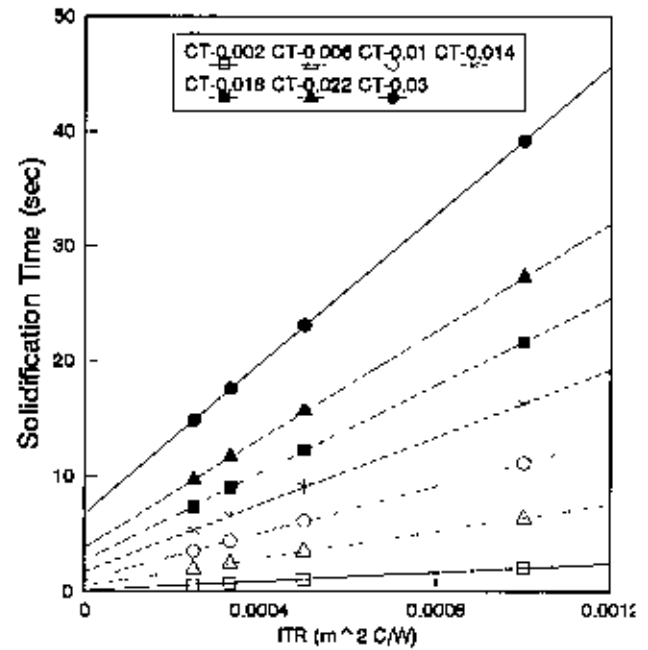
FIG. 3.12 EFFECT OF HEAT TRANSFER COEFFICIENT ON SOLIDIFICATION TIME
FOR 75 C MOULD TEMP. (a) SH=0 C, (b) SH=20 C, (c) SH=40 C, (d) SH= 60 C
FOR Cu CASTINGS IN CI MOULD
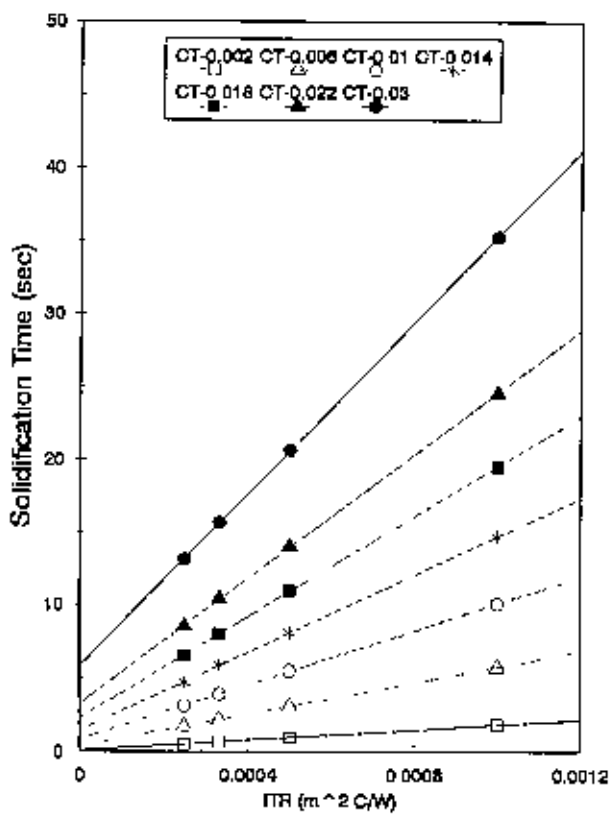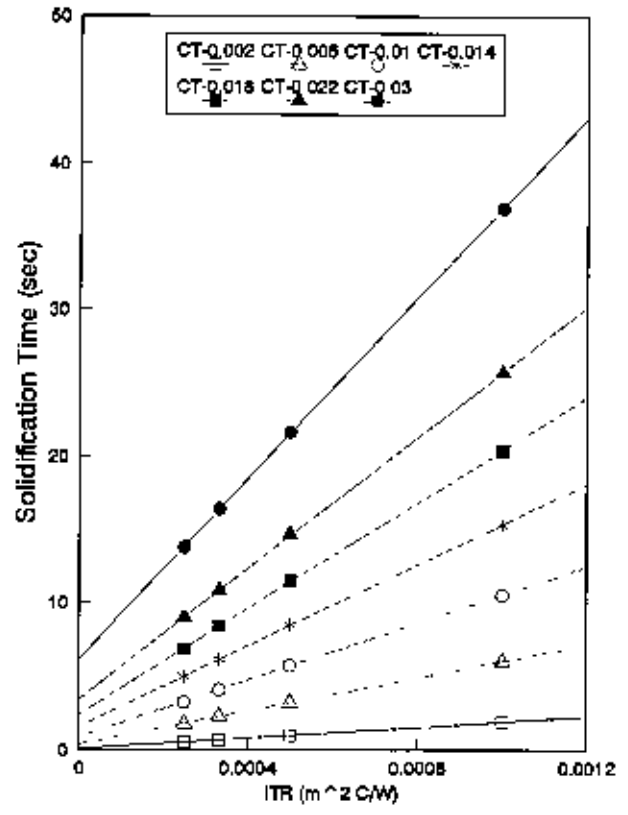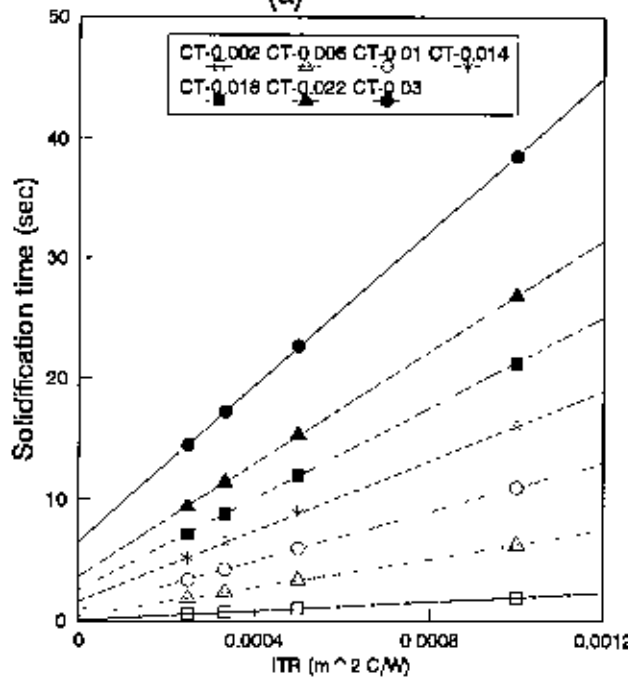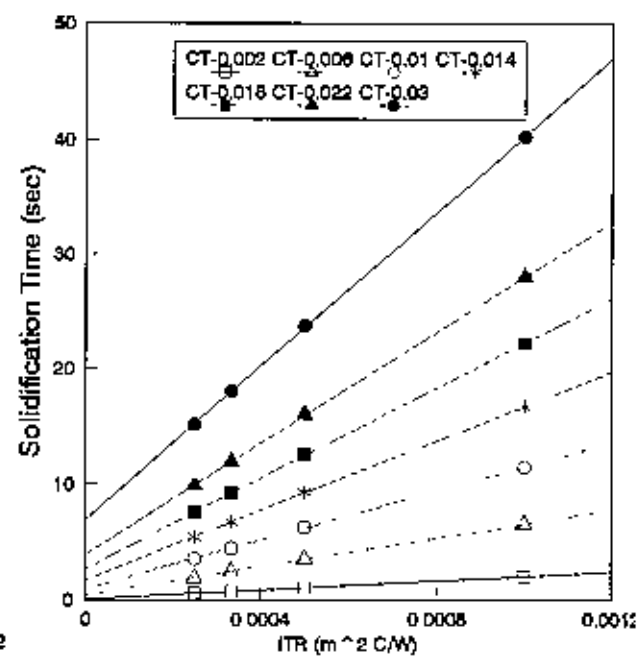
FIG. 3.13 EFFECT OF HEAT TRANSFER COEFFICIENT ON SOLIDIFICATION TIME
100 C MOULD TEMP. (a) SH = 0 C, (b) SH = 20 C, (c) SH= 40 C, (d) SH=60 C
Cu CASTINGS IN CI MOULD
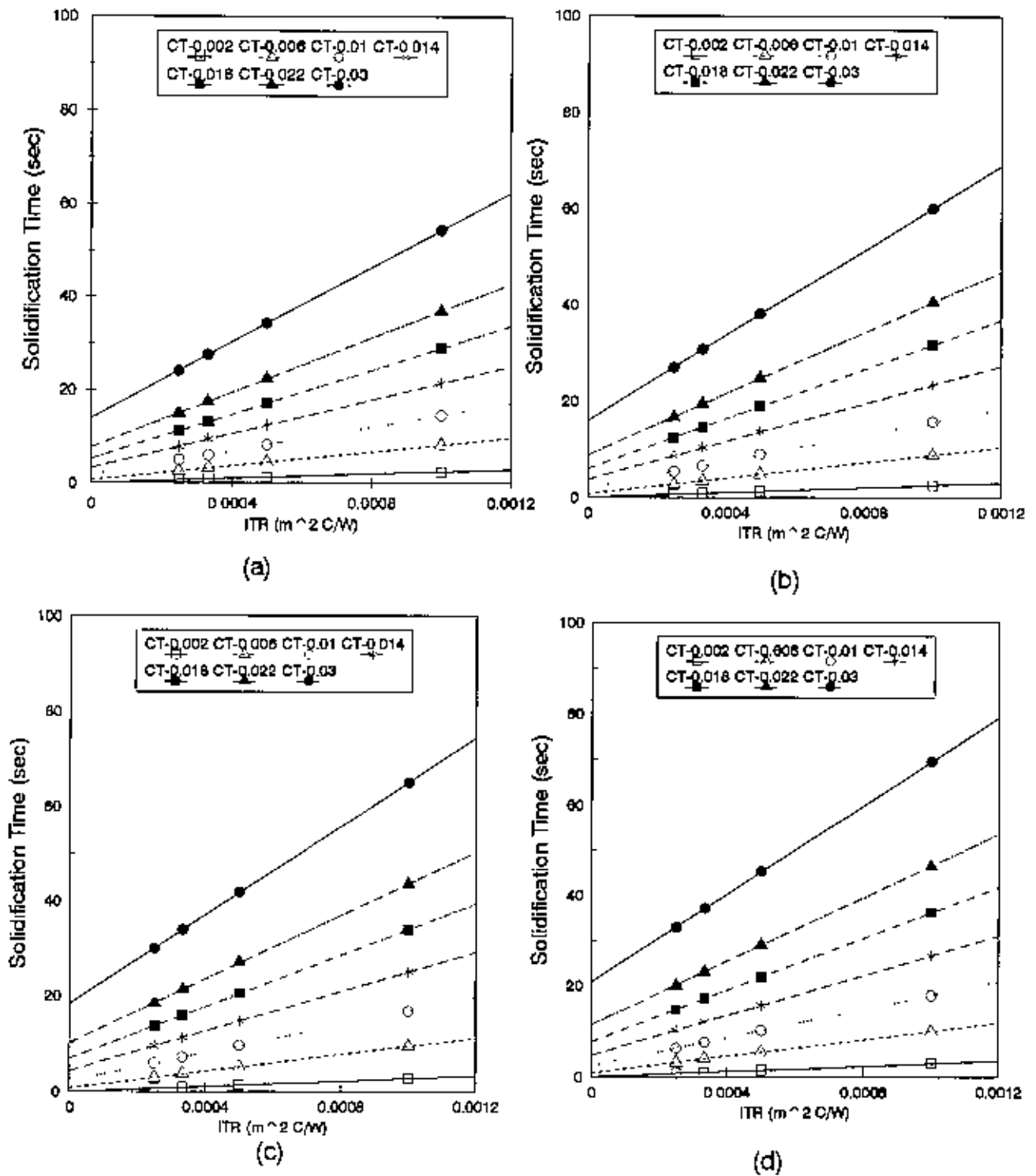
FIG. 3.14 EFFECT OF HEAT TRANSFER COEFFICIENT ON SOLIDIFICATION
TIME FOR 25 C MOULD TEMP, (a) SH=0 C, (b) SH=20 C,
(c) SH=40 C, (d) SH=60 C FOR Zn CASTINGS IN CI MOULD
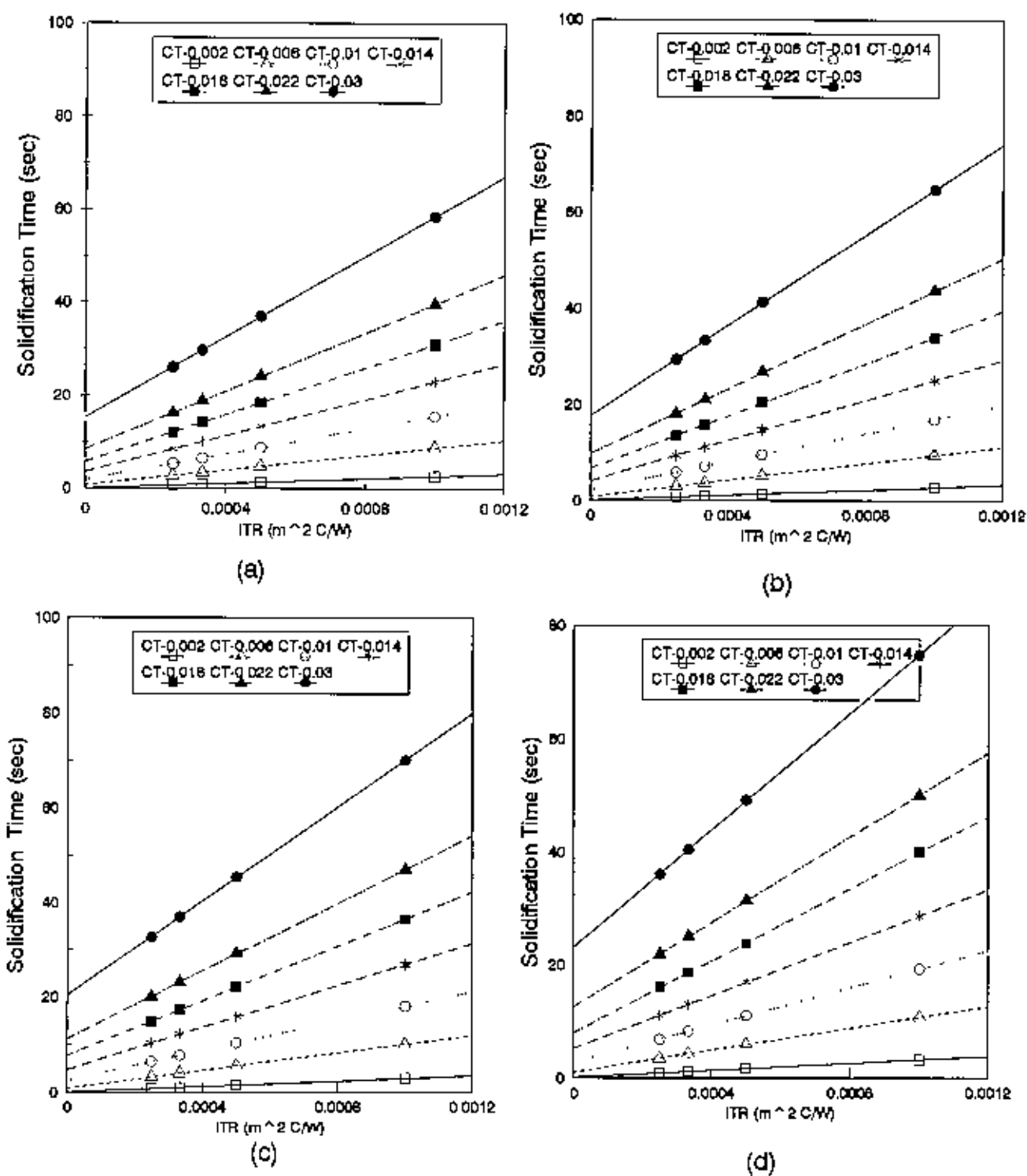
FIG. 3.15 EFFECT OF HEAT TRANSFER COEFFICIENT ON SOLIDIFICATION
TIME FOR 50 C MOULD TEMP. (a) SH=0 C, (b) SH=20 C,
(c) SH=40 C, (d) SH=60 C FOR Zn CASTINGS IN CI MOULD
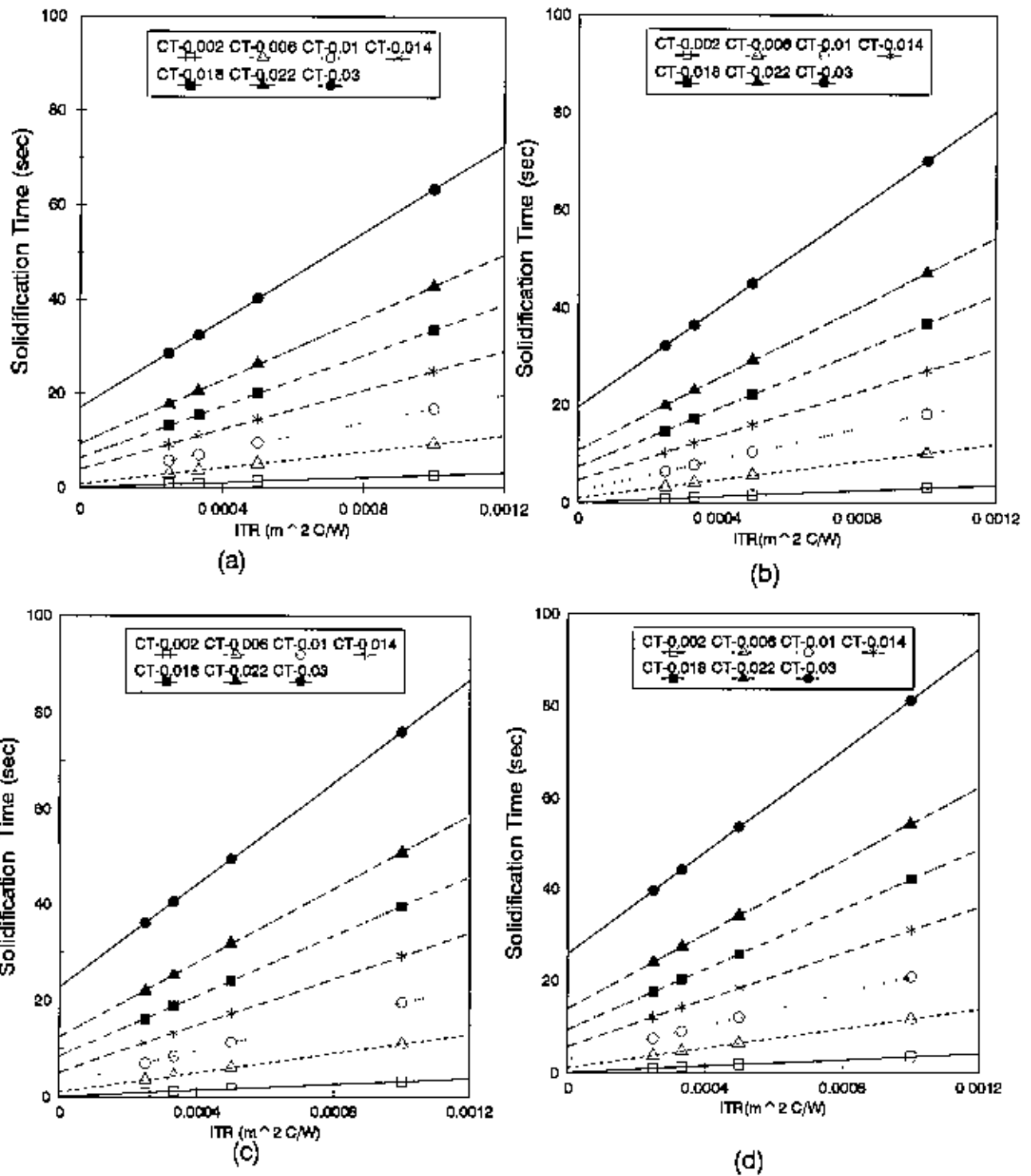
FIG. 3.16 EFFECT OF HEAT TRANSFER COEFFICIENT ON SOLIDIFICATION
TIME FOR 75 C MOULD TEMP. (a) SH=0 C, (b) SH=20 C,
(c) SH=40 C, (d) SH=60 C FOR Zn CASTINGS IN CI MOULD
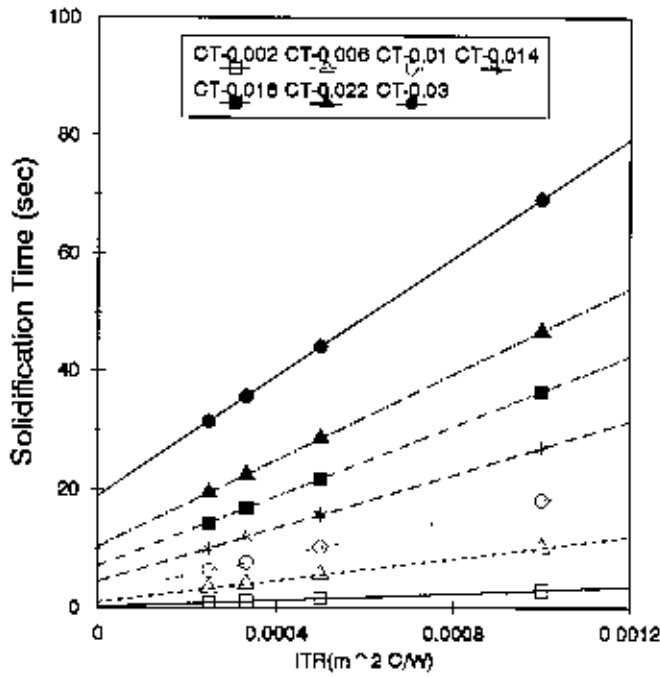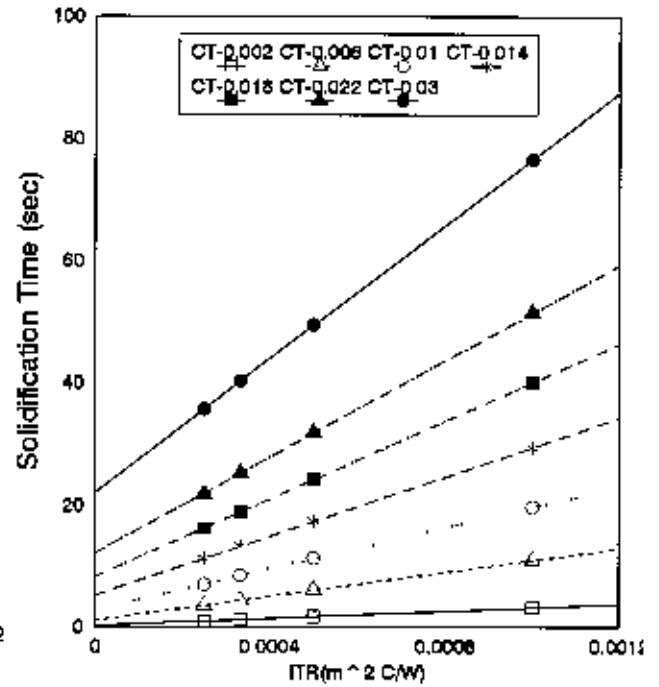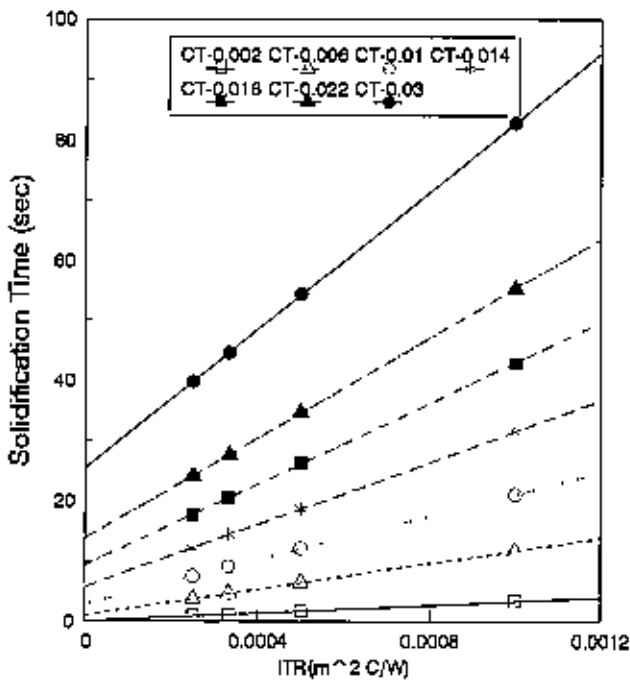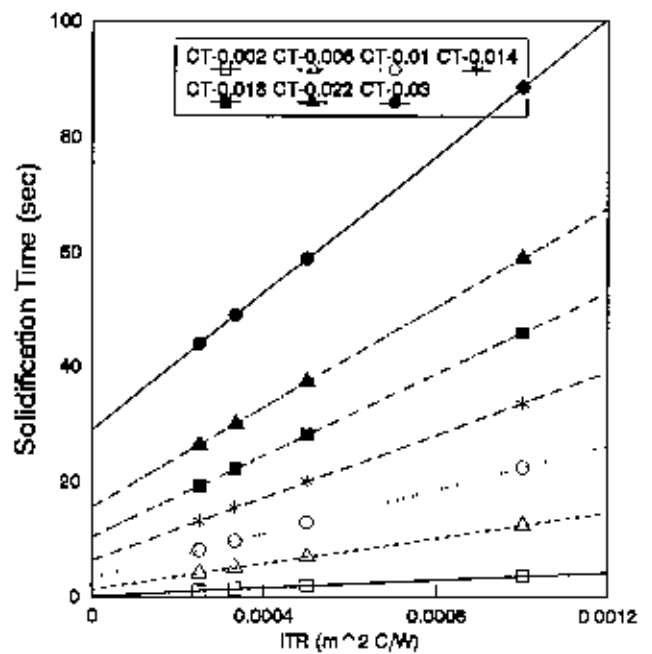
FIG. 3.17 EFFECT OF HEAT TRANSFER COEFFICIENT ON SOLIDIFICATION TIME
FOR 100 C MOULD TEMP. (a) SH=0 C, (b) SH=20 C,
(c) SH=40 C, (d) SH=60 C FOR Zn CASTINGS IN CI MOULD
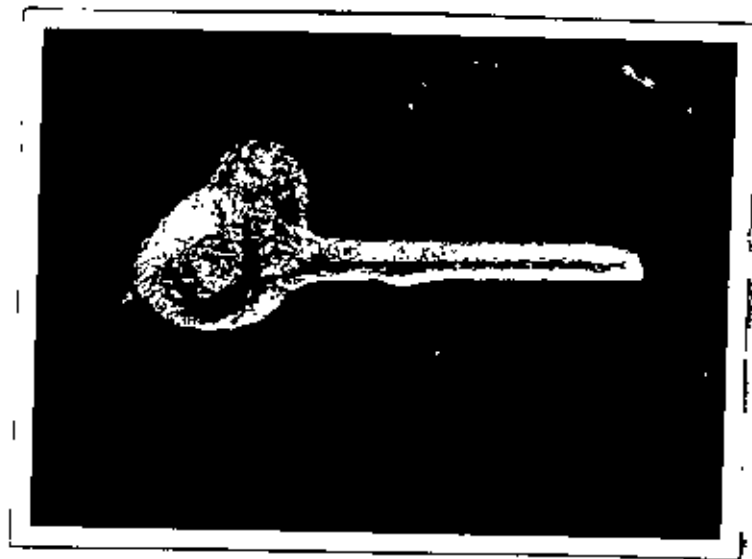
FIG. 3.18 PHOTOGRAPH OF PLATE SHAPED ALUMINIUM CASTING IN
SEMI-INFINITE SAND MOULD

FIG. 3.19 TRANSIENT HF AND HTC FOR 0.022m CASTING IN SEMI-INFINITE SAND MOULD
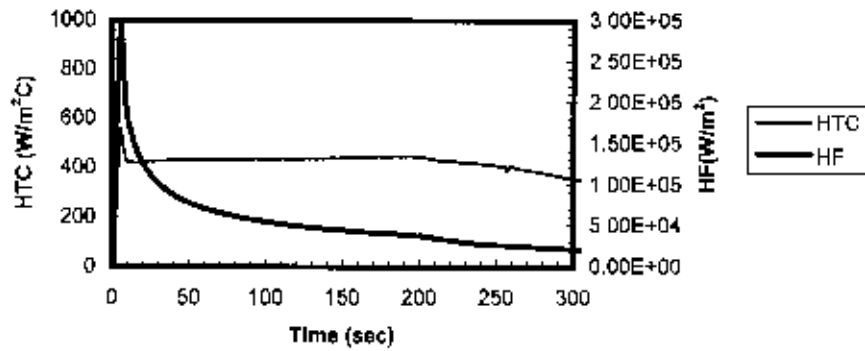
FIG. 3.20 ESTIMATED AND MEASURED T1 FOR AL CASTING IN SEMI-INFINITE SAND MOULD
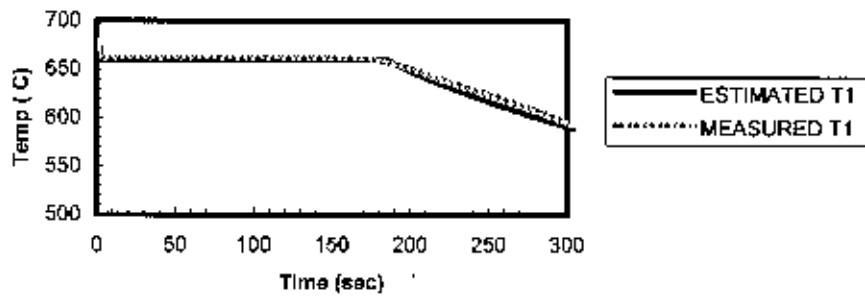
FIG. 3.21 ESTIMATED AND MEASURED T2 FOR AL CASTING IN SEMI-INFINITE SAND MOULD
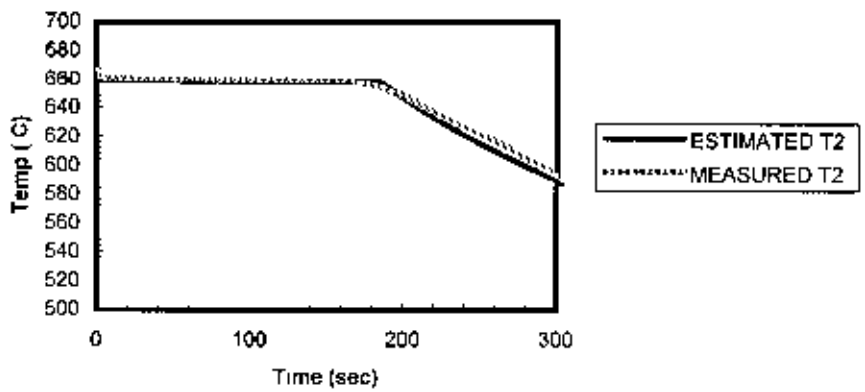
FIG. 3.22 ESTIMATED AND MEASURED T3 FOR AL CASTING IN SEMI-INFINITE SAND MOULD
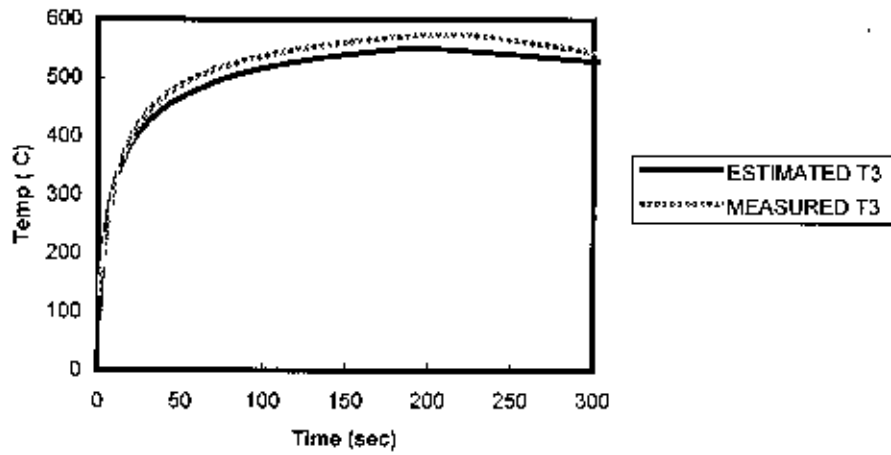
FIG. 3.23 ESTIMATED AND MEASURED T4 FOR AL CASTING IN SEMI-INFINITE SAND MOULD
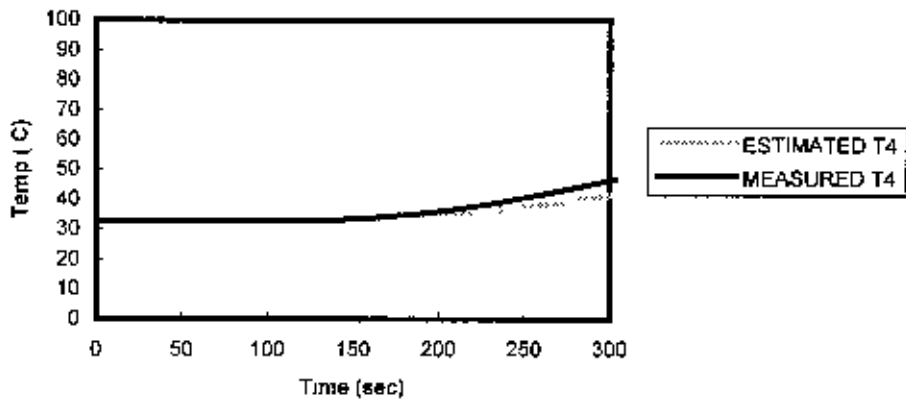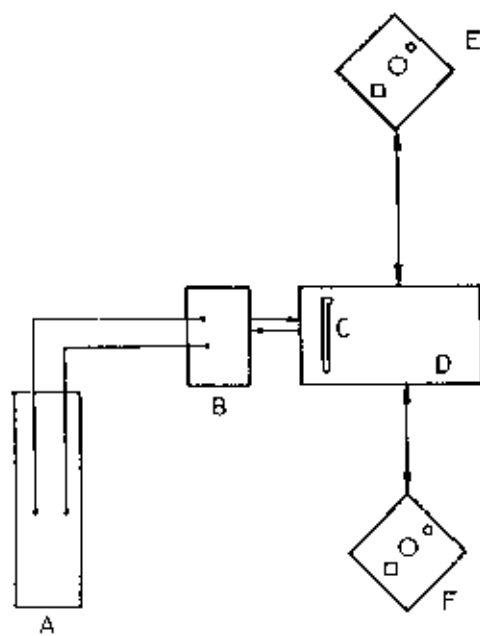
A - Casting Set up
B - Data Logger.)
C - IEEE 488 Card
D - Computer
E - Temperature File
F - Heatflux File

FIG. 4.1 DIFFERENT MODULES OF
THE DATA ACQUISITION SYSTEM

300

25 50   100

50

TOP VIEW

ⵁ12 5

25

12

T1
T2
T3
T4

50
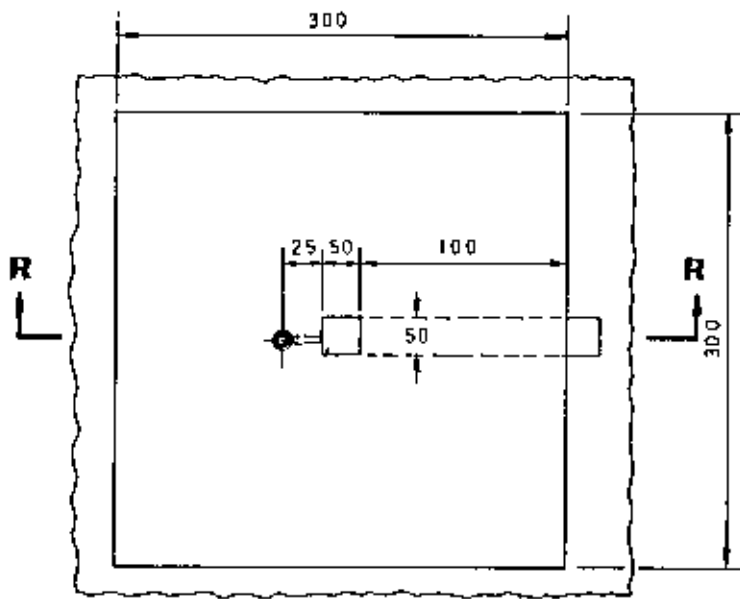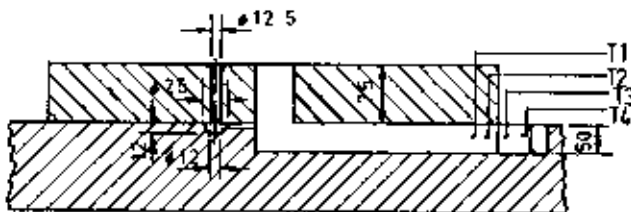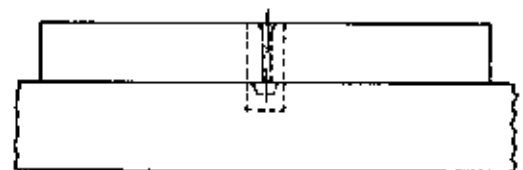
SECTION-RR

R.H.S. VIEW

FIG. 4·2 ONE BAR CASTING WITH ONE CHILL AT THE END
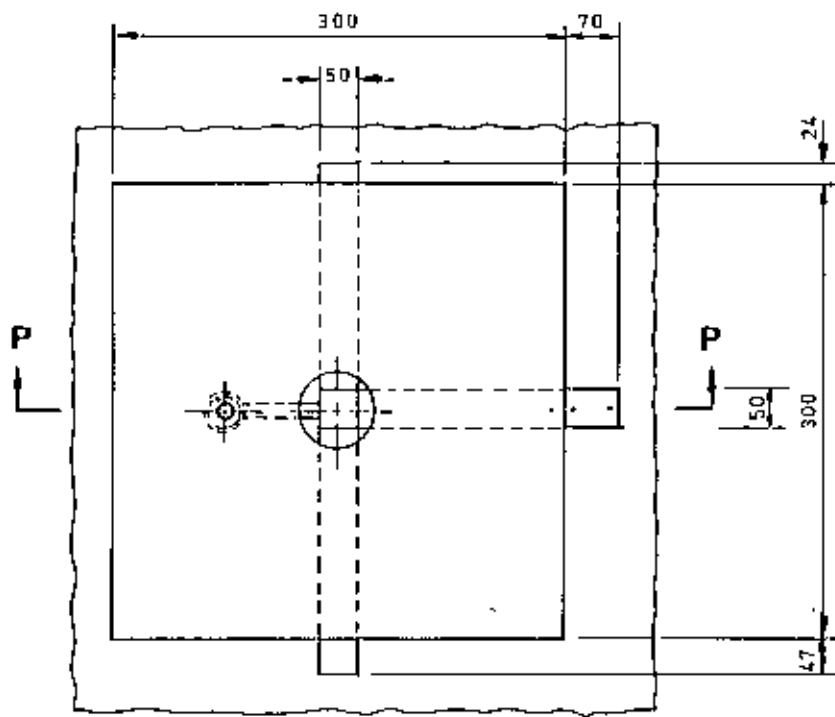
TOP VIEW
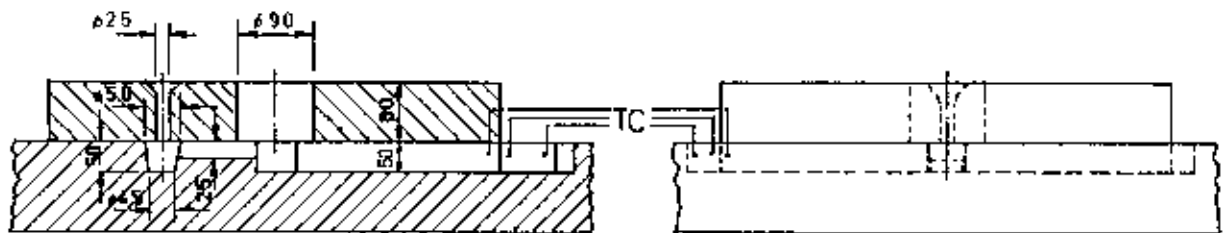
SECTION-PP   R.H.S. VIEW

FIG. 4.3   3-BAR CASTING WITH THREE CHILLS AT THE END
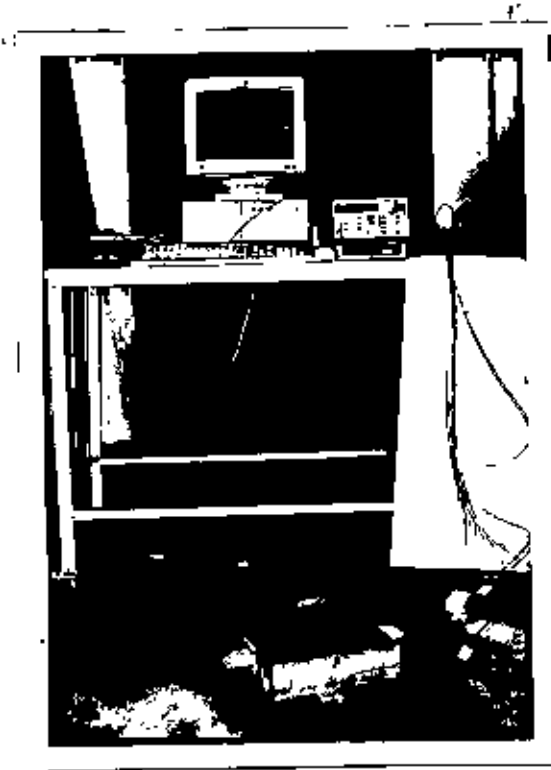
FIG. 4.4 SET UP FOR 3-BAR SHAPED CASTING SHOWING MOULD
ASSEMBLY, THERMOCOUPLES, DATA LOGGER AND COMPUTER
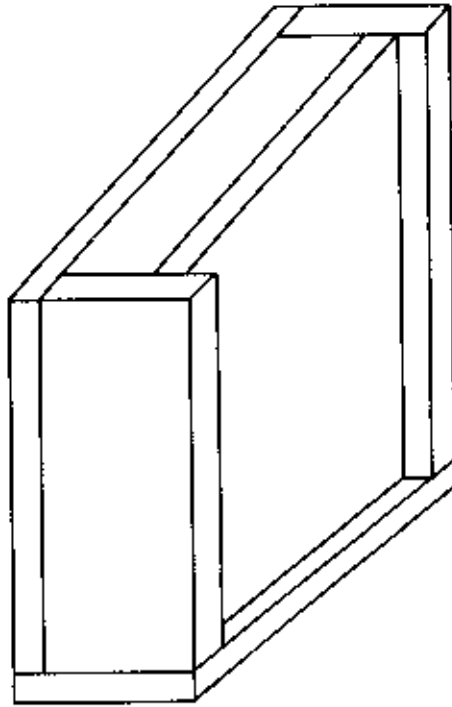
FIG. 4.5 MOULD FOR PLATE
SHAPED CASTING.
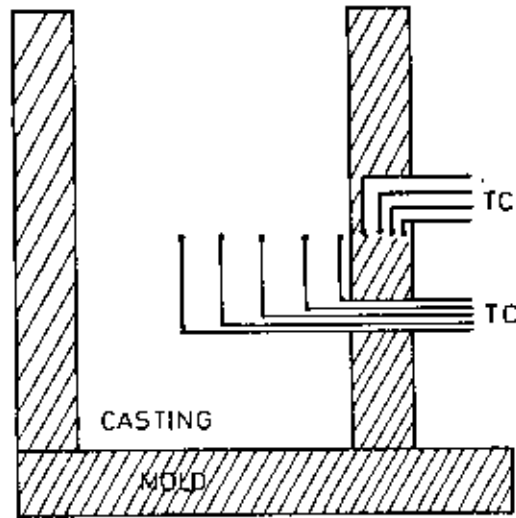
FIG. 4.6 LOCATION OF THE THERMOCOUPLES
IN CASTING AND MOULD.
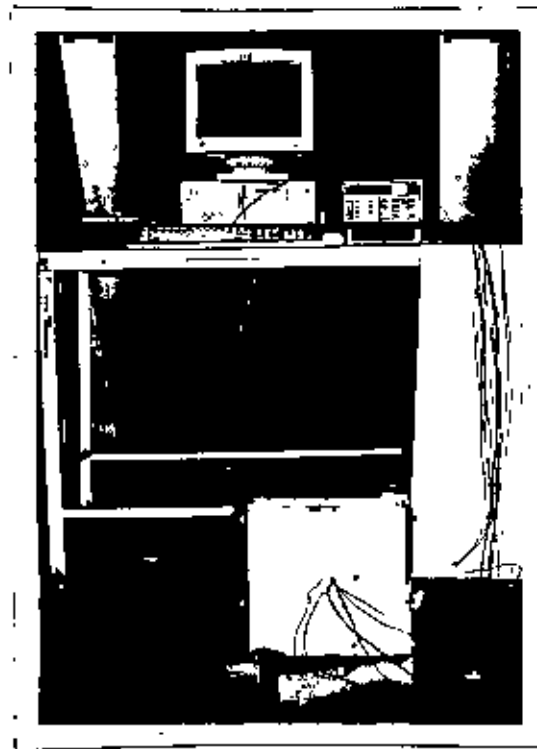
FIG. 4.7 SET UP FOR PLATE SHAPED CASTING SHOWING MOULD
ASSEMBLY, THERMOCOUPLES, DATA LOGGER AND COMPUTER
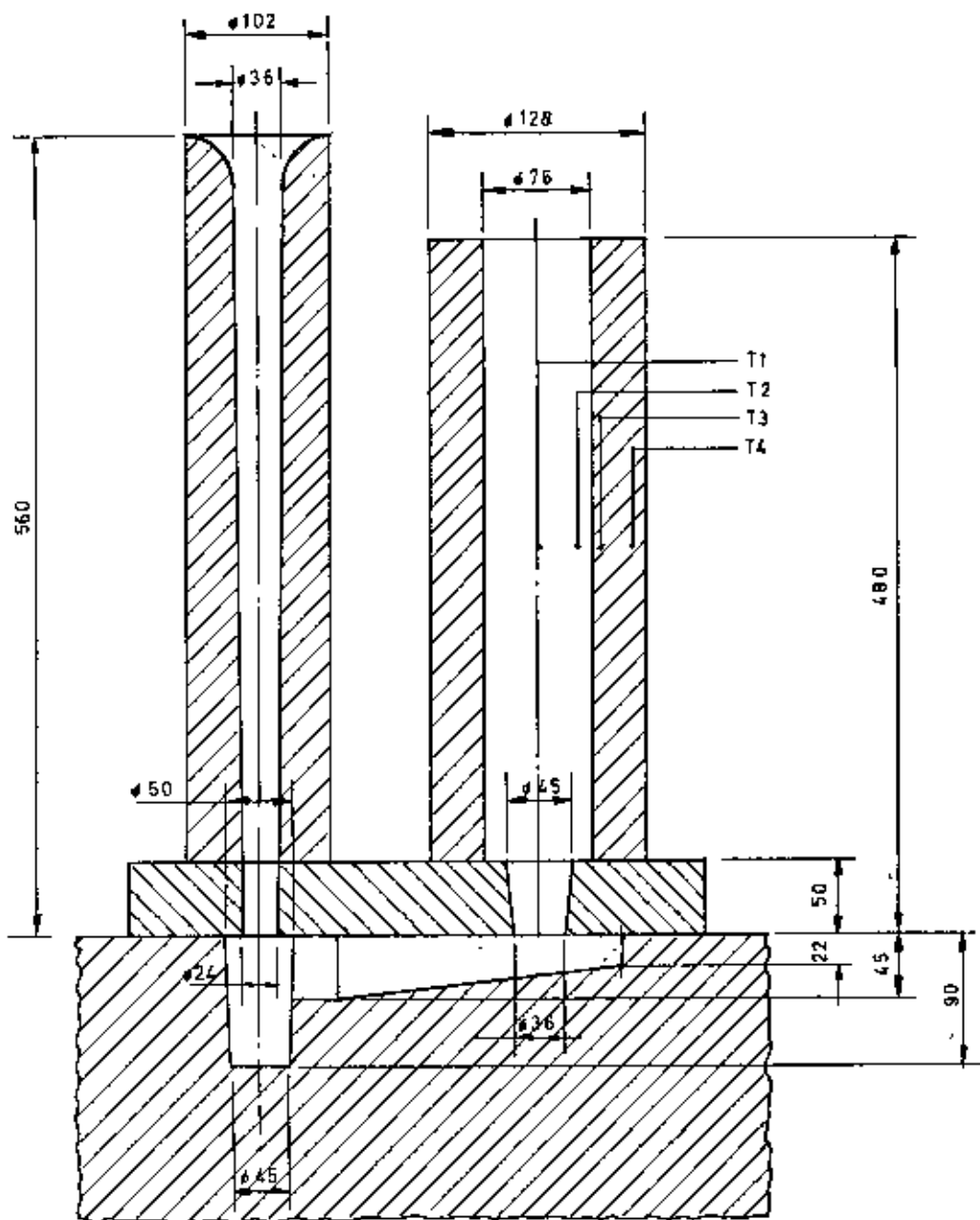
FIG. 4.8 MOULD ASSEMBLY FOR CYLINDRICAL CASTING.
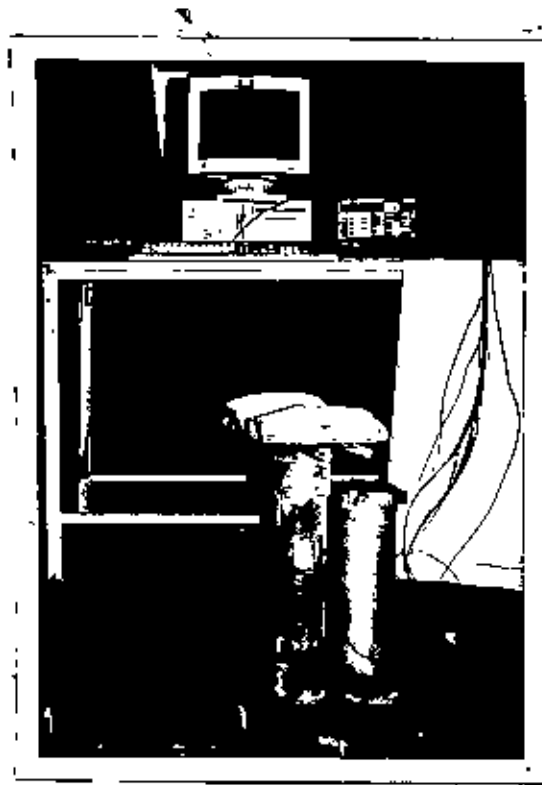
FIG. 4.9 SET UP FOR CYLINDRICAL SHAPED CASTING SHOWING MOULD
ASSEMBLY, THERMOCOUPLES, DATA LOGGER AND COMPUTER

FIG. 5.1 A PORTION OF TIME TEMPERATURE DATA FROM A TYPICAL EXPERIMENT

Time (sec)	T1	T2	T3	T4
120	31.9	31.4	30.7	31.1
121	33.8	31.8	30 7	31 1
122	38 2	32.8	30.7	31.1
123	38.6	33.2	30.7	31 1
124	40	33 9	30.7	31.1
125	43 1	34.9	30.7	31 1
126	45.1	35 9	30 8	31 1
127	47 7	36.8	30.8	31.1
128	50.2	37.7	30.8	31.2
129	53.3	38.5	30 9	31.2
130	57.8	40 3	30.9	31.2
131	61.4	42	31	31.2
132	65.4	43.6	31.1	31.3
133	121.8	53.5	37.5	31.3
134	574 4	531.1	46.3	31.3
135	632.1	620.8	53.5	31.5
136	662.3	655.8	59 2	32 2
137	677 3	653.9	65.1	33.8
138	686.4	661.5	73.3	36.1
139	682.7	653 9	82 1	38 9
140	685 5	650	91	42.1
141	683 2	651.1	99.9	45.6
142	680	651	108 5	49 4
143	675 2	651 6	116 6	53 6
144	673.7	650 5	124.3	57.9
145	668.2	649.3	131 7	62 2
146	667.8	648 4	139	66.6
147	665.4	647.4	146	71.1
148	664.5	646.5	152.8	75.7
149	664.4	645.6	159.3	80.2
150	663.9	644.7	165.5	84.7
151	663.4	643.9	171.2	89.1
152	662.5	643.1	176.6	93.5
153	662.2	642.3	181 7	97.9
154	661 5	641 6	186 6	102 4
155	661	640 8	191 3	106 9
156	661	640.1	195.7	111.3
157	660 7	639.3	200.1	115.8
158	660 4	638.6	204.3	120.3
159	660.3	637.9	208.4	124.7
160	660.1	637.2	212 4	129.1
161	660 1	636 7	216 4	133 6
162	660	636 1	220 2	138
163	659.9	635.6	224.1	142.4
164	659.8	635.2	227.8	146.9
165	659.8	634.7	231 5	151.2
166	659.8	634 3	235.1	155.5
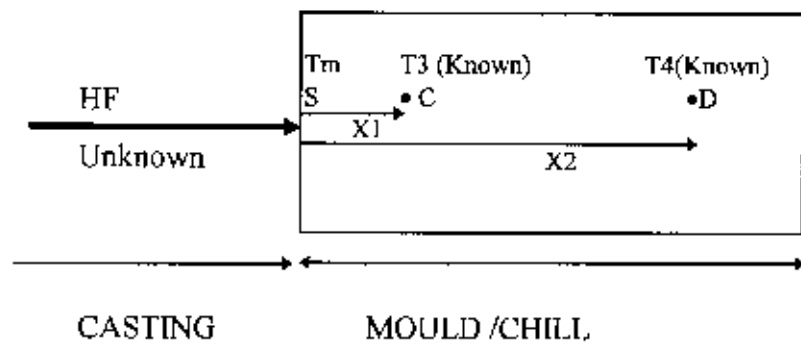
FIG. 5.2 INVERSE HEAT CONDUCTION PROBLEM IN 1-D HEAT FLOW

FIG. 5.3 THE FLOW CHART FOR THE DETERMINATION OF HF
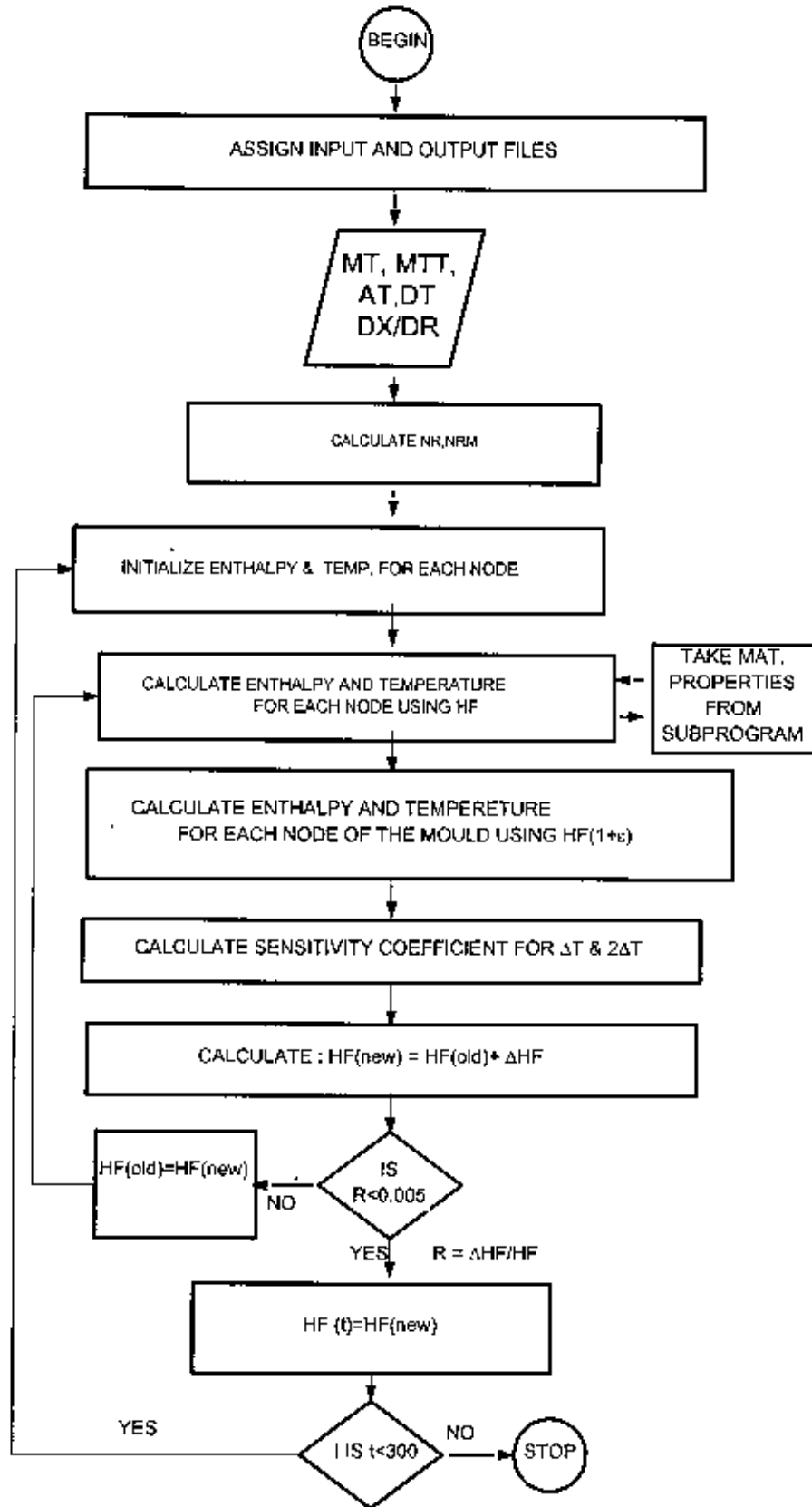
FIG. 6.1.1 TEMP-TIME PROFILES OF BAR SHAPED CASTING FOR 24mm CHILL (PT-760 C)
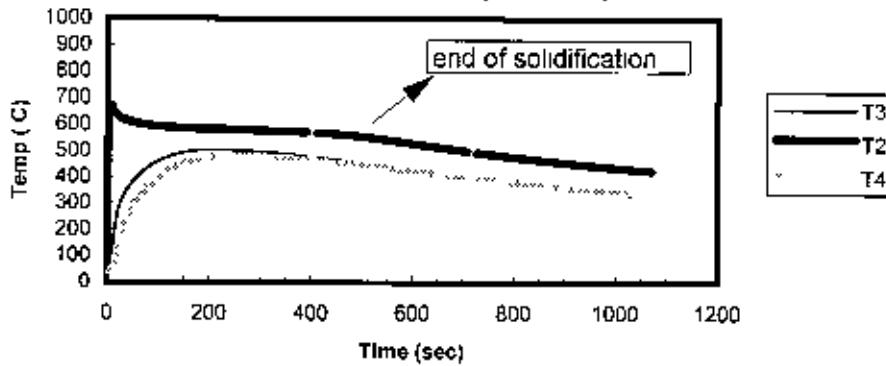
FIG. 6.1. 2a EFFECT OF SUPERHEAT ON TEMP-TIME PROFILES AT C, T3-t, FOR 24mm CHILL
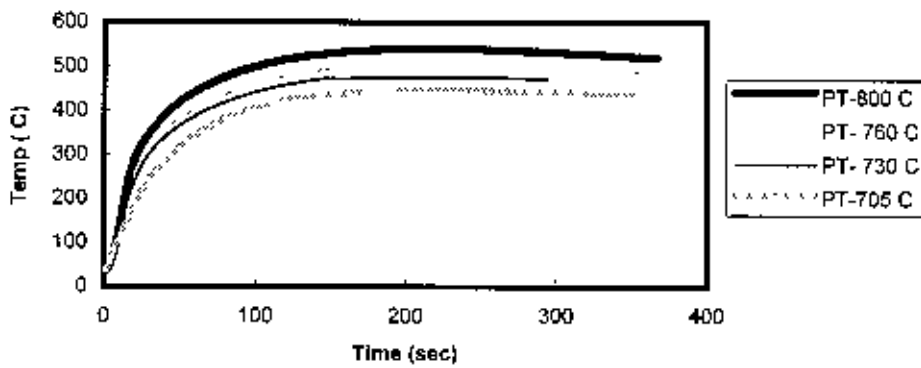
FIG. 6.1.2b EFFECT OF CHILL THICKNESS ON TEMP-TIME PROFILES AT C, T3-t, FOR POURING TEMP-705 C
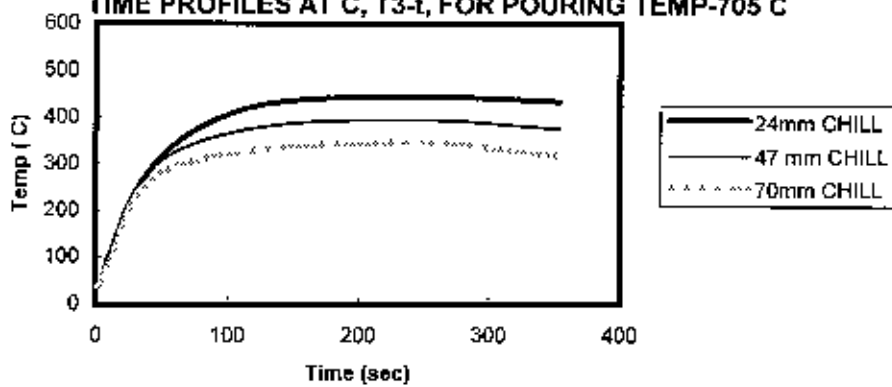
FIG. 6.1.2c EFFECT OF CHILL THICKNESS ON TEMP-TIME PROFILES AT C, T3-t, FOR POURING TEMP-730 C
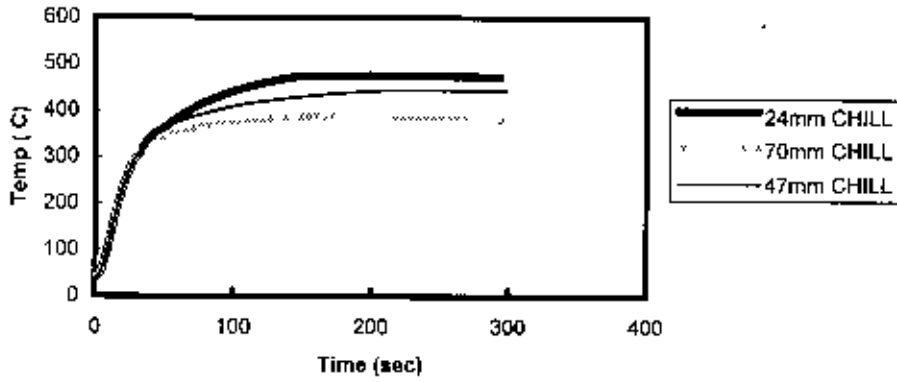
FIG. 6.1.3a EFFECT OF SUPERHEAT ON TEMP-TIME PROFILES AT D,T4-t, FOR 24mm CHILL
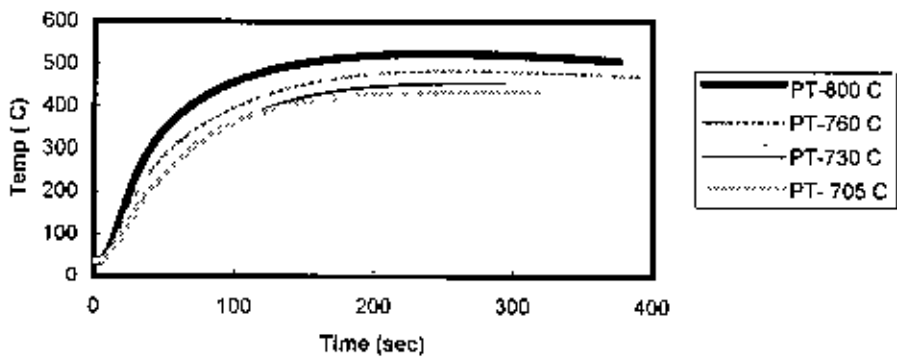
FIG. 6.1.3b EFFECT OF CHILL THICKNESS ON TEMP-TIME PROFILES AT D, T4-t, FOR POURING TEMP-705 C
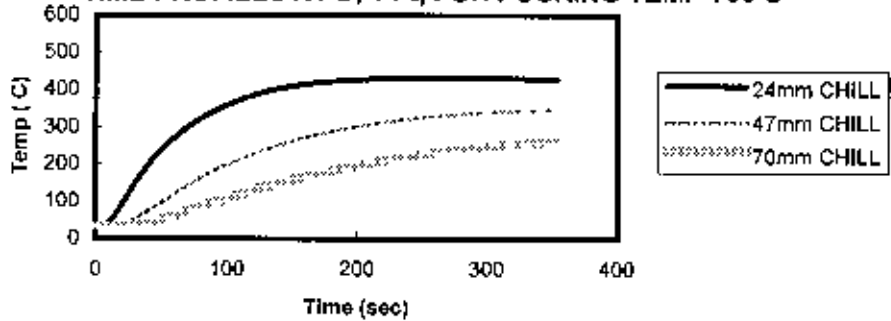
FIG. 6.1.4 EFFECT OF SUPERHEAT ON TEMP-TIME PROFILES AT B, T2-t, FOR 24mm CHILL
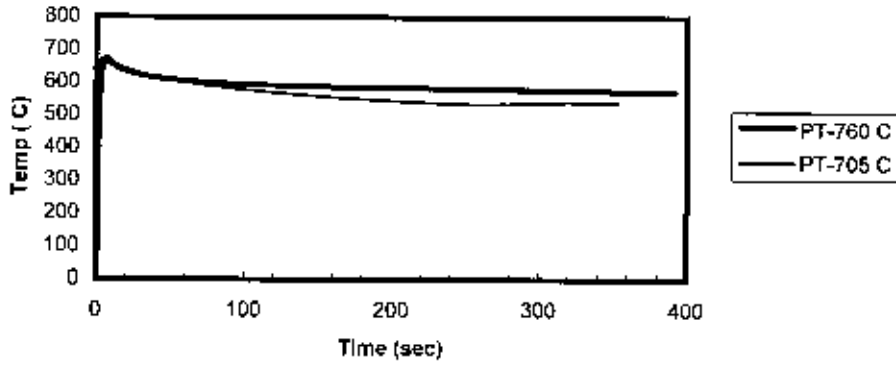
FIG. 6.1.5 EFFECT OF CHILL THICKNESS ON TEMP-TIME PROFILES AT B, T2-t, FOR POURING TEMP- 705 C
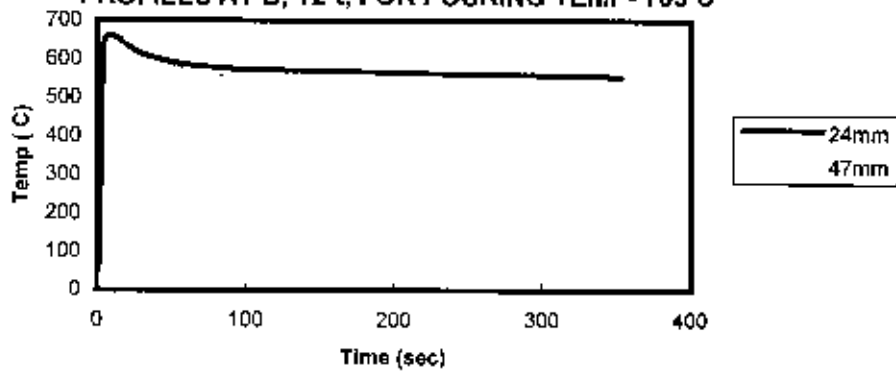
FIG. 6.1.6a EFFECT OF SUPERHEAT ON HF-TIME CURVES FOR 24mm CHILL
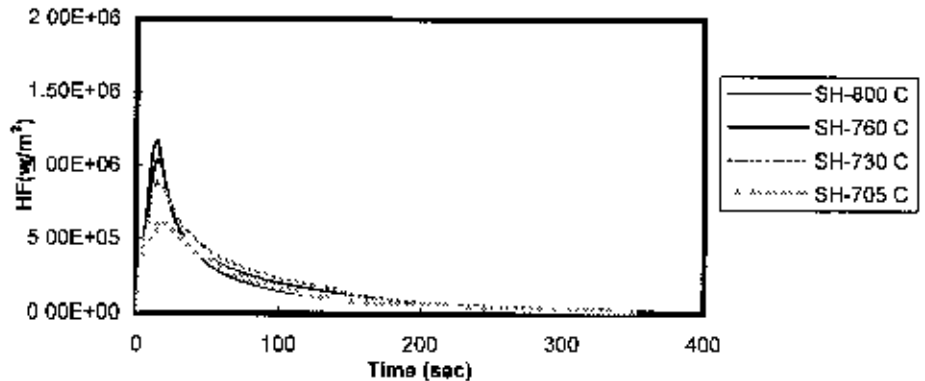
FIG. 6.1.6b TEMP/HF-TIME PROFILE SHOWING LIQUID METAL INTERFACE AT HFmax (PT-950 C)

Time of HFmax and cange in slope of Tm
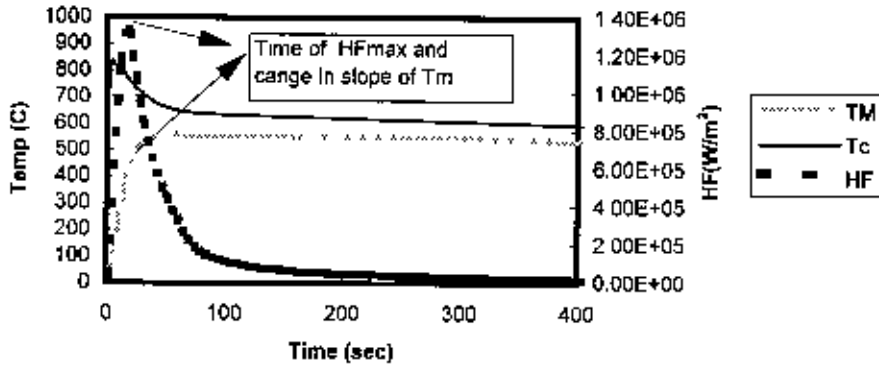
FIG. 6.1.6c TEMP/HF-TIME PROFILE SHOWING INTERFACE AT MELTING POINT AT HFmax (PT-760 C)

Time of HFmax and change in slope of Tm
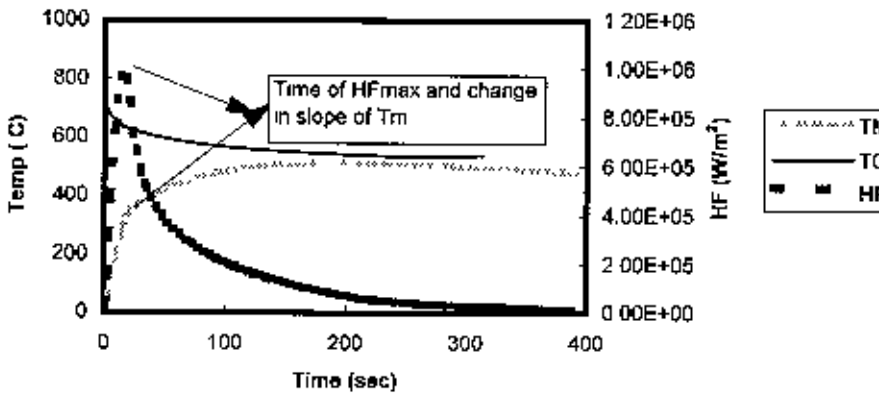
FIG. 6.1.6d TEMP/HF-TIME PROFILE SHOWING SOLIDIFIED SKIN AT HFmax (PT-705 C)

Time of HFmax and change in slope of Tm
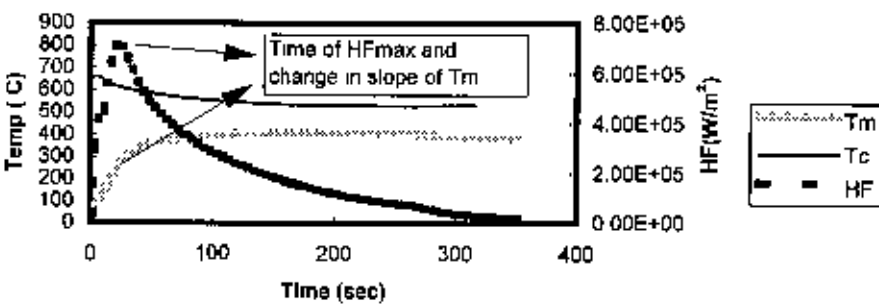
FIG. 6.1.7a EFFECT OF CHILL THICKNESS ON HF-TIME CURVES FOR PT-800 C
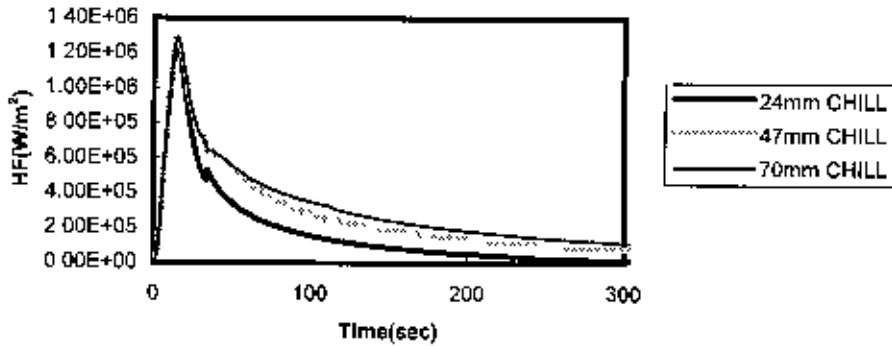
FIG. 6.1.7b EFFECT OF CHILL THICKNESS ON HF-TIME CURVES FOR PT-760 C
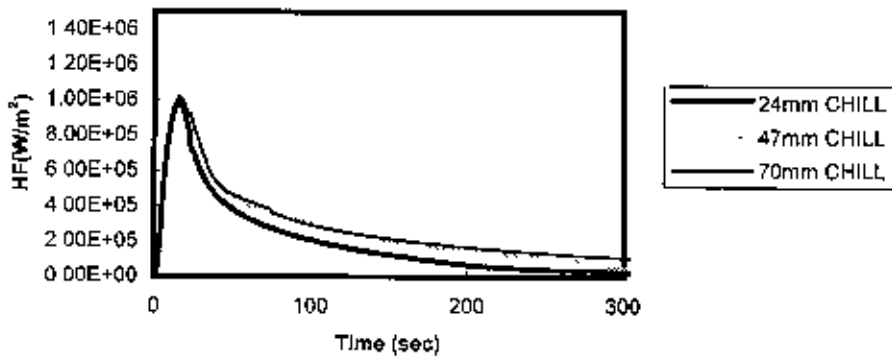
FIG. 6.1.8 EFFECT OF SUPERHEAT ON TOTAL HF FOR DIFFERENT CHILLS
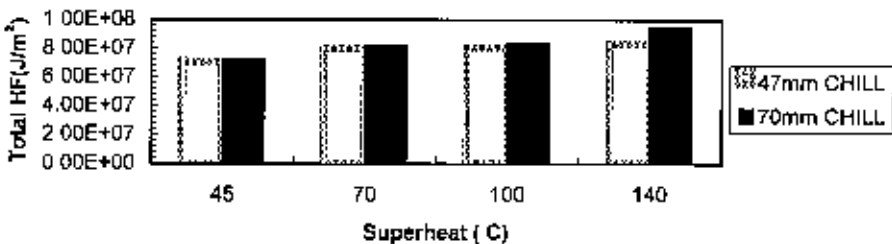
FIG. 6.1.9 MEASURED AND MODELED TEMPERATURE
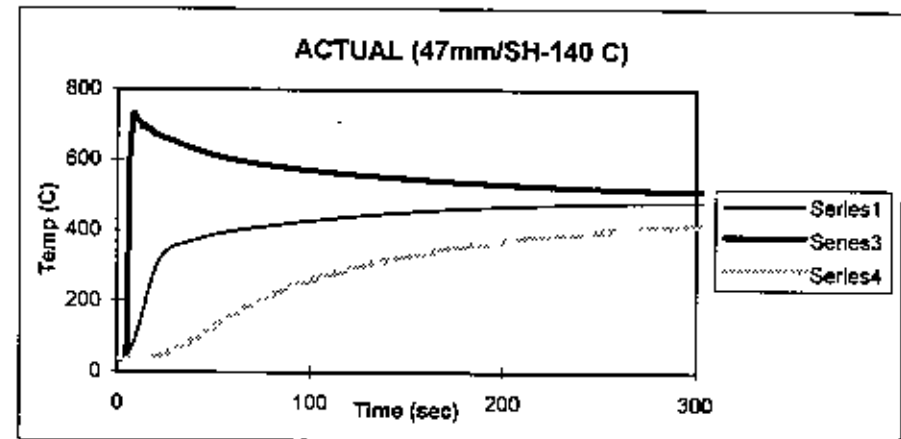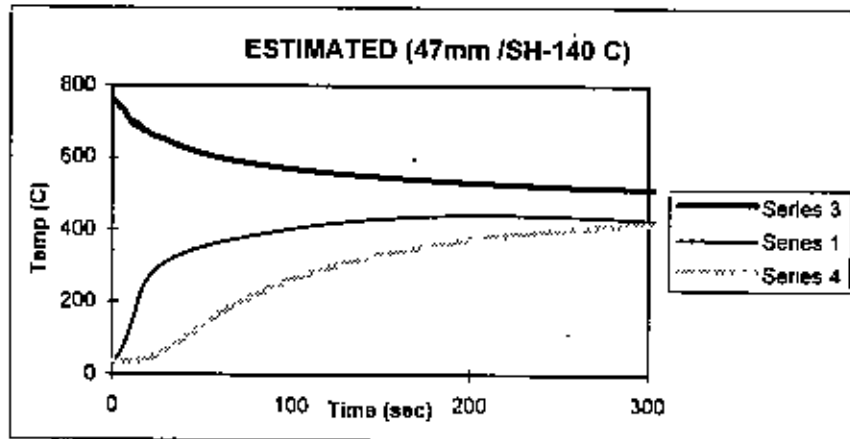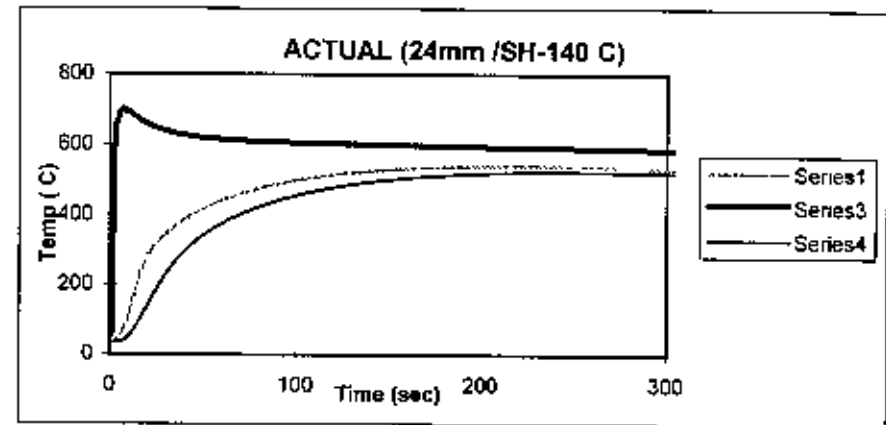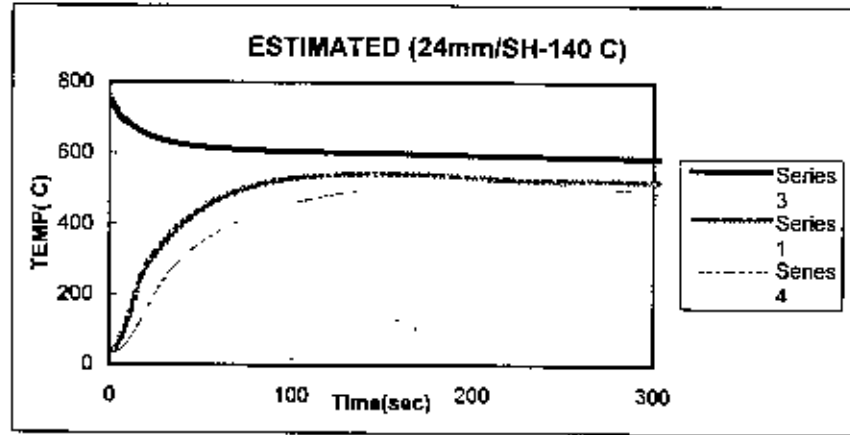
Series 1== T2   Series 3== T3   Series4== T4

ESTIMATED (24mm/SH-140 C)

ACTUAL (24mm /SH-140 C)

ESTIMATED (47mm /SH-140 C)

ACTUAL (47mm/SH-140 C)

FIG. 6.1.9 MEASURED AND MODELED TEMPERATURE

Series 1== T2   Series 3== T3   Series4== T4

ESTIMATED (70mm /SH-140 C)

ACTUAL (70mm /SH-140 C)

ESTIMATED (24mm /SH-100 C)

ACTUAL (24mm /SH-100 C)

FIG. 6.1.9 MEASURED AND MODELED TEMPERATURE

Series 1== T2   Series 3== T3   Series4== T4

ESTIMATED (47mm/ SH-100 C)

ACTUAL (47mm /SH-100 C)

ESTIMATED (70mm /SH-100 C)

ACTUAL (70mm /SH-100 C)

FIG. 6.1.9 MEASURED AND MODELED TEMPERATURE

Series 1== T2   Series 3== T3   Series4== T4

ESTIMATED (24mm /SH-70 C)

ACTUAL (24mm /SH-70 C)

ESTIMATED (47mm /SH-70 C)

ACTUAL (47mm /SH-70 C)

FIG. 6.1.9 MEASURED AND MODELED TEMPERATURE

Series 1== T2   Series 3== T3   Series4== T4

ESTIMATED (70mm /SH-70 C)

ACTUAL (70mm /SH-70 C)

ESTIMATED (24mm /SH-45 C)

ACTUAL (24mm /SH-45 C)

FIG. 6.1.9 MEASURED AND MODELED TEMPERATURE

Series 1== T2   Series 3== T3   Series4== T4

ESTIMATED (47mm /SH-45 C)

ACTUAL (47mm /SH-45 C)

ESTIMATED (70mm /SH-45 C)

ACTUAL (70mm /SH-45 C)
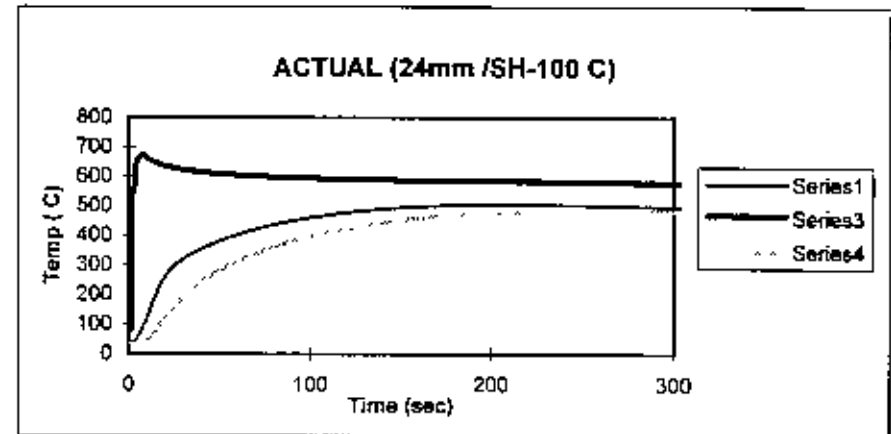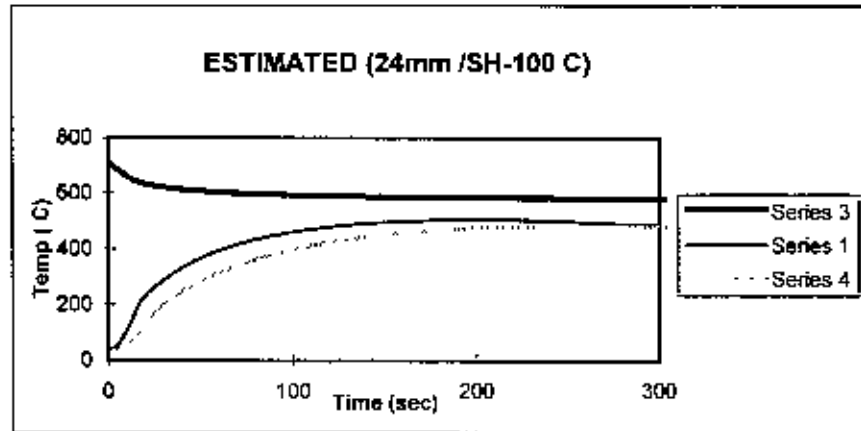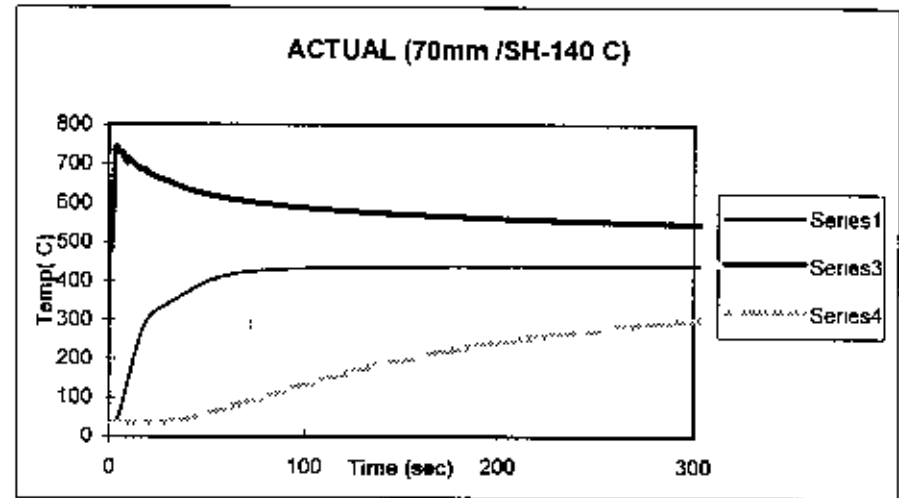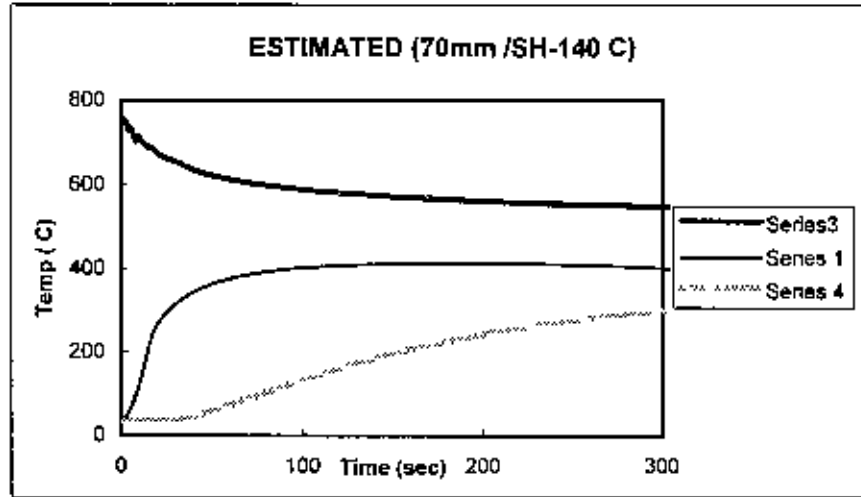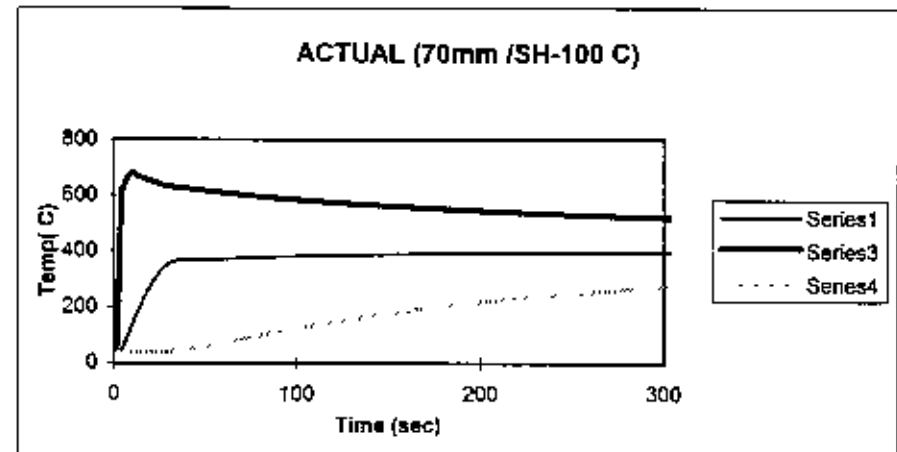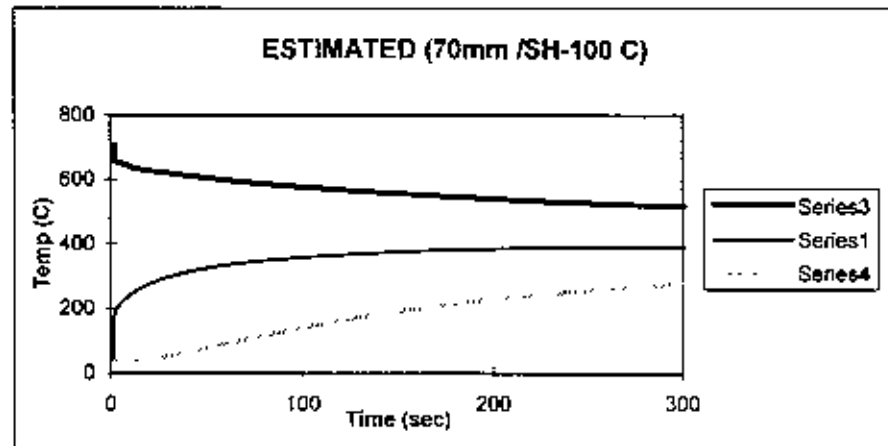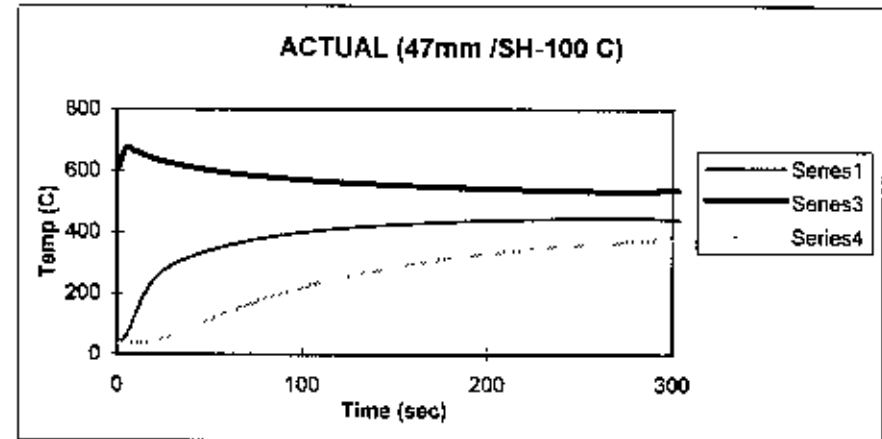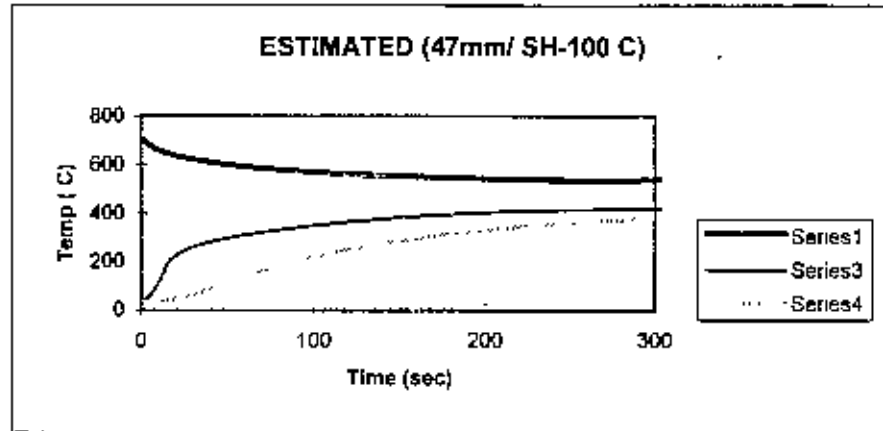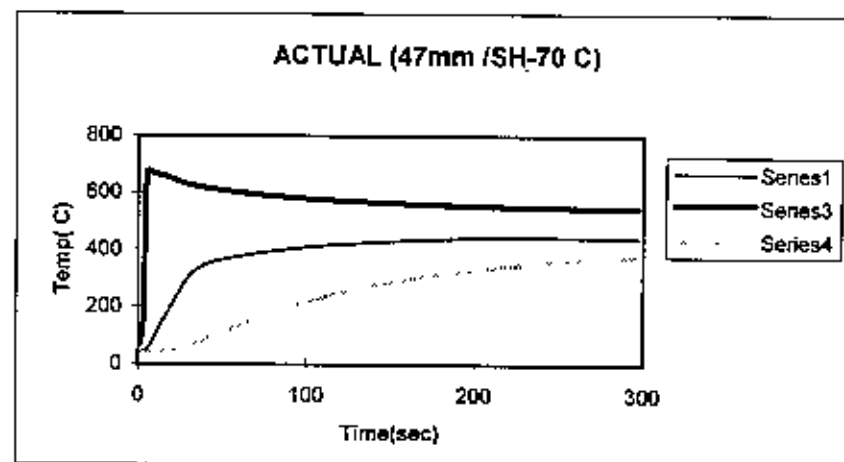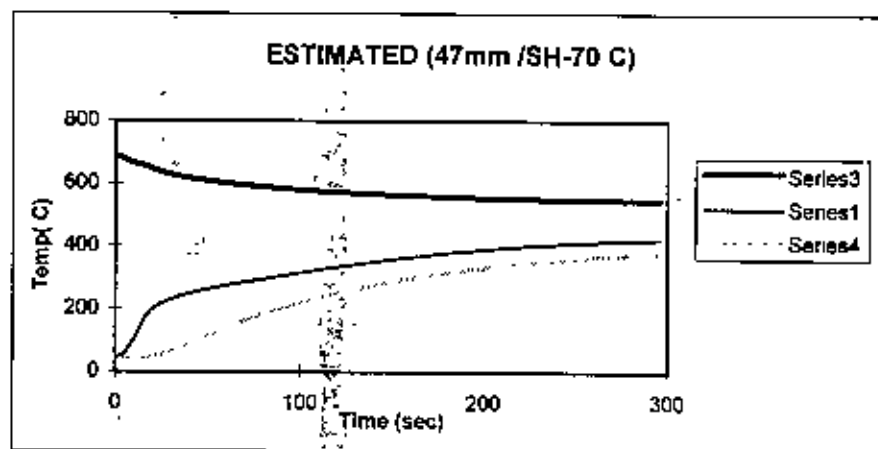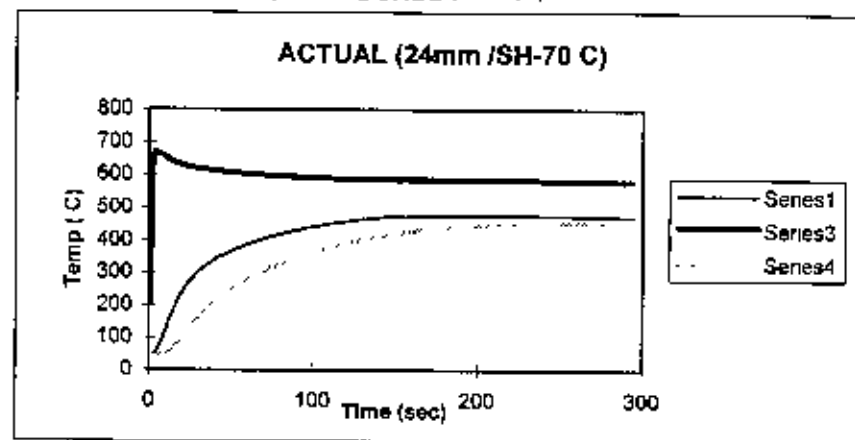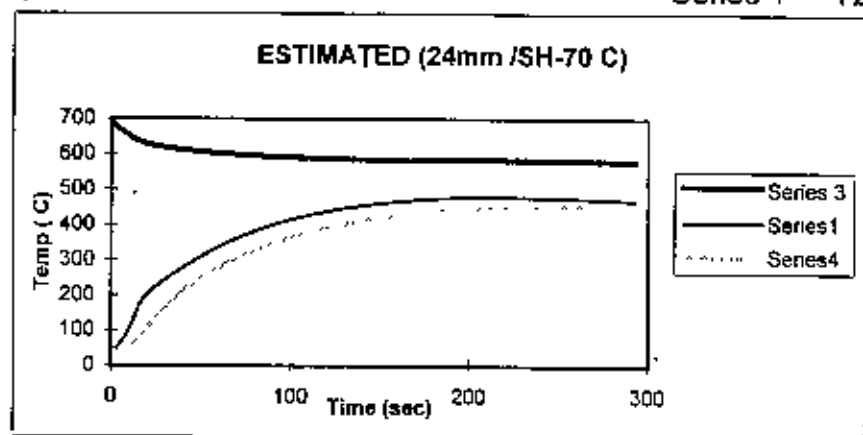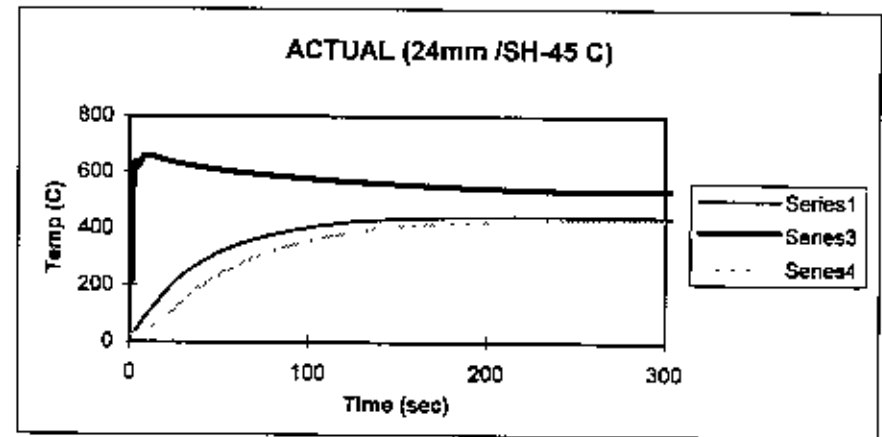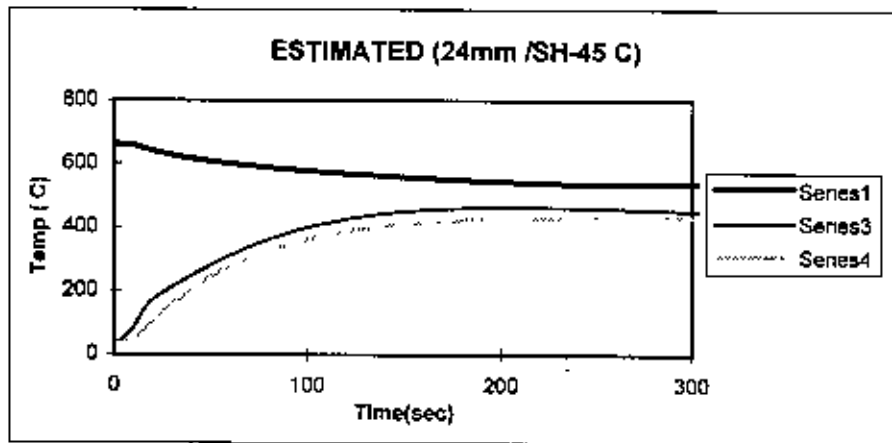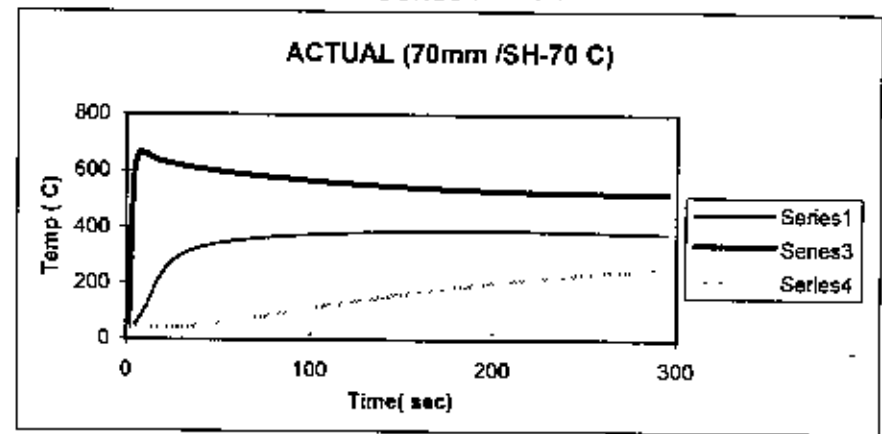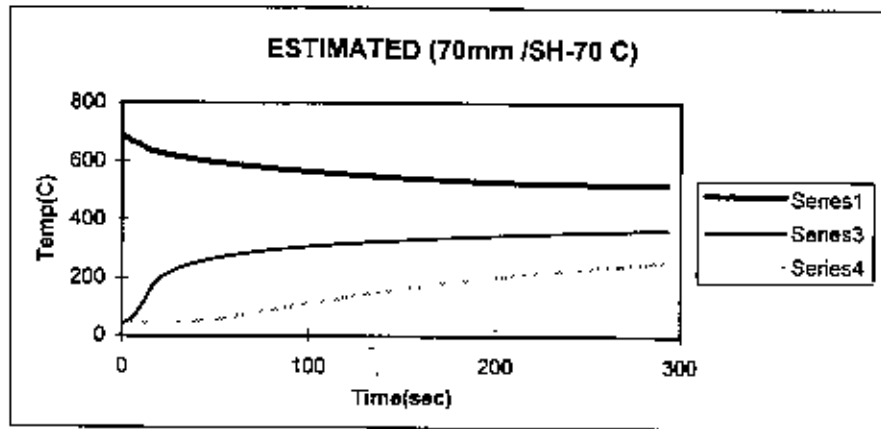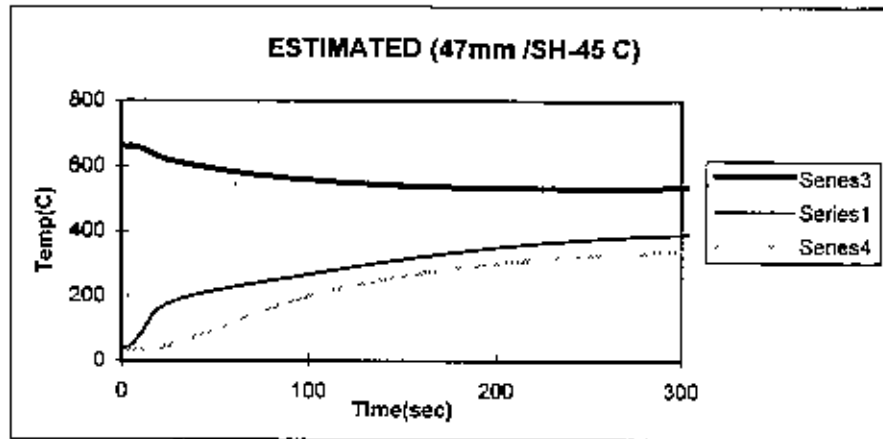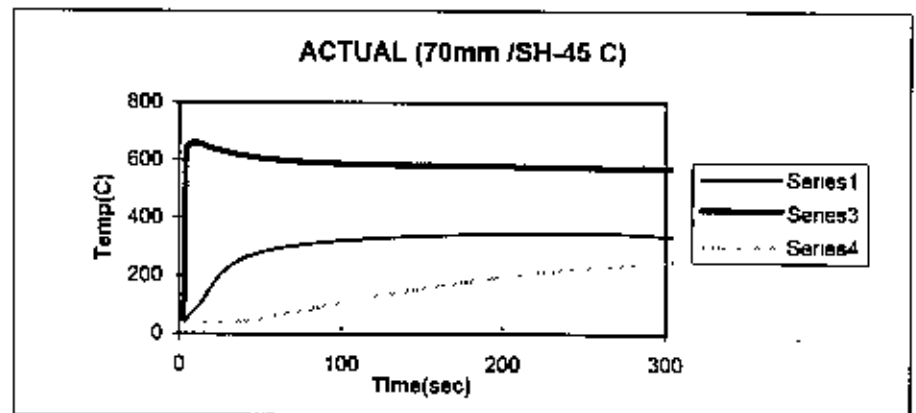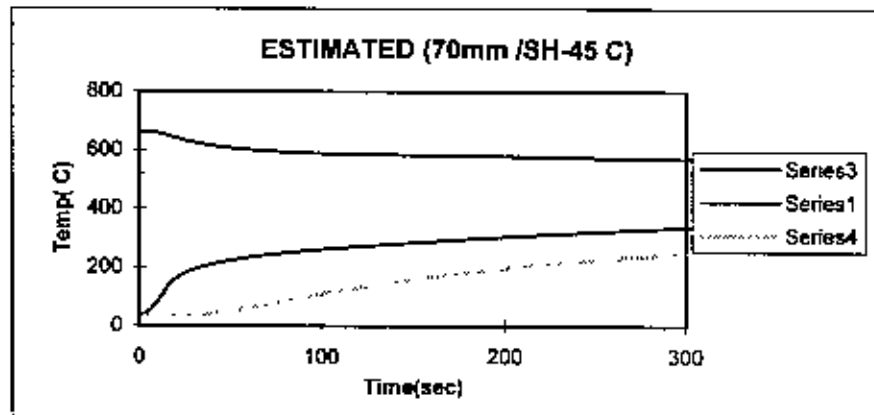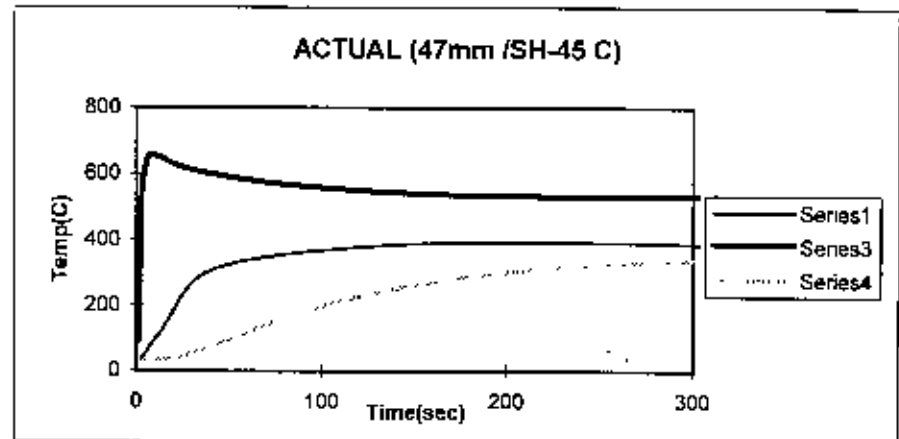
FIG. 6.1.10a EFFECT OF SUPERHEAT ON HTC-TIME CURVES FOR 47mm CHILL
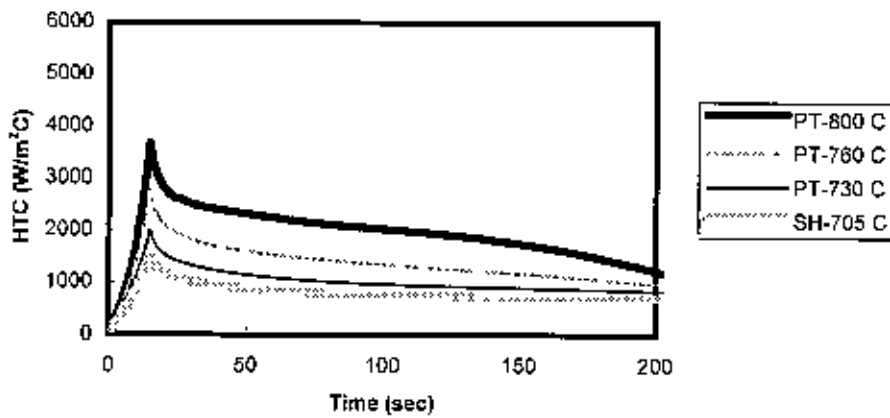
FIG. 6.1.10b EFFECT OF CHILL THICKNESS ON HTC-TIME CURVES FOR PT-730 C
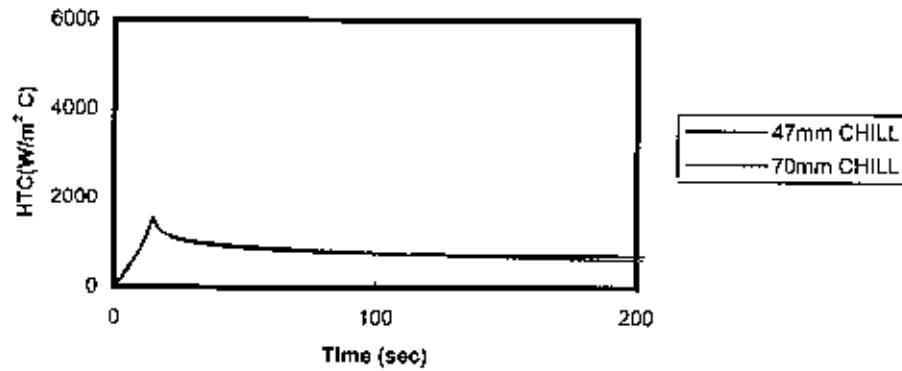
FIG. 6.2.1 TEMP-TIME PROFILES FOR 68mm PLATE CASTING (PT-750 C)
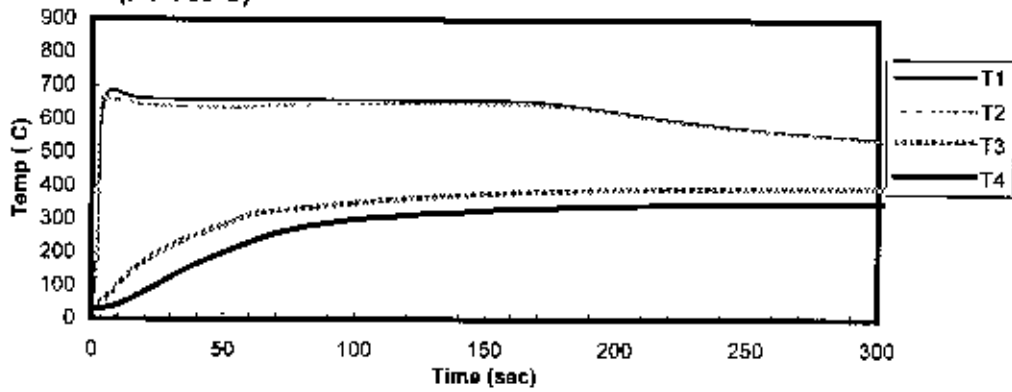
FIG. 6. 2.2a EFFECT OF SUPERHEAT ON HEATING CURVES OF MOULD AT C, T3-t, FOR 68mm PLATE CASTING
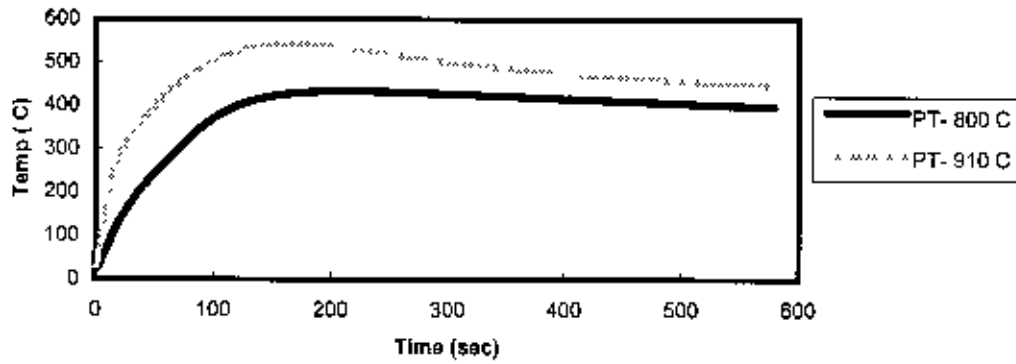
FIG. 6.2.2b EFFECT OF SUPERHEATON HEATING CURVES OF MOULD AT C, T3-t, FOR 52mm PLATE CASTING
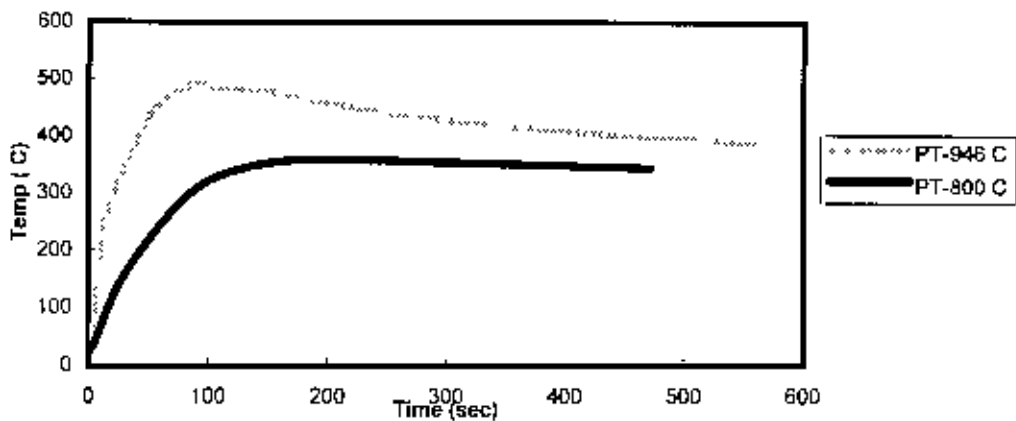
FIG. 6.2.3a EFFECT OF CASTING THICKNESS ON HEATING CURVES OF MOULD AT C, T3-t, FOR POURING TEMP -800 C
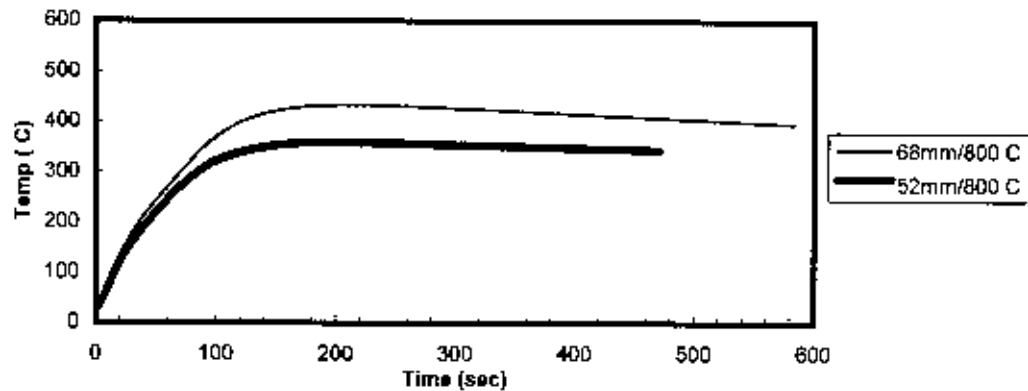
FIG. 6.2.3b EFFECT OF CASTING THICKNESS ON HEATING CURVES OF MOULD AT C, T3-t, FOR POURING TEMP-850 C
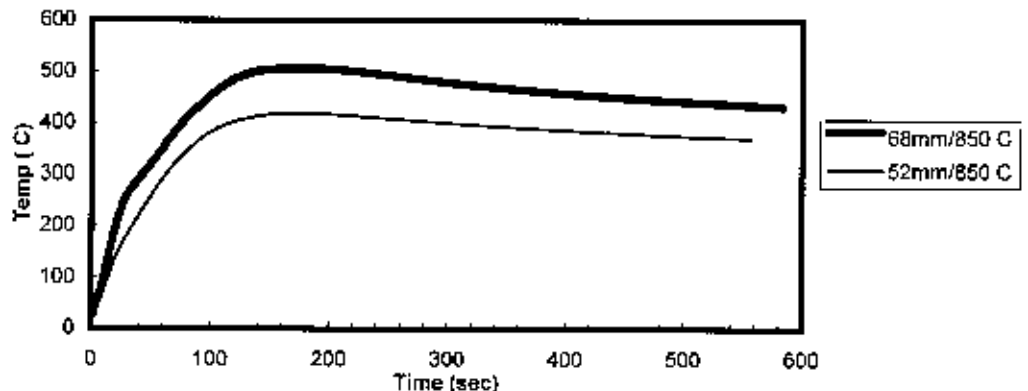
FIG. 6. 2.4a EFFECT OF SUPERHEAT ON HEATING CURVES OF MOULD AT D, T4-t, FOR 68mm PLATE CASTING
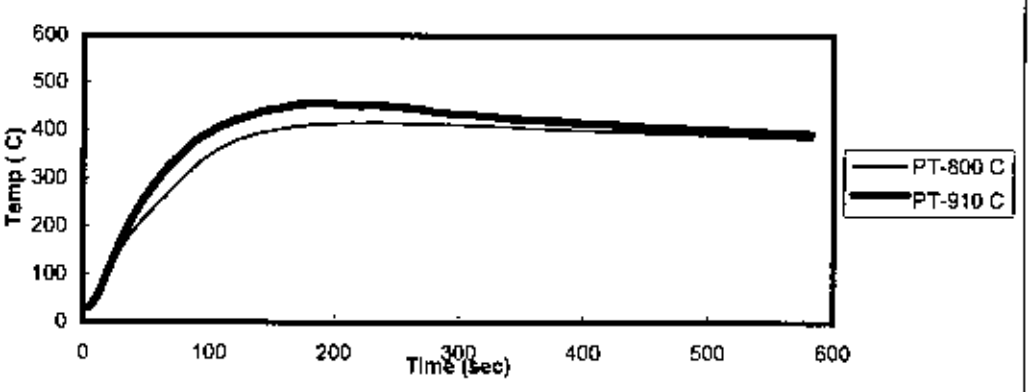
FIG. 6. 2.4b EFFECT OF SUPERHEAT ON HEATING CURVES OF MOULD AT D, T4-t, FOR 52mm PLATE CASTING

Temp (C) vs Time (sec)

Legend:
PT-946 C
PT-800 C
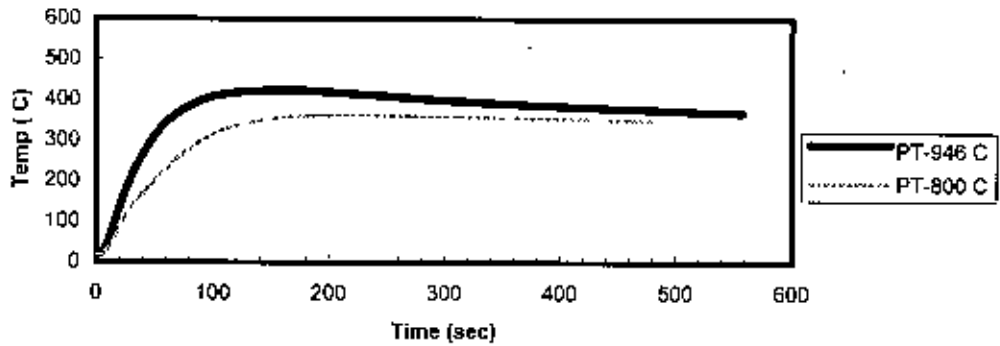
FIG. 6.2.5a EFFECT OF CASTING THICKNESS ON HEATING CURVES OF MOULD AT D, T4-t, FOR POURING TEMP-800 C

Temp (C) vs Time (sec)

Legend:
68mm
52mm
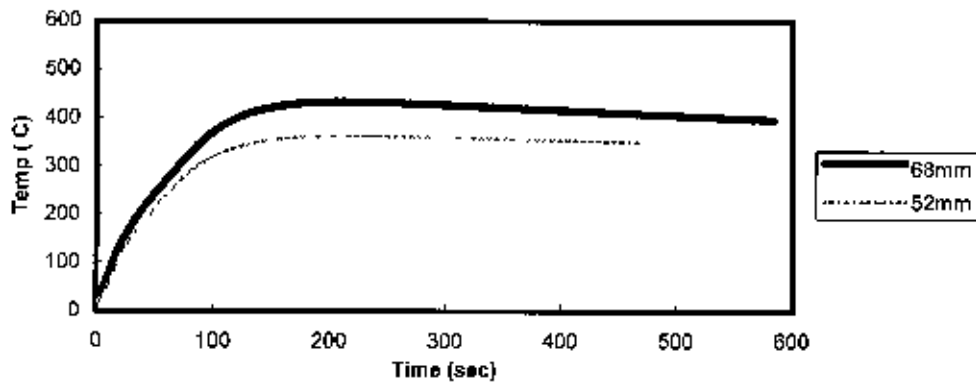
FIG. 6.2.5b EFFECT OF CASTING THICKNESS ON HEATING CURVES OF MOULD AT D, T4-t, FOR POURING TEMP-850 C

Temp (C) vs Time(sec)

Legend:
68mm
52mm
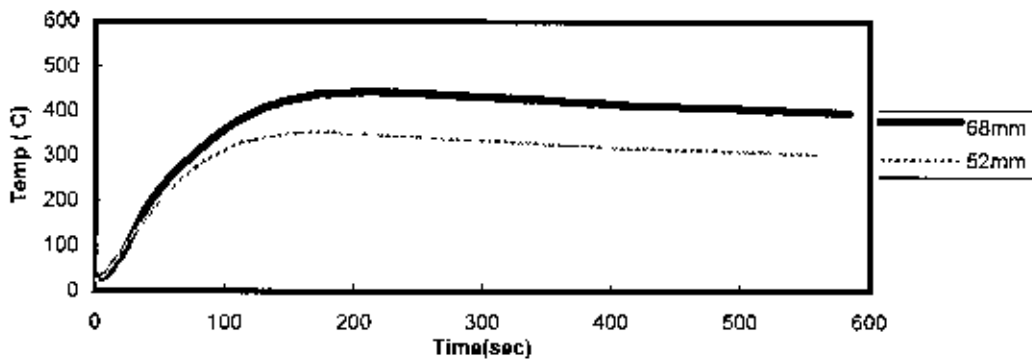
FIG. 6.2.6 EFECT OF CASTING THICKNESS ON COOLING CURVES OF CASTING AT CENTRE, T1-t, FOR POURING TEMPERATURE 850 C
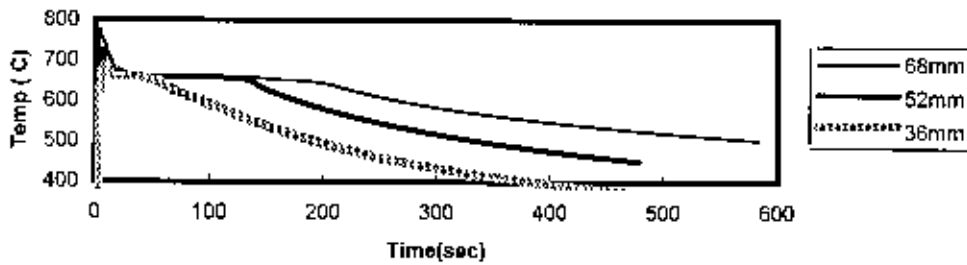
FIG.6.2.7 EFFECT OF POURING TEMPERATURE ON COOLING CURVES OF CASTING AT B, T2-t, FOR 68mm CASTING
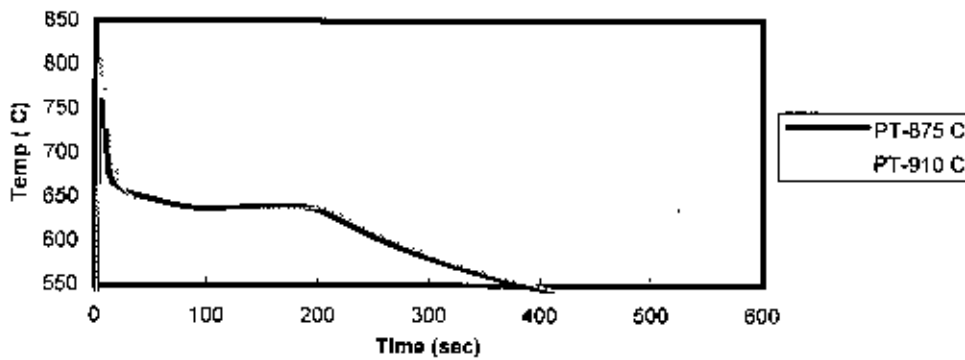
FIG. 6.2.8 EFECT OF CASTING THICKNESS ON COOLING CURVES OF CASTING AT B, T2-t, FOR POURING TEMPERATURE 850 C
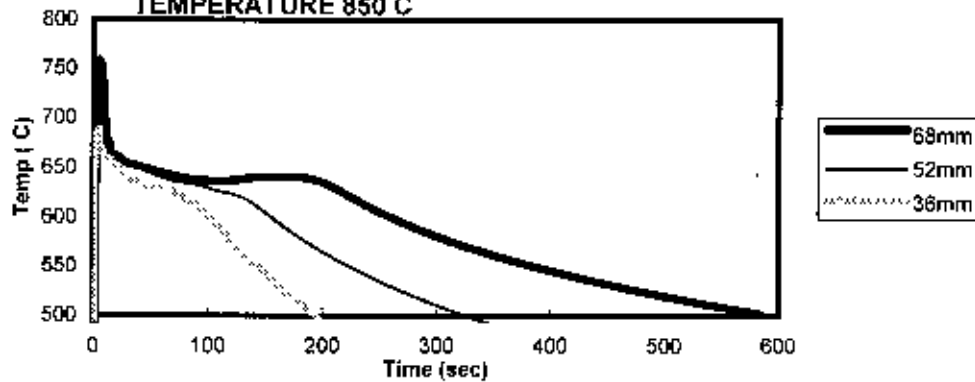
FIG. 3.2.9a EFFECT OF SUPERHEAT ON HF-TIME CURVES FOR 68mm CASTINGS
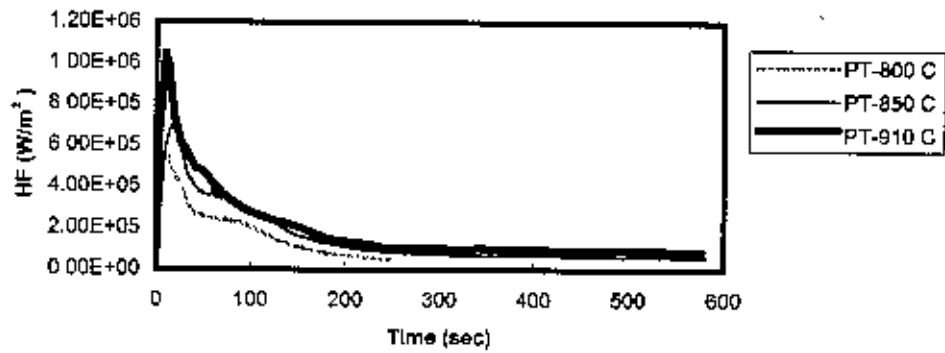
FIG. 6.2.9b EFFECT OF SUPERHEAT ON HF-TIME CURVES FOR 52mm CASTINGS
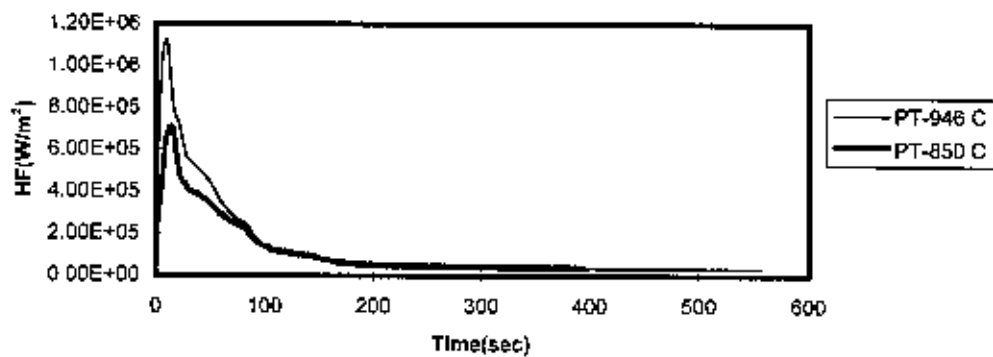
FIG. 6.2.9c SHOWING LIQUID SURFACE AT HFmax (PT-910 C, CT-68mm)
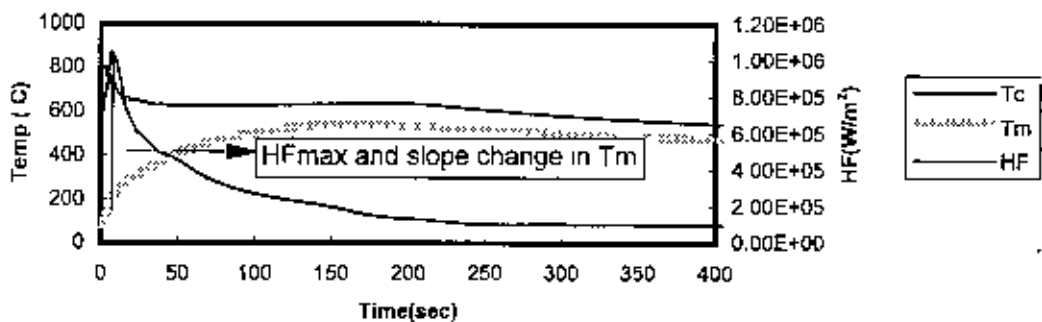
FIG. 6.2.9d SHOWING SOLIDIFICATION STARTS AT HFmax
(PT-925 C, CT-52mm)

HFmax and slope change in Tm
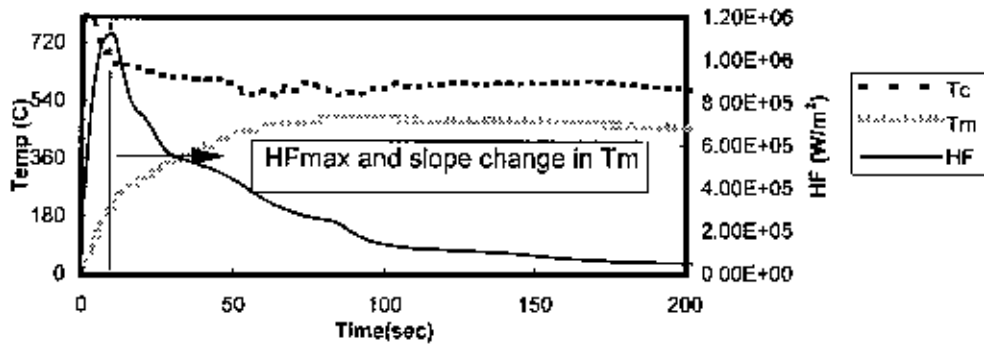
FIG. 6.2.9e SHOWING SOLIDIFIIED SKIN AT HFmax (PT-875 C,
CT-36mm)

HFmax and slope change in Tm
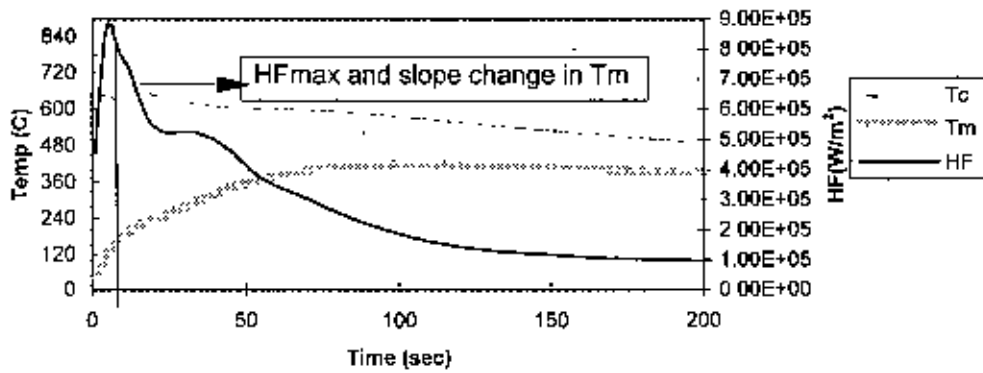
FIG. 6.2.10 EFFECT OF CASTING THICKNESS ON HF-TIME CURVES (PT- 850 C)

Legend:
- ········ 68 mm
- ——— 52 mm

X-axis: Time (sec)
Y-axis: HF (W/m²)

FIG. 6.2.11 EFFECT OF SUPERHEAT ON HFmax

Legend:
- □ 52mm
- △ 36mm
- ✕ 68mm

X-axis: SH (C)
Y-axis: HFmax(W/m²)
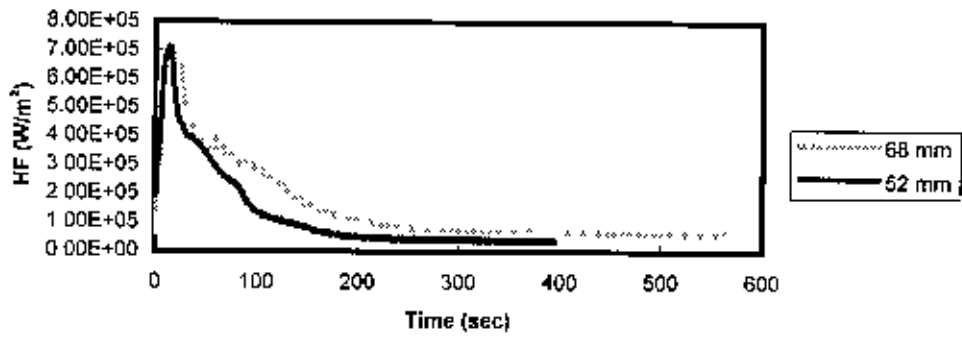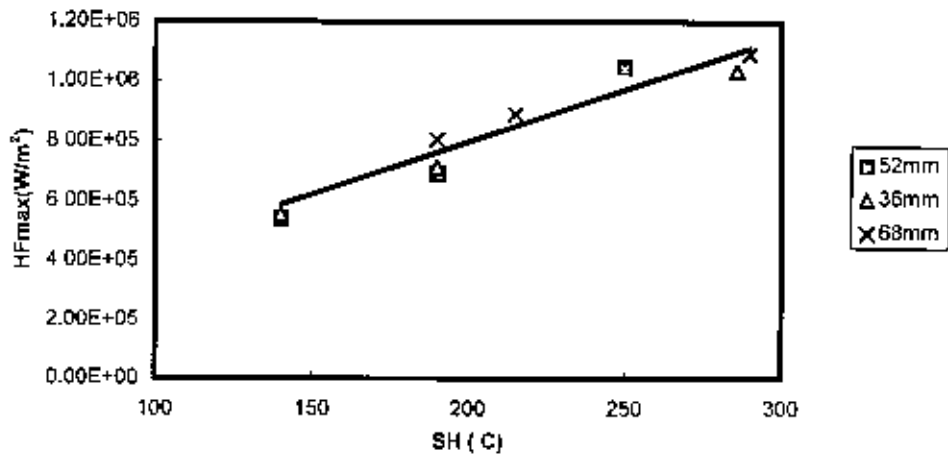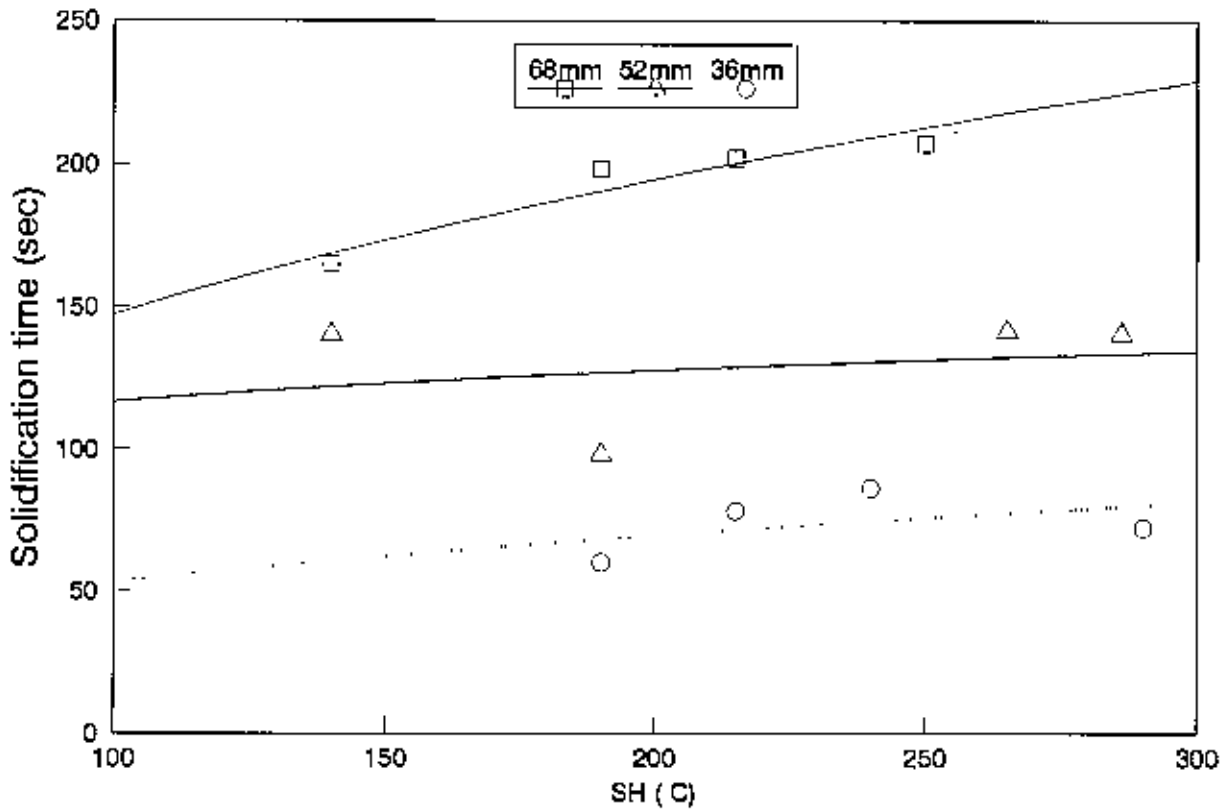
FIG. 6.2.12a EFFECT OF SUPERHEAT ON SOLIDIFIICATION TIME FOR PLATE
SHAPED AL CASTING IN CI MOULD
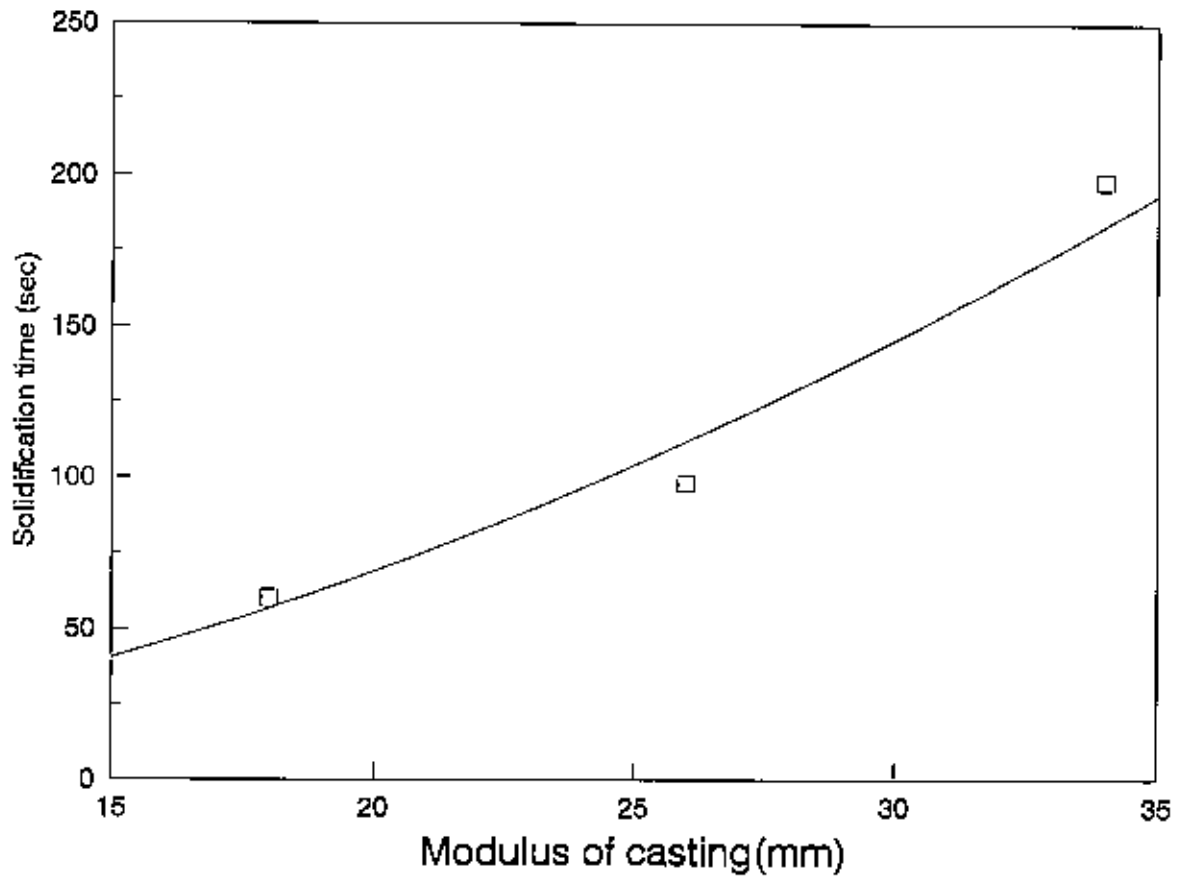
FIG. 6.2.12b EFFECT OF MODULUS OF CASTING ON SOLIDIFCATION TIME

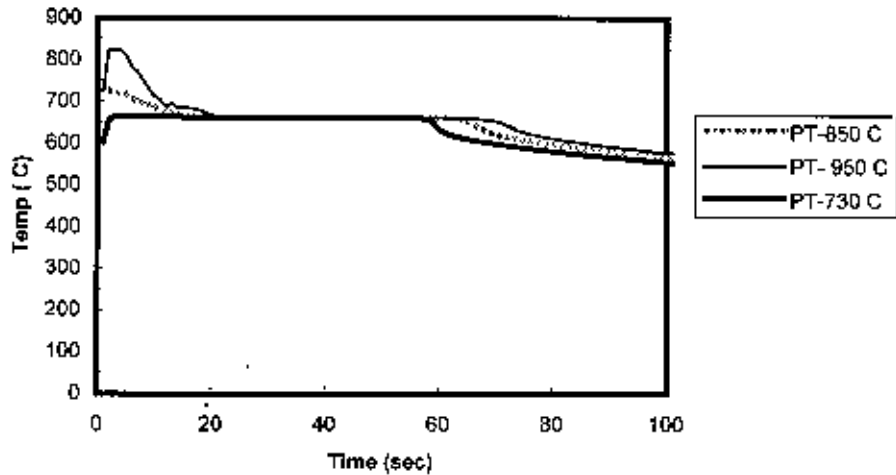FIG. 6.3.1 TEMP-TIME PROFILES OF CYLINDRICAL ALUMINIUM CASTING (MT-107 C, PT-950 C)
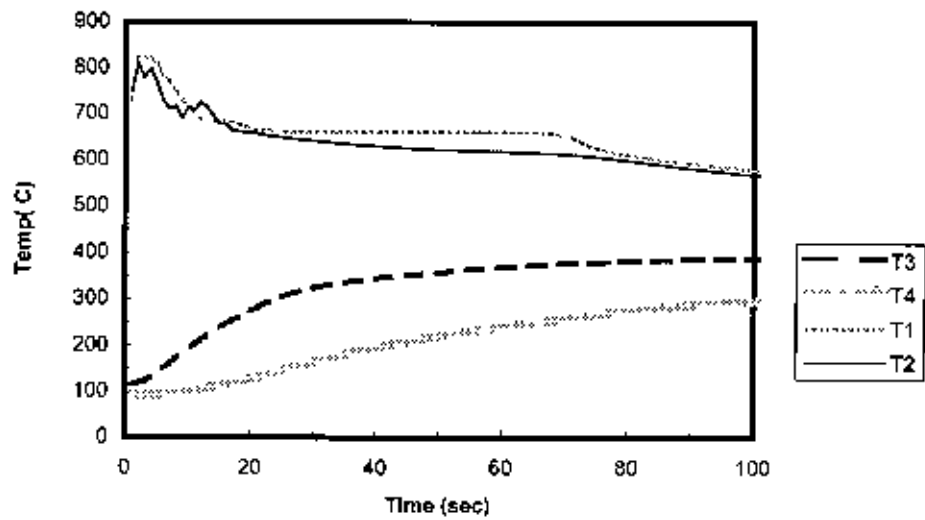
FIG 6.3.2a EFFECT OF SUPERHEAT ON TEMP-TIME PROFILES OF MOULD AT C, T3-t, FOR 82 C INITIAL MOULD TEMP
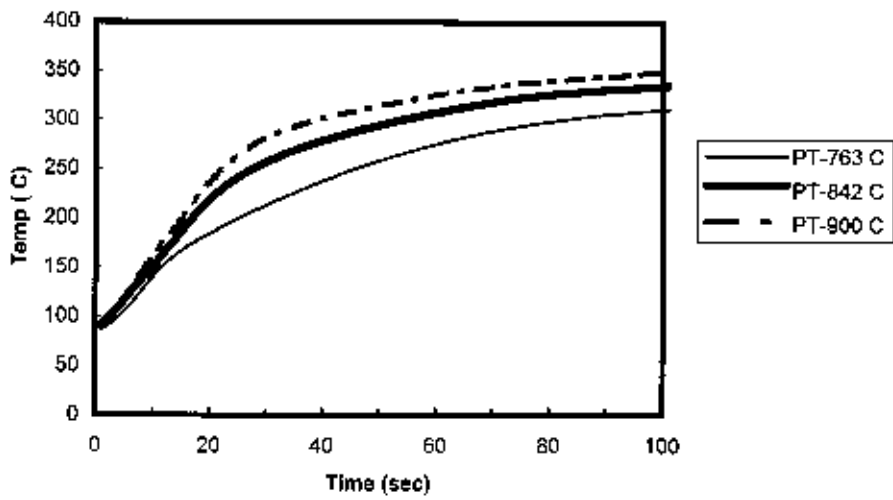
FIG. 6.3.2b EFFECT OF SUPERHEAT ON TEMP-TIME PROFILES OF MOULD AT C, T3-t, FOR 107 C INITIAL MOULD TEMP
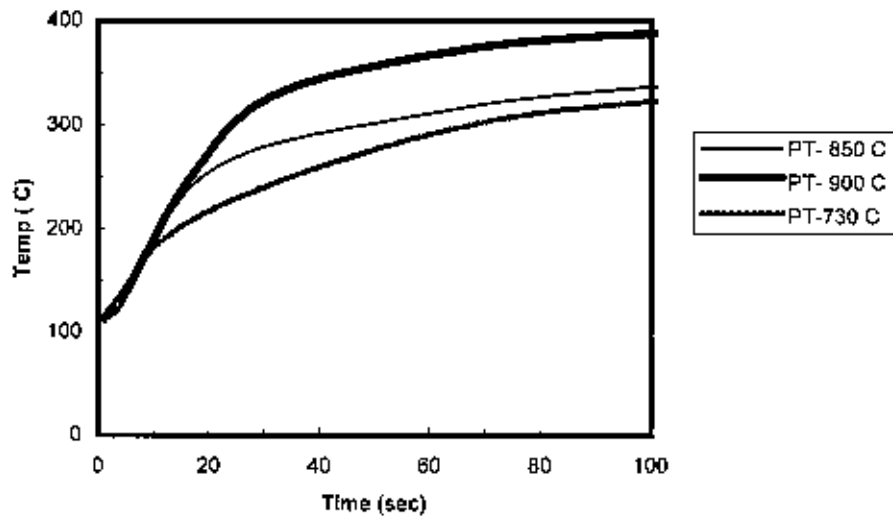
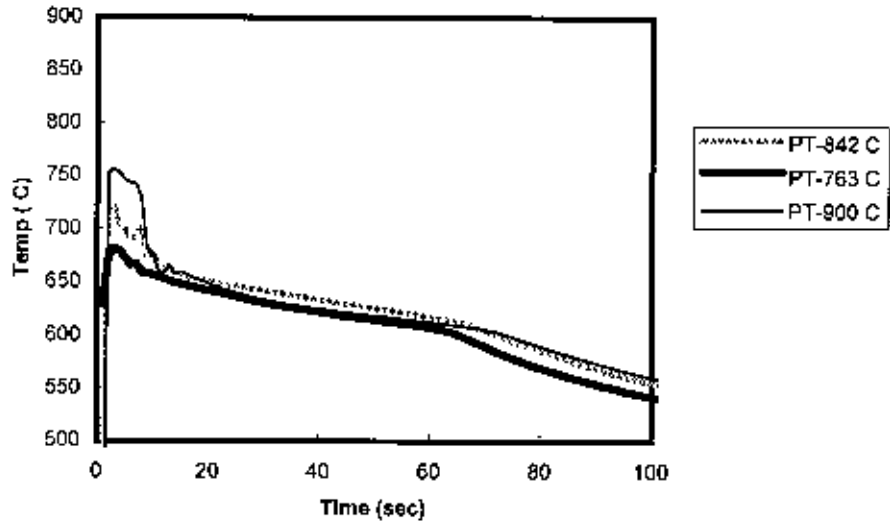FIG. 6.3.3a EFFECT OF SUPERHEAT ON TEMP-TIME PROFILES OF MOULD AT D, T4-t, FOR 82 C INITIALMOULD TEMP
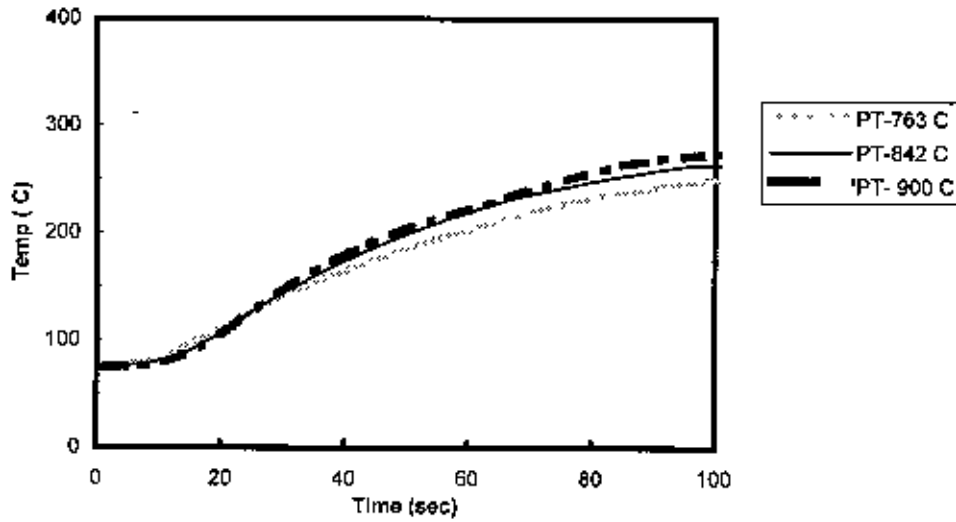
FIG. 6.3.3b EFFEECT OF SUPERHEAT ON TEMP-TIME PROFFILES OF MOULD AT D, T4-t, FOR 107 C INITIAL MOULD TEMP
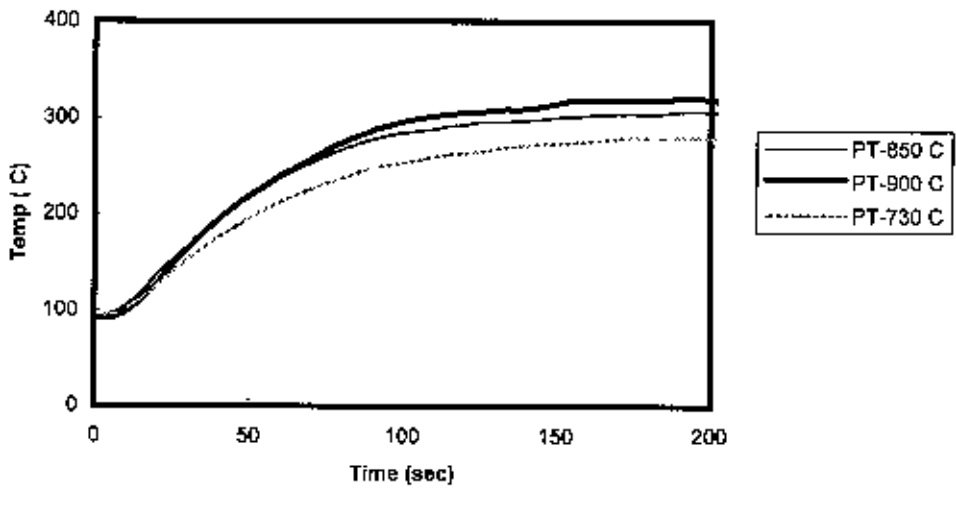
FIG. 6.3.4a EFFECT OF SUPERHEAT ON TEMP-TIME PROFILES OF CASTING AT A, T1-t, FOR 82 C INITIAL MOULD TEMP
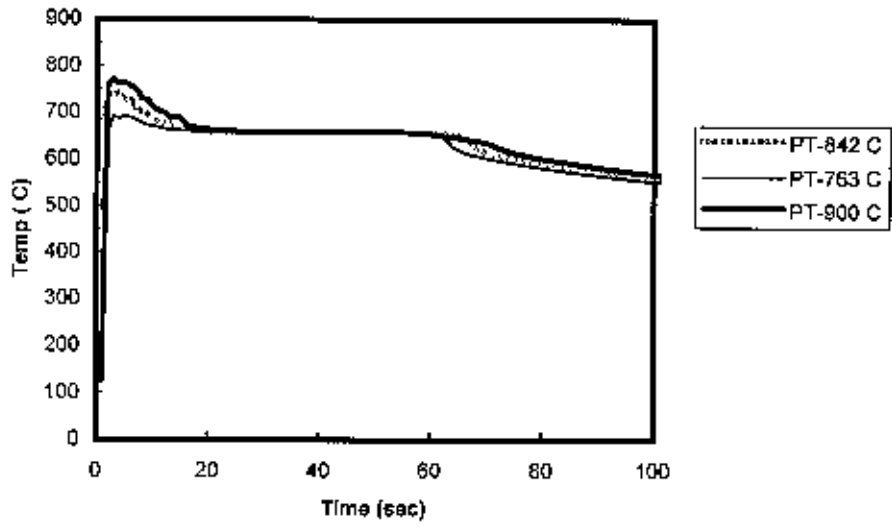
FIG. 6.3.4b EFFECT OF SUPERHEAT ON TEMP-TIME PROFILES OF CASTING AT A, T1-t, FOR 107 C INITIAL MOULD TEMP

FIG. 6.3.5a   EFFECT OF SUPERHEAT ON TEMP-TIME PROFILES OF CASTING AT B, T2-t, FOR 82 C INITIAL MOULD TEMP

FIG.6.3.5b EFFECT OF SUPERHEAT ON TEMP-TIME PROFILES OF CASTING AT B, T2-t, FOR 107 C MOULD TEMP
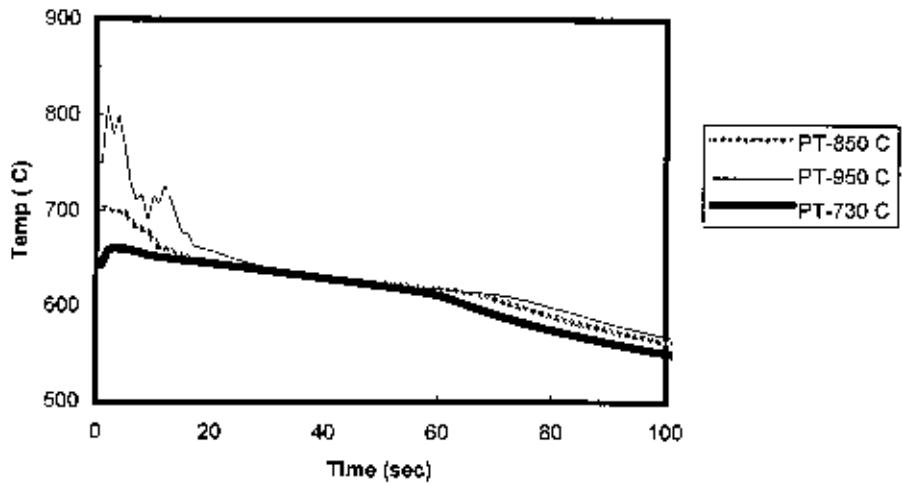
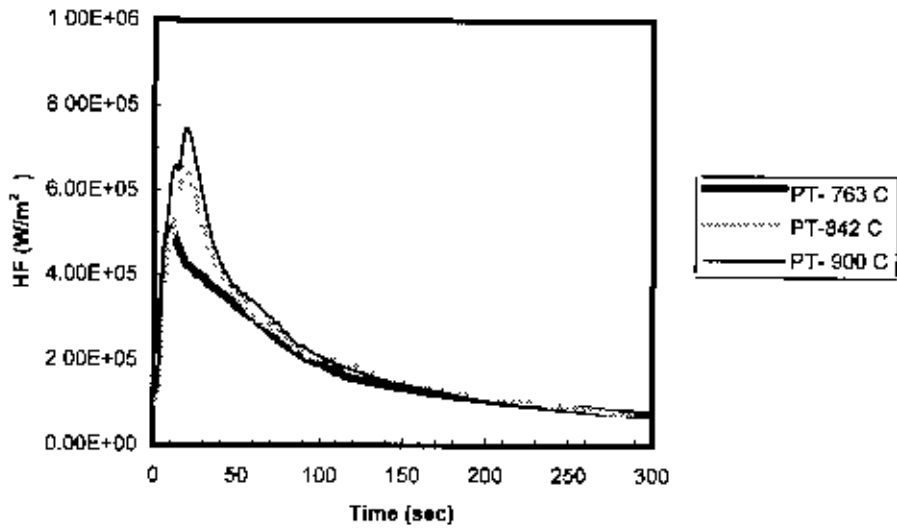FIG. 6.3.6a EFFECT OF SUPERHEAT ON HF-TIME CURVES FOR 82 C INITIAL MOULD TEMP

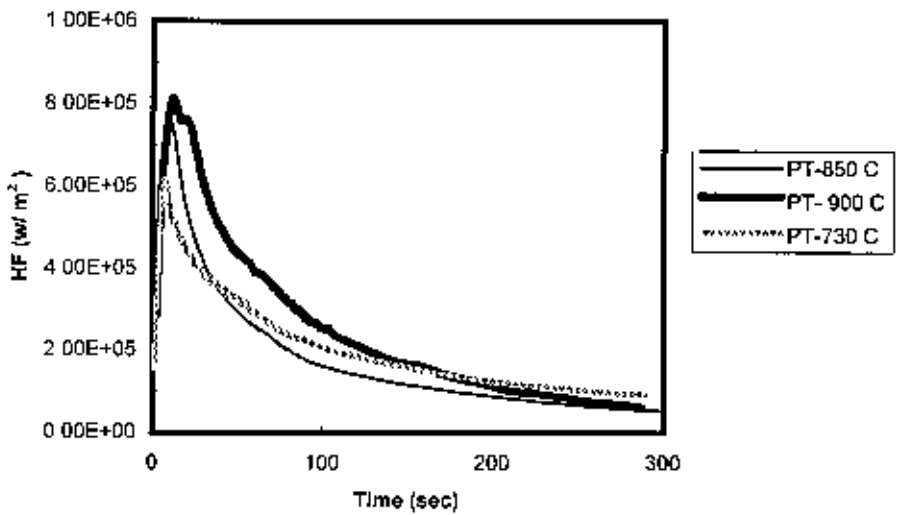FIG. 6.3.6b EFFECT OF SUPERHEAT ON HF-TIME CURVES FOR 107 C INITIAL MOULD TEMP

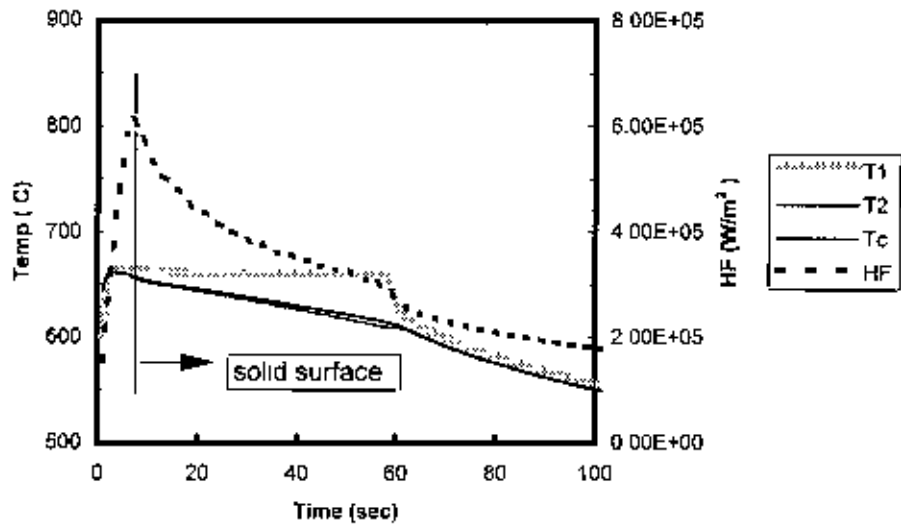FIG. 6.3.7 SHOWING SOLIDIFICATION STARTS BEFORE THE END OF FILLING (PT-730 C, MT-107 C)
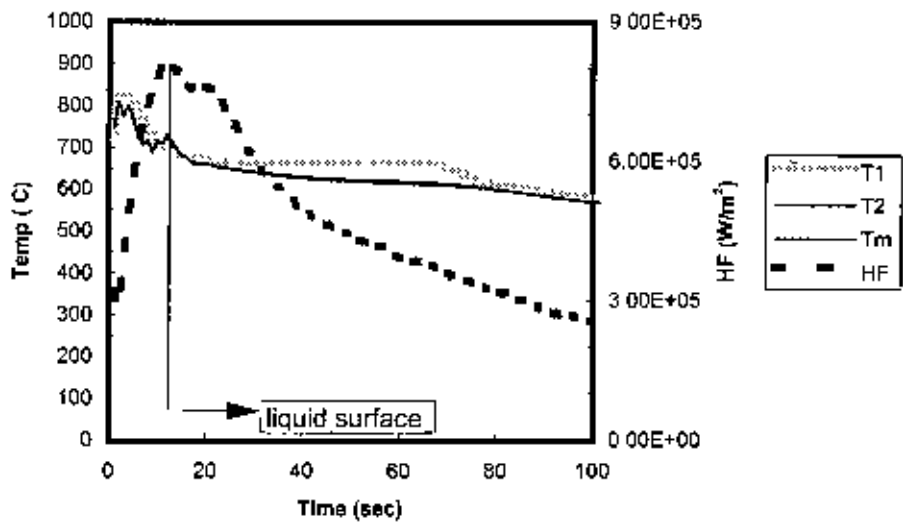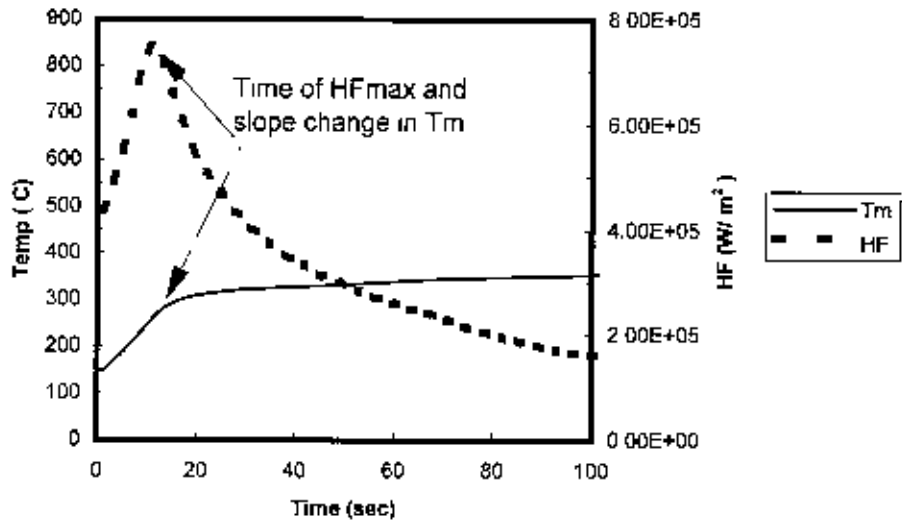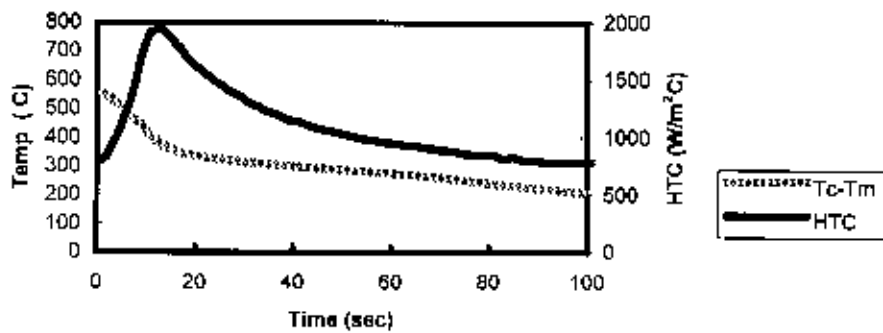

FIG. 6.3.8 SHOWING LIQUID SURFACE AT THE END OF FILLING (PT-950 C, MT-107 C)

FIG. 6.3.9 TIME OF HFmax AND SLOPE CHANGE IN Tm (MT-107 C, PT-850 C)

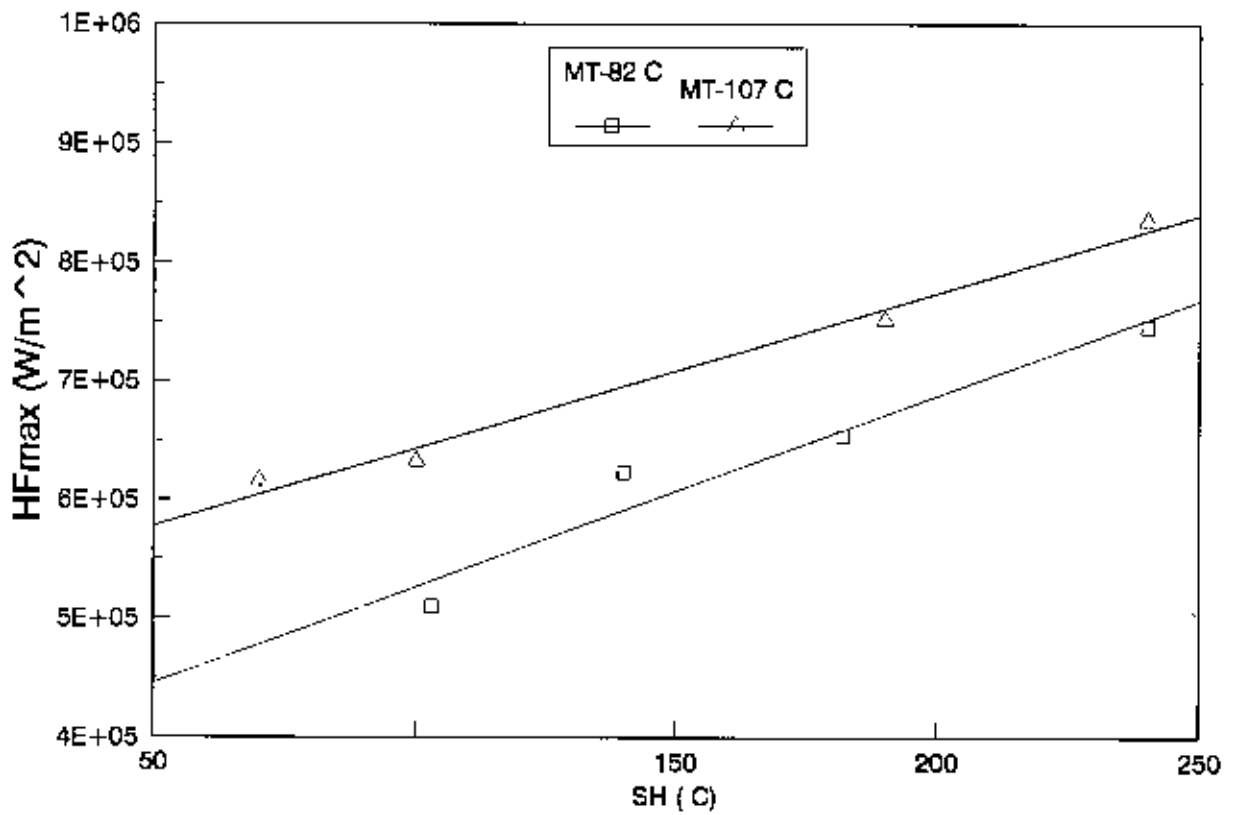FIG. 6.3.10   HTC AND Tc-Tm FOR CYLINDRICAL CASTING (MT-107 C, PT-850 C)

FIG. 6.3.11 EFFECT OF INITIIAL MOULD TEMPERATURE ON HFmax-SH CURVES

FIG. 6.3.12a EFFECT OF SUPERHEAT ON HTC-TIME CURVES AT 82 C INITIAL MOULD TEMP
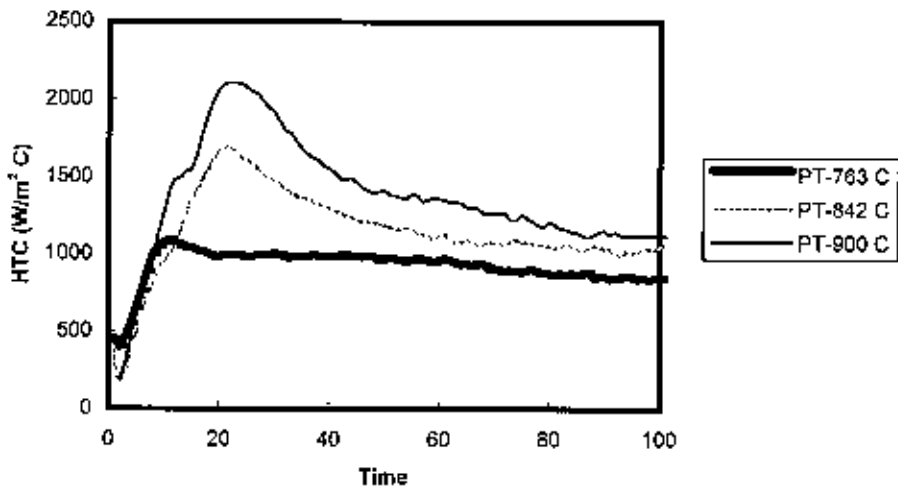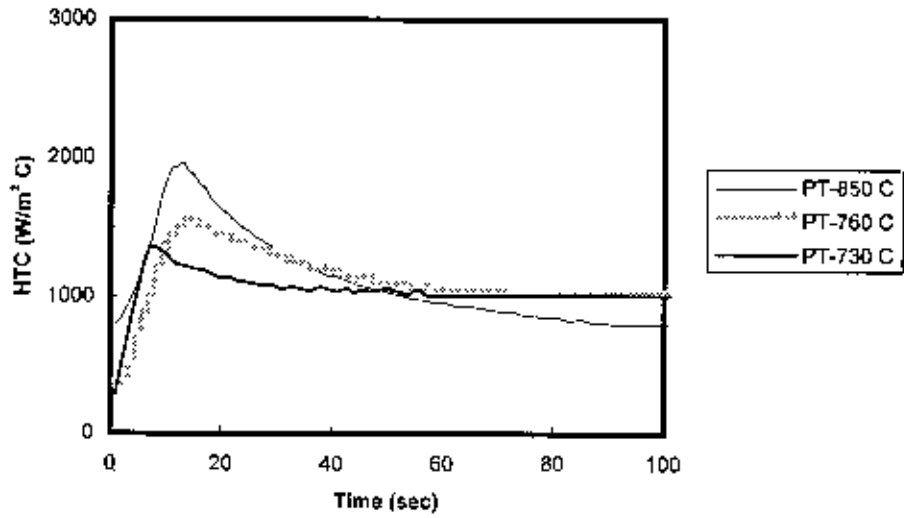

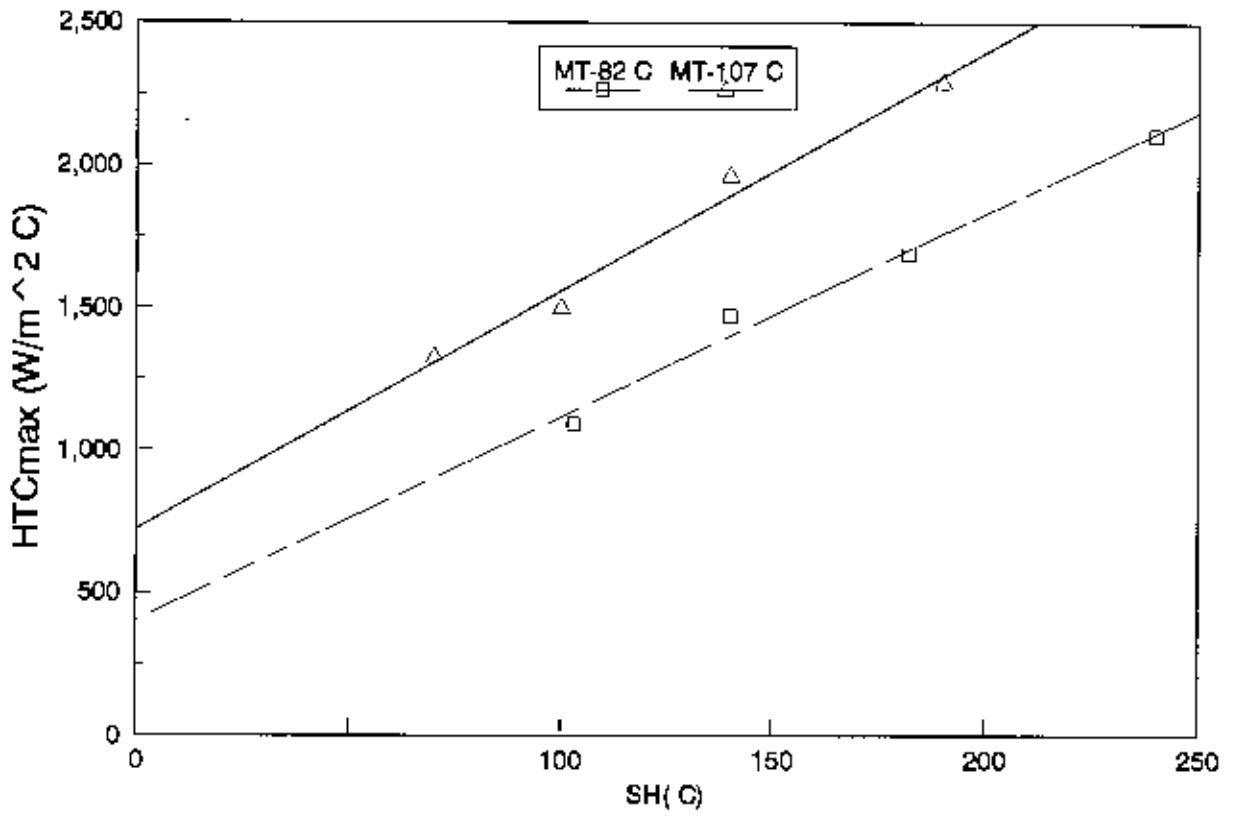FIG.6.3.12b EFFECT OF SUPERHEAT ON HTC-TIME CURVES AT 107 C INITIAL MOULD TEMP

FIG. 6.3.13 EFFECT OF INITIAL MOULD TEMPERATURE ON HTCmax-SH CURVES
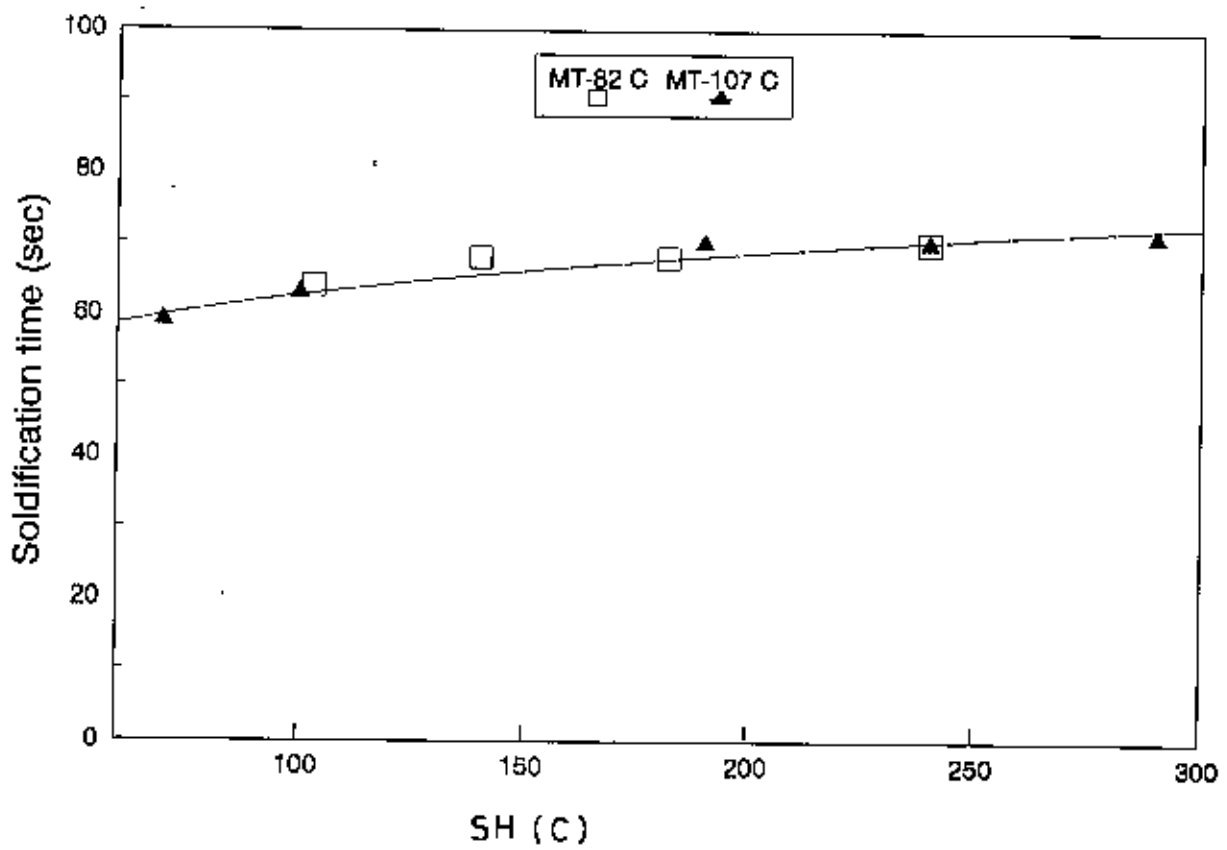
FIG. 6.3.14 EFFECT OF SUPERHEAT ON SOLIDIFICATION TIME

AT DIFFERENT MOULD TEMPERATURE

APPENDIX -A

Transient Heat Conduction Equation (Rectangular System):

$$\left(K\frac{\partial^2 T}{\partial x^2} + \frac{\partial K}{\partial T} * \left(\frac{\partial T}{\partial x}\right)^2 \right) = \rho \frac{\partial H}{\partial t}$$

Nodal Representation of Casting and Mould :
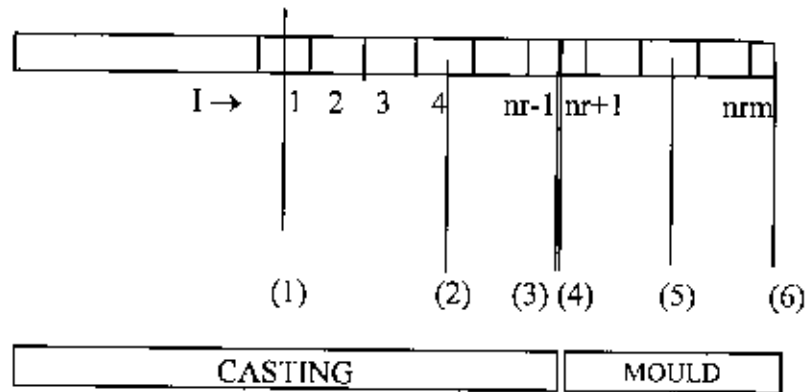
Here, I represents the node number.

Nodal Specification:

Nodes are taken as full node in the casting and mould region and half node at the interface (both in casting and mould) and at the external surface.

(1) Centre Node (in casting , I = 1)

(2) Middle nodes (in casting, I = 2 .. nr-1)

(3) Interfacial node (in casting, I = nr)

(4) Interfacial node (in mould, I = nr)

(5) Middle nodes (in mould. I = nr+1 .. nrm-1)

(6) Surface node }(in mould, I = nrm)

Finite Difference Approximation:

The replacement of time and space derivatives by finite difference involves expressing the derivatives in terms of a truncated Taylor series. In one dimensional space, the space derivatives of the equation can be represented by the central difference form as below

$$\frac{\partial^2 T}{\partial x^2} = \frac{T_{i+1} - 2T_i + T_{i-1}}{\Delta x^2}$$

$$\frac{\partial T}{\partial x} = \frac{T_{i+1} - T_{i-1}}{2\Delta x}$$

$$\frac{\partial H}{\partial t} = \frac{H_{i,j+1} - H_{i,j}}{\Delta t}$$

Explicit Finite Difference Equations:

Replacing the derivatives of the transient heat conduction equation, the following FDA equations are obtained :

In the casting,

$$K\left(\frac{T_{i+1} - 2T_i + T_{i-1}}{DX^2}\right) + Y*\left(\frac{T_{i+1} - T_{i-1}}{DX}\right)^2 = \rho\frac{H^{i+1} - H^i}{DT}, \text{ where } Y = \frac{\partial K}{\partial T}$$

$$K\left(\frac{T_{i+1} - 2T_i + T_{i-1}}{DX^2}\right) + Y*\left(\frac{T_{i+1} - T_{i-1}}{DX}\right)^2 = \frac{H^{j+1} - H^j}{Z} \quad \text{, where } Z = DT/\rho$$

$$H^{j+1} = H^j + Z*\left[\frac{K}{DX^2}\left(T_{i+1} - 2T_i + T_{i-1}\right) + Y\left(\frac{T_{i+1} - T_{i-1}}{2DX}\right)^2\right] \text{ for I=2 ..nr-1} \qquad (2)$$

Thus,

$$H^{j+1} = H^j + Z*\left[\frac{2K}{DX^2}\left(T_{i+1} - T_i\right)\right] \qquad\qquad \text{for I = 1} \qquad (1)$$

$$H^{j+1} = H^j + Z*\left[\frac{K}{DX^2}\left(T_{i-1} - T_i\right) - \frac{FR}{DX} + Y\left(\frac{FR}{K}\right)^2\right] \qquad\qquad \text{for I=nr} \qquad (3)$$

In the mould,

$$H^{j+1} = H^j + Z * \left[\frac{K}{DX^2}(T_{i+1} - T_i) + \frac{FR}{DX} + Y\left(\frac{FR}{K}\right)^2 \right] \qquad \text{for } I = nr \qquad (4)$$

$$H^{j+1} = H^j + Z * \left[\frac{K}{DX^2}(T_{i+1} - 2T_i + T_{i-1}) + Y\left(\frac{T_{i+1} - T_{i-1}}{2DX}\right)^2 \right] \text{for } I = nrm+1, nrm-1 \quad (5)$$

$$H^{j+1} = H^j + Z * \left[\frac{K}{DX^2}(T_{i-1} - T_i) - \frac{FRE}{DX} + Y\left(\frac{FRE}{K}\right)^2 \right] \qquad \text{for } I = nrm \qquad (6)$$

Here, FR = heat flux from casting to mould
FRE = heat flux from mould to environment

Transient Heat Conduction Equation (Cylindrical System):

$$\left(K\left(\frac{\partial^2 T}{\partial x^2} + \frac{1}{r}\frac{\partial T}{\partial r} \right) + \frac{\partial K}{\partial T} * \left(\frac{\partial T}{\partial x} \right)^2 \right) = \rho\frac{\partial H}{\partial t}$$

Explicit Finite Difference Equations:

In the casting,

For I=1

$$H^{j+1} = H^j + Z * \left[\frac{4K}{DR^2}(T_{i+1} - T_i) \right] \qquad (1)$$

For I=2..nr-1

$$H^{j+1} = H^j + Z * \left[\frac{K}{DR^2}\left\{ \left(\frac{2I-3}{2I-2}\right)T_{i-1} - 2T_i + \left(\frac{2I-1}{2I-2}\right)T_{i+1} \right\} + Y\left(\frac{T_{i+1} - T_{i-1}}{2DR}\right)^2 \right] \quad (2)$$

For I=nr

$$H^{j+1} = H^j + Z * \left[-\frac{FR}{DR} + \frac{K}{DR^2}(T_{i+1} - T_i) - \frac{FR}{(i-1)*DR} - \frac{K}{(i-1)DR^2}*(T_{i+1} - T_i) + Y\left(\frac{FR}{K}\right)^2 \right]$$

$$(3)$$

In mould,

For I=nr

$$H^{J+1} = H^J + Z*\left[\frac{FR}{DR} + \frac{K}{DR^2}\left(T_{i+1} - T_i\right) + \frac{FR}{(i-1)*DR} - \frac{K}{(i-1)DR^2}*\left(T_{i+1} - T_i\right) + Y\left(\frac{FR}{K}\right)^2\right]$$

(4)

For I=nr+1.. nrm-1

$$H^{j+1} = H^J + Z*\left[\frac{K}{DR^2}\left\{\left(\frac{2I-3}{2I-2}\right)T_{i-1} - 2T_i + \left(\frac{2I-1}{2I-2}\right)T_{i+1}\right\} + Y\left(\frac{T_{i+1} - T_{i-1}}{2DR}\right)^2\right]$$

(5)

.

For I=nrm

$$H^{J+1} = H^J + Z*\left[-\frac{FRE}{DR} + \frac{K}{DR^2}\left(T_{i-1} - T_i\right) - \frac{FRE}{(i-1)*DR} + \frac{K}{(i-1)DR^2}*\left(T_{i-1} - T_i\right) + Y\left(\frac{FRE}{2DR}\right)^2\right]$$

(6)

Here, FR   = heat flux from casting to mould

FRE = heat flux from mould to environment

APPENDIX -B

THERMOPHYSICAL PROPERTIES OF CASTING AND MOULD MATERIAL

Aluminium

Thermal conductivity (W/m C)

$K = 189.0 + 0.142T$	$T < 663.0$
$K = 210.56 + 4.75(663.0 - T)$	$663.0 \leq T < 690.0$
$K = 400$	$T \geq 690.0$

Specific Heat (J/Kg C)

$C = 1130$	$T > 660$
$C = 857 + 0.0587*T$	$T < 660$

Latent heat (J/Kg)
$L = 4.02 \times 10^5$

Density (Kg/m³)
$\rho = 2700$

Zinc

Thermal conductivity (W/m C)

$K = 115.115 - 0.047T$	$T < 419$
$K = 67.63 - 0.0115T$	$T > 419$

Specific heat (J/Kg C)

$C = 376.80 + 0.2093T$	$T < 419$
$= 494.026 + 0.042 T$	$T > 419$

Latent heat (J/Kg)
$L = 1.13 \times 10^5$

Density (Kg/m³)

$\rho = 7183.99 - 0.9T$	$T < 419$
$= 7022.94 - 0.96T$	$T > 419$

Copper

Thermal conductivity (W/m C)
$K = 418$

Specific heat (J/Kg C)
$C = 393.55+.084T$ T<1084
$\quad = 460.54$ T>1084

Latent heat (J/Kg)
$L = 2.05 \times 10^5$

Density (Kg/m^3)
$\rho = 9086.667 - 0.667T$ T<1084
$\quad = 8660.0 - 0.7T$ T>1084

Sand

Thermal conductivity (W/m C)

$K = 1.865 - 2.33E{-}3T + 2.06E{-}7T^2$	T>760
$K = 1.27 - 2.147E{-}3T + 1.83E{-}6T^2 + 1.26E{-}9T^3$	760>T>538
$K = 1.22 - 1.96E{-}3T + 1.68E{-}6T^2 + 1.51E{-}9T^3$	538>T>371
$K = 1.01 - 1.01E{-}3T + 2.85E{-}7T^2 + 1.15E{-}9T^3$	371>T>204
$K = 0.86 - 1.01E{-}4T - 1.15E{-}6T^2 + 2.18E{-}9T^3$	204>T

Specific heat (J/Kg C)

$C = 1085.19 - 0.09T$	T>760
$C = 1038.30 + 0.15T$	760>T>538
$C = 996.43 + 0.23T$	538>T>371
$C = 820.59 + 0.678T$	371>T>204
$C = 703.36 + 1.20T$	204>T

Density (Kg/m^3)
$\rho = 1515.0$

Emissivity
$\varepsilon = 0.7$

AFS grain fineness
No- 60

Grey Cast Iron

Thermal conductivity (W/m C)

$K = 43.5 - 8.5E-3T$ $T < 235$

$K = 54.43 - 0.055$ $235 \leq T < 335$

$K = 39.25 - 0.0098T$ $T \geq 335$

Density (Kg/m^3)

$\rho = 7885.5 - 0.36T$ $T < 780.0$

Emissivity

$\varepsilon = 0.8$

Specific heat (J/Kg C)

$C = 542.97 + 0.133T$ $T < 661.7$

Chemical Composition

C - 3.0%

Si - 1.5%

Mn - 0.2%

S - 0.05%

P - 0.05%

Heat transfer coefficient at external surface (W/m^{2}C)

Convective heat transfer coefficient

$h_c = 1.42 \, (\Delta T/L)^{0.25}$ GrPr $-10^4 - 10^9$

$h_c = 1.31 \, (\Delta T)^{0.33}$ GrPr $- 10^9 - 10^{13}$

Radiative heat transfer coefficient

$h_r = \varepsilon\sigma \, ((Tw+273)^4 - (Ta+273)^4)/\Delta T$

Where, L = characteristic length ,

       $\Delta T = Tw - Ta$

       Gr = Grashof number

       Pr = Prandlt number